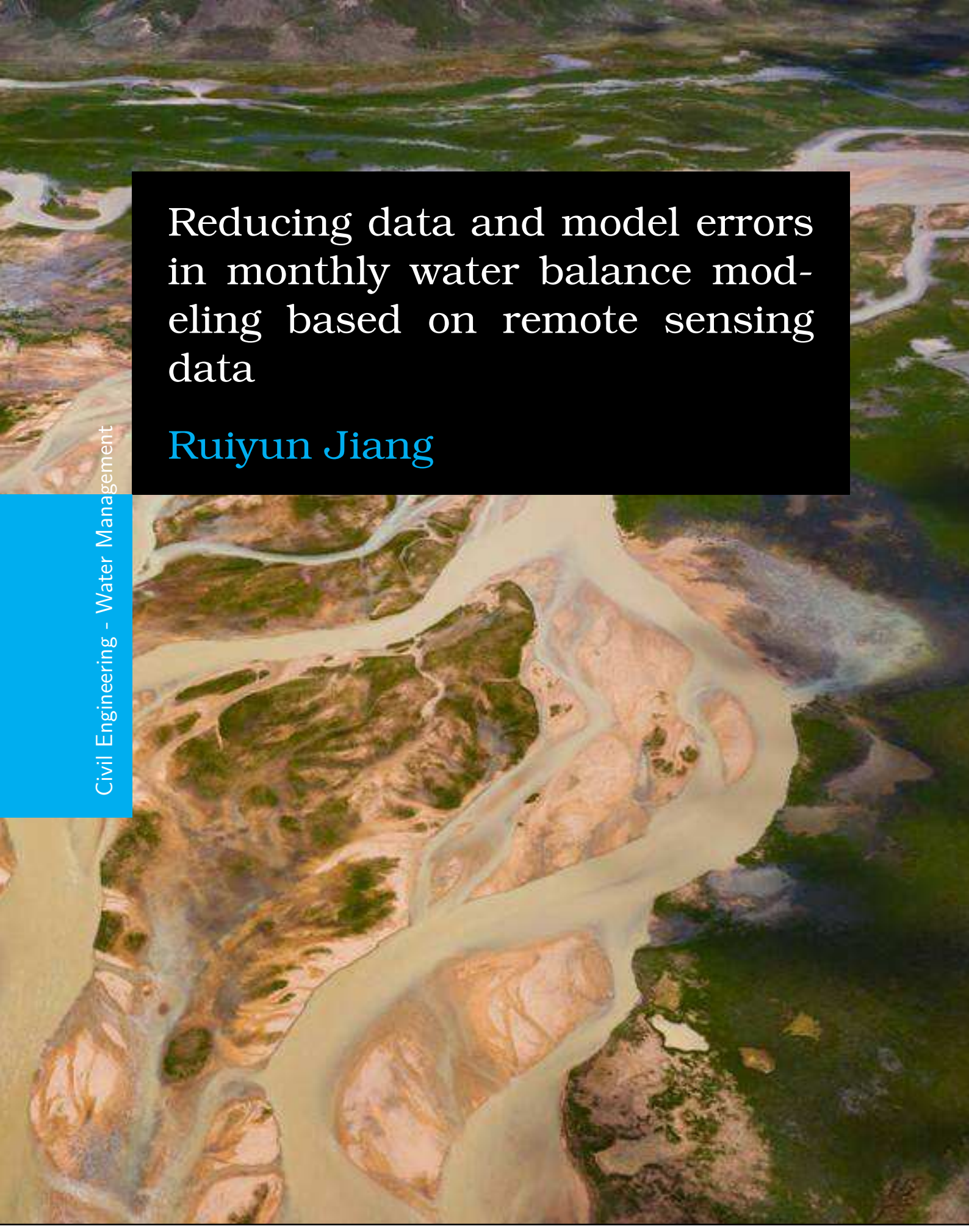

Reducing data and model errors in monthly water balance modeling based on remote sensing data

Ruiyun Jiang

Civil Engineering - Water Management

TU Delft Delft University of Technology

Reducing data and model errors in monthly water balance modeling based on remote sensing data

Master of Science Thesis

Ruiyun Jiang

at Delft University of Technology
to be defended on January 24th, 2022 at 9:45.
An electronic version of this thesis is available at
http://repository.tudelft.nl/

Faculty of Civil Engineering and Geosciences (CEG) · Delft University of Technology

Supervisor: Dr.ir.Gerrit Schoups
Thesis committee: Dr. Markus Hrachowitzand Dr. Ronald van Nooyen

Abstract

The water balance model has long been an indispensable tool for quantifying water supply and demand and regulating water resources. By convention, hydrologists use in-situ measurements of river discharge for model calibration. Whereas hardly is it possible for areas suffering from data storage. Researchers have been working on methods dealing with this problem for many years. Satellite datasets are potential substitutes for the in-situ observation of hydrological variables. This research proposes a monthly strategy using satellite time series as model inputs and aims to apply this strategy in the absence of gauged data for discharge simulations and predictions. Instead of streamflow, the strategy uses variables like actual evapotranspiration (ETa) and/or terrestrial water storage anomalies (TWSA) for calibration. The research challenges lie in the situation that there can be significant errors in data derived from satellite products. Also, hydrological models designed for discharge simulation cannot necessarily function well when calibrated on other terms. This boils down to the research questions as follow:

1. How large are water balance data errors and to what extent can they be reduced?

2. How large are water balance model errors and to what extent can they be reduced?

3. To what extent does quantifying and reducing data and model errors eliminate trade-offs in fitting multiple datasets?

The strategy is constructed based on an error estimation and water balance data fusion method and the original and the advanced version of the Water Partition and Balance model (Wapaba), then tested in the Smoky Hill River catchment. When using unprocessed data, the water balance is not closed for the basin. The discharge simulation has the fitting precision index the Box-Cox transformed root mean squared error (TRMSE) in the range of 0.70 - 1.43 for different datasets and in calibration and validation period. Indexes of discharge fitting σ exceed 1.66. After closing the water balance with the mean value time series of all fluxes, TRMSE decreases to 0.55. Considering data uncertainties, TRMSE is further declined to 0.29 and σ drops to 0.46. After that, the model structure is also improved. When using the modified model to calibrate on only ETa and TWSA for calibration (TRMSE for discharge = 0.87), the performance is similar to that of using the original Wapaba on all fluxes (TRMSE for discharge = 0.86). The fitting precision index σ for TWSA also decreases.

The research demonstrates the effectiveness of the data fusion method in correcting satellite time series and sheds light on the potential of application of this strategy in the ungauged area through the comparison of different calibration cases. After modification, the strategy is able to reproduce the flow regime, without using in-situ data, to the same degree as all three hydrological components (discharge, actual evapotranspiration and water storage) are used for calibration.

Acknowledgments

This thesis would not have been possible without the devoted help of people around me. I hope to use this chance to express my gratitude to my supervisor Dr. ir. Gerrit Schoups. He has made available his support in many ways. I tend to procrastinate when faced with difficulties, but he encouraged me to get started. Also, his crucial guidance helped me find methods of dealing with problems in the research. Although I did have a hard time doing this research, I still feel so lucky since I can have this opportunity to know a nice person as he is. I would like to thank my committee members as well. Dr. Markus Hrachowitz and Dr. Ronald van Nooyen always asked questions that could make me think. Sometimes thoughts escape from my mind easily, but they help me seize them.

I hope to thank my beloved friends. Xin Huang and Mengdi Li generously shared their opinions on this study, which inspired me greatly. Le Zhang, Chen Fa and Ning Cai took care of me a lot in life. Jinjie Mao and Zhe Hou were concerned about my mental health.

I owe my deepest gratitude to my parents for their unconditional trust and support (even though my dad is a terrible cook). In this special covid period, I never feel too bad because I know I am surrounded by their love. Lastly, I want to thank myself for everything.

List of Abbreviations

Abbreviation	Full form
CHIRPS	Climate Hazards Group InfraRed Precipitation with Station data
CSR	Center for Space Research
DE	Differential Evolution
EC	Eddy Covariance
Ei	Interception loss
Ep	Potential evapotranspiration
ET	Evapotranspiration
ETa	Actual evapotranspiration
GLEAM	Global Land Evaporation Amsterdam Model
GLUE	The generalized likelihood uncertainty estimation
GRACE	Gravity Recovery and Climate Experiment
JPL	Jet Propulsion Laboratory
MC	Monte Carlo
MCS	Monte Carlo Simulation
MODIS	Remotely sensed Moderate Resolution Imaging Spectroradiometer
P	Precipitation
Q	Discharge
RMSE	root mean square error
SEBAL	Surface Energy Balance Algorithm
SSEBop	the Operational Simplified Surface Energy Balance
SWAT	Soil and Water Assessment Tool
TRMSE	The Box-Cox transformed root mean squared error
TWS	Terrestrial Water Storage
TWSA	Terrestrial Water Storage Anomalies
Wapaba	The Water Partition and Balance

Table of Contents

1 Introduction **1**

1-1 Background and problem description . . . 1

1-2 Methods for parameter calibration . . . 2

1-3 Satellite data used in model calibration . . . 3

1-4 Methods for data and model error correction . . . 5

1-5 Research questions . . . 6

1-6 Thesis structure . . . 7

2 Case study **9**

2-1 Study Area . . . 9

2-2 Monthly water balance data . . . 12

2-2-1 Overview . . . 12

2-2-2 Precipitation time series . . . 12

2-2-3 Evaporation time series . . . 13

2-2-4 Terrestrial water storage . . . 14

2-2-5 Discharge time series . . . 14

2-3 Monthly water balance model . . . 14

3 Methodology **19**

3-1 Quantifying and reducing data errors using data fusion . . . 19

3-2 Quantifying and reducing model errors using model calibration and evaluation . . . 22

3-2-1 Calibration scheme . . . 22

3-2-2 Objective function . . . 25

4 Results **29**
4-1 Data fusion . . . 29
4-1-1 Data fusion results . . . 29
4-2 Efficiency analysis . . . 33
4-2-1 Case a: using raw data for calibration . . . 33
4-2-2 Case b: Using clean data and calibration on Q . . . 35
4-3 Model structure analysis . . . 39
4-3-1 Case c: calibration on ETa, TWSA and discharge . . . 39
4-3-2 Case d: calibration on ETa and TWSA . . . 39
4-3-3 Case e: model structure modification and calibration on ETa, TWSA and discharge . . . 42
4-3-4 Case f: model structure modification and calibration on ETa and TWSA . 45

5 Discussion **51**
5-1 The significance of water balance data errors and their reduction . . . 51
5-2 The significance of errors in water balance models, and model error reduction . . 52
5-3 The effectiveness of quantifying and reducing data and model errors . . . 52
5-3-1 Effects of reducing water balance data errors . . . 53
5-3-2 Effects of accounting for precipitation uncertainty . . . 53
5-3-3 Effects of model structure modification . . . 54

6 Conclusions and prospects **57**
6-1 Research conclusions . . . 57
6-2 Prospects for further study . . . 58

A Dataset information **59**

B Water balance check **63**

C Other simulation results **67**

References **73**

Chapter 1

Introduction

1-1 Background and problem description

Water balance models are essential tools for quantifying water supply and demand and solving practical water resource problems. They are designed to give a clearer comprehension of crucial processes that affect the hydrological cycle. Monthly models have been widely applied for the estimation of monthly stream flows, medium and long-term forecasting of water resources, and water resources management (C. Y. Xu & Singh, 1998).

The most commonly used assessments of discharge are based on simulations of discharge together with gauge-based observations (Famiglietti & Rodell, 2013). In practice, one oft-mentioned problem is that water balance models based on physical mechanisms need the support of a large number of spatiotemporal distribution data, but manual observation is always time-consuming and laborious. Modeling suffers from short ground observations and their limited spatial and temporal representatives. The missing, long-overdue or inaccurate information on runoff complicates the prediction of monthly water resources.

In recent years, the development of remote sensing products has led to increased availability of satellite datasets on various hydrological variables, which proves the possibility of their utilization in hydrological modeling, makes up for the insufficiency of conventional station observations and brings unprecedented opportunities for model evaluation and improvement (Lu et al., 2015). The current thesis proposes research to build an improved monthly water balance strategy that allows using satellite time series for calibration and to evaluate the applicability of the strategy as a valuable tool for streamflow simulations and predictions in poorly gauged river basins. The research starts with a literature review on approaches to correct errors in satellite remote sensing data, commonly used hydrological model calibration methods, together with existing methodologies to use satellite data of hydrological components for model calibration and evaluation.

1-2 Methods for parameter calibration

In conceptual models, parameters cannot be directly measured and thus require optimization through calibration, so that satisfactory agreement can be obtained between observed and simulated counterparts of some components related to the water balance (Rientjes, Muthuwatta, Bos, Booij, & Bhatti, 2013). Water balance models are usually calibrated by using streamflow time series observed at one or a few locations in the river basin (Muthuwatta et al., 2009), since calibration on streamflow, which is an integrated response of a watershed, controls many model processes. Moreover, the in-situ measurement of streamflow is relatively easy (compared with the ground observation of terrestrial water storage) and the extent of uncertainty in measured streamflow can often be estimated (Yassin et al., 2017). There are various methods for hydrological model calibration and evaluation using streamflow data alone.

The traditional methods generally used for hydrological model calibration are single-criterion optimization and multi-criteria optimization. The former is a straightforward and scrutable approach but suffers from some restrictions when dealing with complicated models with a great number of parameters. The latter enables the full use of field measurements and is useful for reducing parameter uncertainty (Cao, Bowden, Davie, & Fenemor, 2006). For example, Cao et al. (2006) adopt a multi-variable and multi-site approach for SWAT model calibration and evaluation by using extensive field measurements; while Hallema and Moussa (2009) use multi-objective functions related to volume, peak flow, and the Nash-Sutcliffe coefficient in addition to extensive data collection.

Another widely used method is to assess the fidelity of the hydrological model based on Bayesian statistical inference (Yassin et al., 2017), which is highly effective in providing a general and natural probabilistic strategy that explains the hydrological model and its parameter uncertainty at the same time (e.g., Y. M. Xu, Lin, and Li, 2015). The uncertainty analysis method based on Bayesian theory assumes that the model parameters obey a random vector of a joint distribution, and uses the Bayesian method to calculate the posterior probability distribution of the parameters and calculate the uncertainty confidence interval of the predictor (Wei, 2017). Yang (2007) uses Bayesian inference to tackle the problem of non-identifiability of distributed parameters. In the research of Jeremiah, Sisson, Marshall, Mehrotra, and Sharma (2011), they implement a sequential Monte Carlo approach so as to obtain posterior parameter estimates in eastern Australia, and this approach results in great efficiency in parameter space exploration. The generalized likelihood uncertainty estimation (GLUE) strategy represents prediction uncertainty within the context of Monte Carlo (MC) analysis coupled with Bayesian estimation and propagation of uncertainty. The GLUE method is flexible and easy to apply (Blasone et al., 2008). For example, Ma and Chen (2014) propose the parameter uncertainty analysis of the Xinanjiang model in the Dongyang River Basin based on the GLUE method. The range of uncertainty contains most of the measured discharge, which demonstrates that using the GLUE method to quantify uncertainty of the Xinanjiang model in the study area is feasible. However, the measured discharge cannot be included in the upper and lower bounds of the simulated discharge, indicating that the parameter ranges cannot cover all values.

Another different method is sensitivity analysis, which is popular and efficient for model parameterization, especially in model reduction or for reducing of the number of parameters needing calibration. Through the identification, the noninfluential factors and insensitive

components of the model structure can be constrained or removed (Razavi & Gupta, 2015). The sensitivity analysis procedure helps to significantly simplify the model or analysis and to reduce the workload of manual calibration. A sensitivity analysis that accommodates a large number of parameters while considers several output variables can be applied for a water quality model (van Griensven et al., 2006) as well as quantity mathematical models (da Silva et al., 2015), and obtain successful results. Bock, Hay, McCabe, Markstrom, and Atkinson (2016) implement the Fourier Amplitude Sensitivity Test (FAST) global-sensitivity algorithm on a monthly water balance model to generate parameter sensitivities. In the study of da Silva et al. (2015), the parameters that influenced the surface runoff and baseflow were optimized manually, and the resulting parameter set was used for simulation and evaluation.

1-3 Satellite data used in model calibration

As the growing complexity of hydrological models brings more degrees of freedom, using streamflow alone in traditional calibration methods is not sufficient to adequately capture some components (e.g., water storage) in the basin and subsequently to close the water balance (Yassin et al., 2017). To constrain the model performance, many studies evaluated the potential of satellite remote sensing-based hydrological components data.

One common approach is calibrating hydrological models using observed streamflow data and satellite time series of another hydrological component (Muthuwatta et al., 2009). Comparisons of model performances reveal that simulations incorporating water balance variables other than discharge reduce optimal combinations of multiple parameters (i.e., equifinality, which corresponds to more than one parameter combination leading to similar results (Immerzeel & Droogers, 2008)). Besides, the comparisons increase the probability of finding a parameter set that represents the actual hydrological simulations of the basin (Muthuwatta et al., 2009).

Some studies of Gravity Recovery and Climate Experiment (GRACE) outline its potential to detect and improve the understanding of water storage and its change within the basin (Sun, Green, Swenson, & Rodell, 2012; V. Ferreira, Gong, He, Zhang, & AndamAkorful, 2013), since it has a solid hydrological signal over the selected study area (Deus, Gloaguen, Krause, 2013). Incorporating GRACE-derived terrestrial water storage changes (TWSC) data during model parameterizations can improve hydrological model performances since GRACE data can be used to constrain the ratio between ET and TWSC and to improve the estimates of hydrological variables (Lo, Famiglietti, Yeh, & Syed, 2010; Yassin et al., 2017; Bai, Liu, & Liu, 2018). For example, Tangdamrongsub et al. (2017) argue in their study that GRACE Data Assimilation greatly improves the accuracy of groundwater storage estimates by 25%, although they slightly lower the accuracy of discharge simulation. The research of Yassin et al. (2017) validates that adding an objective function of comparing TWS anomaly against GRACE data reduces errors in the simulation of the total volume of streamflow.

Unlike these previous studies, Rientjes et al. (2013) argue that it remains unclear to what extent the model can reproduce the water balance of the basin by including a state variable such as TWSC in the traditional calibration approach since a state variable can only indirectly influence closure of the water balance of the hydrological model. The ETa time series estimates based on remote sensing are often used in calibrating and evaluating surface,

sub-surface, and river routing parameters, since they can indirectly incorporate the effects of water diversions, and reflect part of the effects of human activities (Muthuwatta et al., 2009; Rajib, Evenson, Golden, & Lane, 2018). The authors use a preference-based multi-variable objective function weighted for streamflow and SEBS-ETa for parameter estimation with Monte Carlo Simulation (MCS). Their results are satisfactory for both terms (better than those on single-variable calibration). Similarly, Muthuwatta et al. (2009) present in their study a stable calibration approach using observed streamflow data and remotely sensed ETa time series estimates from Moderate Resolution Imaging Spectroradiometer (MODIS) carried out with MCS.

In addition to the above two water budget components, precipitation is also essential, since it is a vital input for hydrological models. Many surveys state the deficient ability of remote sensing rainfall estimates, compared to rain gauge measurements, since uncertainties associated with them lead to severe non-linear propagation of errors affecting discharge simulation (Falck, Maggioni, Tomasella, Vila, & Diniz, 2015). Thus, errors in satellite remote sensing precipitation need to be quantified and, if possible, removed ahead of time. The use of remotely sensed streamflow estimates in hydrological modeling directly seems to be plausible (e.g., Hiep et al., 2018), but the information contained in them may not properly bring the evolution of vertical fluxes at various temporal and spatial scales within the basins to researchers (Rajib et al., 2018).

Theoretically, some calibration approaches using data from satellite products can be applied and investigated with or without limited in-situ ground hydro-meteorological data (ungauged areas), to estimate streamflow and to improve the understanding of the hydrological processes (López, Sutanudjaja, Schellekens, Sterk, & Bierkens, 2017). Some of the previous studies arrive at positive conclusions regarding the effects on streamflow simulations from incorporating satellite remote sensing data for model calibration. For example, in the study of Zaitchik, Rodell, and Olivera (2008) and Forman, Reichle, and Rodell (2012), assimilation of GRACE-derived TWS anomalies by using an ensemble Kalman smoother leads to a slight improvement in runoff simulation, and a significant improvement in groundwater simulation. Immerzeel and Droogers (2008) validate the method of using satellite-derived ETa, based on the Surface Energy Balance Algorithm (SEBAL), as a data source for calibrating the process-based hydrological model Soil and Water Assessment Tool (SWAT). However, there are also negative results reported. As is mentioned in the research of Bai et al. (2018), the calibration of hydrological models using GRACE data alone cannot improve the runoff simulations compared with the simple parameter estimates. The primary reason could be that model calibration using GRACE-derived TWS data, which is a state variable, alone improves the parameterization associated with state variables, but cannot improve the parameterization associated with runoff generation and/or routing. In the study of Rientjes et al. (2013), simulation of discharge by using the HBV model calibrated on only remote-sensed ETa results in low performances, because a small error in ETa can cause a relatively large error in discharge, due to the large difference in their volumes.

As stated above, calibration using time series of only one variable can result in incorrect parameterization (i.e., successful reproduction of discharge, but a mismatch of ET and water storage), yet model calibration and evaluation by remote sensing data of multiple variables can also be an option. For instance, López et al. (2017) represent a multi-objective calibration approach that uses a step-wise calibration scheme that attempts to combine the advantages of calibration respectively using satellite time series of actual evaporation and surface soil

moisture. They first adjust all the model parameters on satellite actual evapotranspiration (ETa) and hold constant those that can be clearly identified. The remaining parameters are then calibrated using surface soil moisture. A model calibrated on the two variables achieves a better streamflow simulation performance than using a single one of them. Tian et al. (2017) jointly assimilate GRACE-derived TWS and soil moisture satellite retrievals. The joint assimilation results in better estimates of water storage, groundwater, and surface soil moisture.

Apart from these studies, parameters of hydrological models for basins with spatially sparse and limited ground observation are usually estimated by using regional information. Since the most commonly used hydrological models are conceptual or partly conceptual models, with a clear physical basis, one can assume basins with similar characteristics have similar hydrological behavior and thus can be modeled with similar parameters (Bardossy, 2007). Therefore, hydrological regionalization can be used to transfer model parameter information from gauged (donor) to ungauged basins. For example, Bock et al. (2016) achieve satisfying simulation results in low and median flows across the conterminous United States.

In a nutshell, conventional approaches have a great dependence on the in-situ measurement of streamflow, so its application and effects in poorly gauged areas are severely restricted. Incorporating satellite remote sensing time series of hydrological components together with the runoff observations in the calibration of the water balance model reveals the potential of remote sensing data to improve the understanding of water cycle processes within the basin. Hence, using remote sensing time series of variables like TWSC for model parametrization seems to be a useful alternative in ungauged basins, but the simulation effects of other variables (e.g., streamflow, groundwater) can be either positive or negative.

1-4 Methods for data and model error correction

Despite some success in improving the model performance, the uncertainties in remote sensing data are a limiting factor in their utility for parameter estimation (Yassin et al., 2017). To make use of remote sensing data, unknown errors and bias in data of all balance components precipitation, evapotranspiration, river discharge, and water storage change - need to be quantified and, if possible, removed. One popular error estimation technique is to consider in-situ measurements as relatively accurate and use them as a reference (ground-truth). Sheffield, Ferguson, Troy, Wood, and McCabe (2009) evaluate each of the remotely sensed datasets against observations and off-line data, and atmospheric reanalysis data. Moreira et al. (2019) evaluate uncertainties in precipitation and evapotranspiration with in situ measurements of rain-gauge stations and eddy covariance (EC) sites, respectively. Instead of using a single measurement dataset, it is also feasible to merge multiple non-satellite products for each water budget component, and the non-satellite merged products are assumed to represent the best estimates of each budget term (Sahoo et al., 2011). For example, Sahoo et al. (2011) merge multiple non-satellite products for P and ET by taking their mean. Then they merge all the satellite data to produce a single satellite-only data product for P and ET respectively. The merged products are generated for P and ET by combining the four P and four ET products using weighted values based on their errors with respect to the non-satellite merged products. Another approach is to create a reference dataset using the water budget equation. Moreira et al. (2019) use remote sensing data to calculate the TWSC as a residual of the

simplified water balance equation. They also investigate the difference between the TWSC from the GRACE and the remote sensing water balance.

Without requiring a reference as the true value, an alternative idea to estimate the total water budget from satellite data is to build an ensemble of datasets for the same component. To estimate ET uncertainties, Long, Longuevergne, and Scanlon (2014) use the three-cornered hat method, which does not need a priori knowledge of the true ET value. Y. Zhang et al. (2018) use a constrained Kalman filter data assimilation method under the assumption that they can utilize the deviation from the ensemble means of all data sources for the same water balance flux as a proxy of the uncertainty in individual water balance fluxes.

Another point worth noting is what hydrological variables are considered in studies. Some previous studies only work on the estimation of bias and random errors of one component (e.g., Wei (2017) only considers uncertainty in precipitation data aiming at finding out the influence of uncertainty on model performance.). Many other studies investigate three components of the water balance equation (e.g., Sheffield et al., 2009; Azarderakhsh, Rossow, Papa, Norouzi, and Khanbilvardi, 2011). This helps to account for the interactions between errors in individual water balance components.

Moreover, the estimation of water resource availability at the basin scale requires modeling of all variables of the hydrological system (Abera, Formetta, Borga, & Rigon, 2017). The imperfect model structure can lead to uncertainties as well. First, the conceptual model is just a simňpliňfied rep-reňsenňtaňtion of the natural complex water cycle processes with a limited number of parameters and equations, which cannot completely reflect the temporal and spatial complexity of a river basin. For example, there may be empirical model parameters that are not able to depict the truth comprehensively. The hydrological scale and the time-invariant nature of model parameters also directly affect the uncertainty of the model structure. The former problem can happen if applying the equations and laws of the water cycle obtained from small-scale experimental research to the spatial and temporal scale of an actual watershed. The latter problem is even apparent in catchments where the condition of the substrate changes significantly due to the change of vegetation, the behaviors of animals and human beings, etc. For example, traditional models with time-invariant parameters can consider the direct influence of vegetation on hydrological processes; but it is hard for them to take into account the indirect dynamic effects caused by the change of vegetation (Yu, 2015). Such model simplifications may further limit its ability to accurately represent actual hydrological mechanisms and processes (Wei, 2017).

1-5 Research questions

The long-term goal of the research is to fully benefit from satellite products of the terrestrial water cycle and to conduct good water balance simulations in ungauged watersheds. The hypothesis here is that such ungauged prediction requires both accurate satellite data and a reliable model structure.

The current study aims to answer the following research questions:

1. How large are water balance data errors and to what extent can they be reduced?
2. How large are water balance model errors and to what extent can they be reduced?

3. To what extent does quantifying and reducing data and model errors eliminate trade-offs in fitting multiple datasets?

1-6 Thesis structure

The remainder of the thesis will be set out as follows. Chapter 2 introduces the river basin and data used in the study, as well as the monthly Wapaba rainfall-runoff model. Chapter 3 describes the methodology used for answering the research questions. The results are presented and evaluated in Chapter 4, followed by a discussion in Chapter 5 that uses the results from Chapter 4 to answer the research questions. Finally, conclusions and prospects for further study are presented in Chapter 6.

Chapter 2

Case study

This chapter introduces the study area and datasets of all variables used for modelling. Then, the principle of the chosen model is illustrated.

2-1 Study Area

The scale of data used, as well as the avoidance of inference with hydrological conditions, should be taken into account in study basin selection. The proposed method is tested using a single basin, Smoky Hill River, Kansas, United States.

Figure 2-1 presents the location of the basin. The western half of Kansas has exposures of Cretaceous through sediments, indicating a medium or low permeability of the stratum. This is consistent with the geologic map in Figure 2-2, which makes it manifest that there is a considerable amount of silt, siltstone and claystone in the stratum. The basin area is about 49592.23 km^2. It has the Solomon River and the Saline River as its major tributaries (see Figure 2-3). The latitude and longitude of the gauge station are respectively 38°54′23" and 97°07′03". According to USGS ("USGS 06877600 SMOKY HILL R AT ENTERPRISE, KS. USGS Water Resources", n.d.), the mean flow of Smoky Hill River at Enterprise is about 1449 cubic feet per second.

On the authority of the Kansas Department of Health Environment ("SMOKY-SALINE RIVER BASIN TOTAL MAXIMUM DAILY LOAD", n.d.), the flow condition of the study area has such seasonal features that the lowest flows appear in winter (December to January), while spring and summer (generally April to August) see its highest flows. The peak streamflow appearance time is not fixed, generally between March and September (see Figure A-1 in **Appendix A**). Precipitation and runoff events make high flow events influential to flows in the spring and summer to fall time.

Depending on the satellite products, the annual mean precipitation and potential evapotranspiration are 640 mm and 550 mm. Using the standard provided by CPGPRC ("Climate", 2013), this area is semi-humid. Dominated by a typical Midwest climate, it is very hot in

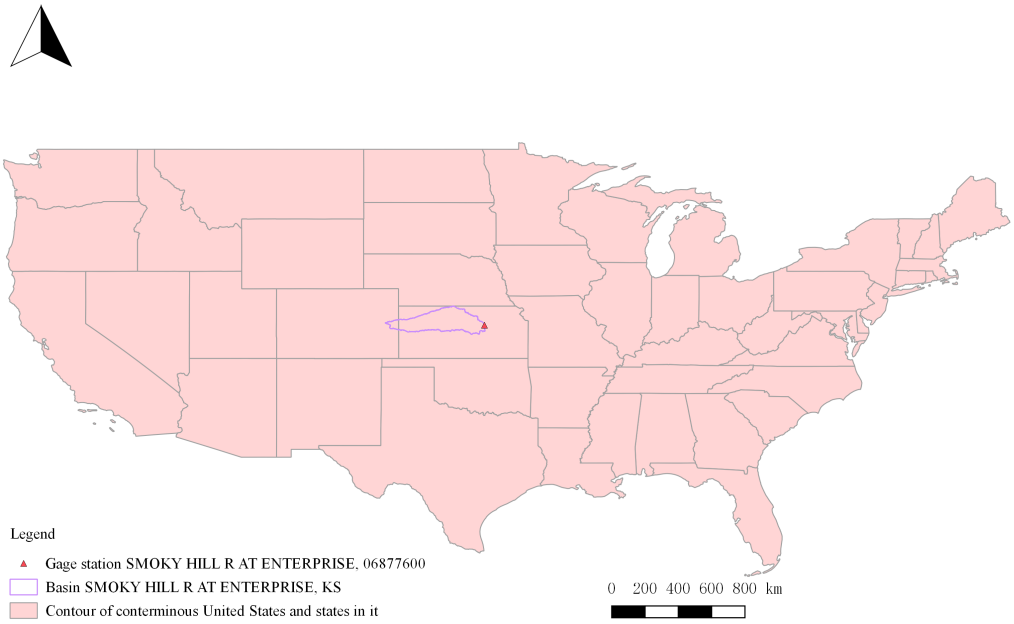

Figure 2-1: The location of the catchment Smoky Hill River at Enterprise. *Note. The Contour of conterminous United States is derived from "US Census Bureau." (2021, October 8).*

summer and cold in the wintertime. In the western part of Smoky hill river basin, the annual average snowfall period is shorter than 20 days, and the annual snowfall is less than 90cm. In the eastern part, the annual snowfall is about 40cm and lasts about 10 days ("NOAAs 19812010 Climate Normals. (n.d.)", n.d.). Although there are minor or moderate spring floods (Hadachek, 2019), snowmelt is not an essential source of streamflow.

This basin lies in the Central Great Plains ecoregion. Compared with other ecoregions, this ecoregion is less impacted by human alteration on hydrologic conditions (Falcone, 2011). The area is distinguished from the adjacent ones by its climate and vegetation. The relatively warmer temperature gives vegetations in Central Great Plains, which are usually grasses, a longer growing period. Shrubs or trees are rare in this area. The most productive crops in this area are winter wheat, sorghum and corn. The primary live stocks are cattle, cow and hog ("USDAs National Agricultural Statistics Service Kansas Field Office (Part of the Northern Plains Regional Field Office)", 2021, September 15). Drought, grazing by animals, and fire are local main disturbance regimes (Chaplin, Cook, Dinerstein, Simms, & Carney, n.d.).

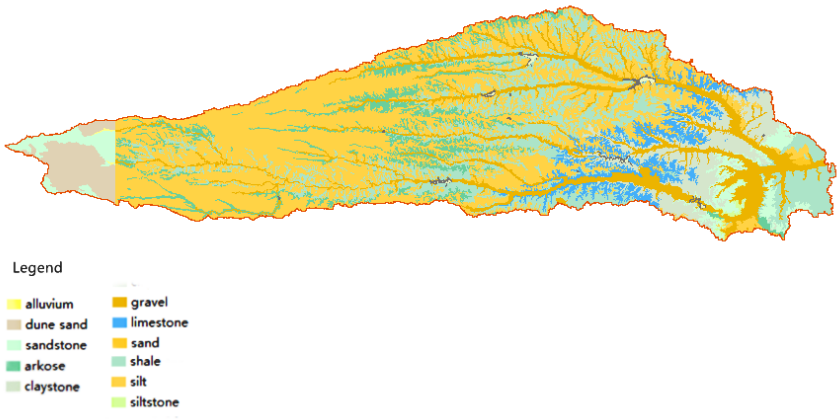

Figure 2-2: The geologic map of the study catchment. *Note. The geologic map is adapted from Geological map of Kansas (Ross, 1992) and Colorado (Green, 1992). The vertical line in the graph is the dividing line between the two states (left Colorado and right Kansas)*

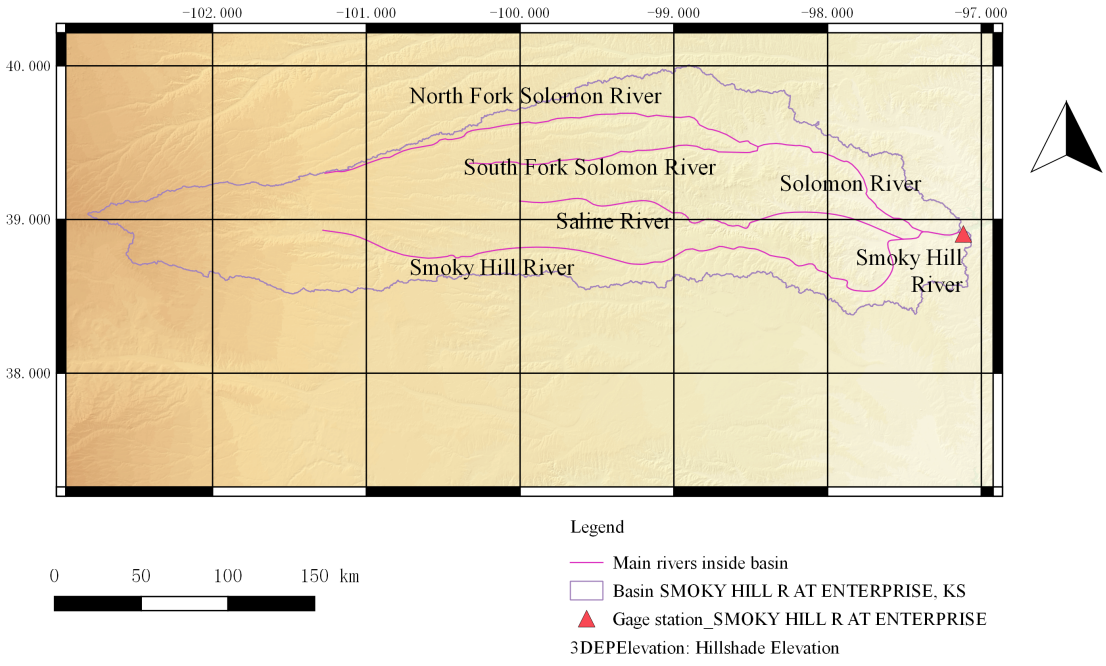

Figure 2-3: The topographic map of the basin with the location of rivers and of the gauge station. *Note. The shapefile of North American rivers is provided by the Natural Earth, Hillshade elevation is provided by "U.S. Geological Survey" (20180618) and the states shapefile (7/21/2015) is derived from ArcGIS Hub.*

Table 2-1: Monthly water balance data

Variable	Symbol	Data source	Resolution	Reference
Precipitation	$Pobs1$	CHIRPS v2.0	0.05°	Funk et al. (2015)
	$Pobs2$	PRISM	4 km	"PRISM Climate Group" (2021)
Evaporation	$Eobs1$	SSEBop v5	1km	Senay and Kagone (2019)
	$Eobs2$	GLEAM v3.5b	0.25°	Miralles et al. (2011)
	Ep			
Water storage	$Sobs$	GRACE	3°	Watkins, Wiese, Yuan, Boening, and Landerer (2015); Wiese, Landerer, and Watkins (2016); Wiese, Yuan, Boening, Landerer, and Watkins (2018); and Landerer et al. (2020)
River discharge	Q	Stream gauges	Basin	"USGS 06877600 SMOKY HILL R AT ENTERPRISE, KS. USGS Water Resources" (2021)

2-2 Monthly water balance data

This section first introduces data sources and the version used in the study. Further information on missing data and data pre-processing is included.

2-2-1 Overview

For the research, two categories of data need to be collected: data utilized as model inputs, and data utilized for the evaluation of model simulation effects. The monthly water balance data collected are summarized in Table 2.1 according to different water balance components. All data are monthly spatially average values over the study basin. Their sources and other information are stated in **sections 2.2.2** to **2.2.5**. This research has been based on monthly data over the period of January 2003 to July 2020.

2-2-2 Precipitation time series

Two monthly precipitation products are employed. The $Pobs1$ and associated standard errors are provided by CHIRPS, which is a 35 more-year quasi-global rainfall dataset (Funk et al., 2015). The unit for CHIRPS is mm per month in this case.

For the remediation of errors and bias in CHIRPS, another precipitation dataset, denoted as $Pobs2$, is included. The $Pobs2$ in Table 2-1 is PRISM Spatial Climate Dataset (in mm), contributing monthly precipitation values for the data fusion. The PRISM climate data are observed from a wide variety of monitoring networks by "PRISM Climate Group" (2021), Oregon State University, http://prism.oregonstate.edu, created 12 June 2021. The resulting datasets incorporate an extensive range of modeling techniques and are available based on monthly modeling.

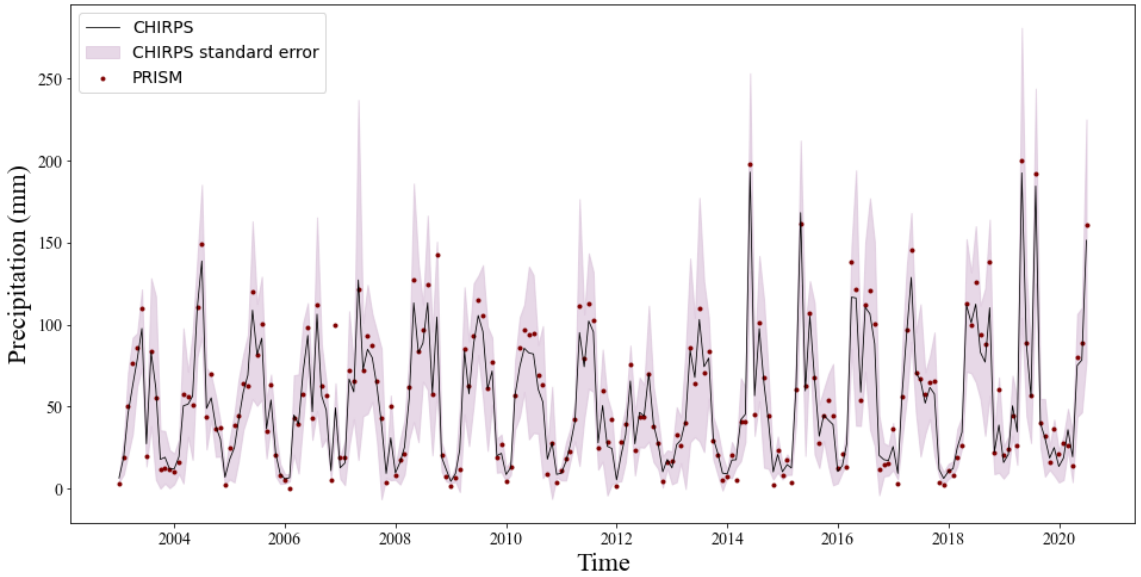

Figure 2-4: Monthly precipitation data for Smoky Hill River at Enterprise during Jan 2003-July 2020. *Note. The longitudinal coordinate precipitation represents the monthly water flux of precipitation and is expressed in depth of water (in this study, mm). The CHIRPS data incorporates standard deviation and a 90% uncertainty band is shown.*

The two datasets are shown in Figure 2-4. They both tend to give higher precipitation in summer to autumn and lower precipitation in winter times.

2-2-3 Evaporation time series

For the determination of errors in evapotranspiration, GLEAM and SSEBop remote sensing products are incorporated. Both datasets are provided in millimeters.

Evapotranspiration is under most conditions considered as the combination of vegetation transpiration, soil surface evaporation and canopy interception loss. The first remote sensing evapotranspiration time series used in the study $Eobs1$ is calculated utilizing the Operational Simplified Surface Energy Balance (SSEBop) model. The Simplified Surface Energy Balance technique, which has specific parameterization for operational applications, is used to build SSEBop. With a thermal index method, it combines ET fractions generated from remotely sensed MODIS thermal imagery with reference ET (Senay & Kagone, 2019). As is shown in Table 2-1, version 5 of the dataset is used and the unit is millimeter.

The Global Land Evaporation Amsterdam Model (GLEAM) is a collection of algorithms that estimate the various components of evapotranspiration independently (Martens et al., 2017; Miralles et al., 2011). The actual evaporation used for the study is denoted as $Eobs2$. The potential ET (including interception loss Ei) provided by GLEAM is denoted as Ep, and is used in the water balance model as an input. Both actual and potential evaporation are in the unit of millimeter per month. For further calculation, units of their fluxes are changed into millimeter.

2-2-4 Terrestrial water storage

GRACE Tellus Monthly Mass Grids provides monthly gravitational anomalies and its symbol is *Sobs*. The dataset is available at: https://podaac-tools.jpl.nasa.gov/drive/files/allData/tellus/L3/gracefo/land_mass/RL06/. The benchmark for the anomaly of terrestrial water storage change is the mean value of January 2004 to December 2010. The anomalies of GRACE-derived TWS data are produced by the Center for Space Research (CSR) at the University of Texas at Austin, as are scaled by the NASA Jet Propulsion Laboratory (JPL).

The data contained in this dataset are units of "Equivalent Water Thickness", which represent mass deviations with regard to the vertical extent of water (in cm and is converted to mm). The *Sobs* contains soil water store and remaining water in groundwater storage. During the simulation period, many data are missing, and the record index indicating data conditions are presented in **Appendix A**.

2-2-5 Discharge time series

The monthly streamflow time series for the study catchments from January 2003 to July 2020 used in the study are the USGS Water Data for the Nation, and the River basin Water Resource Maps and GIS Data is vector digital data GAGES-II: Geospatial Attributes of Gages for Evaluating Streamflow. They are provided by James Falcone, U.S. Geological Survey, Reston, Virginia. The original unit of data provided in cubic feet per second. The chosen time series contains a very dry year (2012) and a very wet year (2019). The original unit of the provided discharge time series is cubic feet per second. For the simulation and comparison, the discharge is expressed in water depth and the unit is converted into millimeter.

2-3 Monthly water balance model

In this section, a five-parameter lumped model is chosen. By using a lumped model, water resources can be estimated without using spatially distributed information. The Water Partition and Balance (Wapaba) monthly hydrological model evolved from the Budyko strategy (L. Zhang, Potter, Hickel, Zhang, & Shao, 2008). The Wapaba model has been validated in many river basins in Australia, Colombia and East-African (Muvundja et al., 2014; Wang et al., 2011). It is suitable for a variety of climatical and hydrological conditions, e.g., tropical, arid, and temperate (John, Fowler, Nathan, Horne, & Stewardson, 2021). According to the research of Bennett and Wang (2017), conceptual models of similar complexity to the Wapaba model perform correctly in the ungauged areas. Thus, under the rational assumption, the Wapaba model can produce analogously acceptable results in catchments without observation.

The model takes in five parameters and two conceptual storages and requires monthly rainfall and potential evapotranspiration as inputs (Li, Wang, & Bennett, 2013). The structure of the Wapaba model is provided in Figure 2-5. The core of the Wapaba model is the use of the consumption curve, as it controls the partitioning among water supply, demand and consumption. Table 2-2 gives the prior bounds of parameters.

The first parameter α_1 depicts the catchment consumption curve. The higher α_1 the less direct runoff there is in the catchment. Moreover, with a higher α_1, the flow will be smoothed and delayed. The evaporative efficiency can be raised with a high value of α_2, which describes the shape of the evapotranspiration curve. The proportion of catchment yield as groundwater is denoted as β. Given a higher value, the recharge rate is faster, suggesting the greater importance of baseflow. Parameter K is a constant of groundwater store time. It is pretty influential to groundwater discharge rate. Flow can be smoothed and delayed if K is very small. The maximum water holding capacity of soil store is denoted as S_{max}. With a high S_{max} value, the hydrograph has longer memory and larger soil moisture (Pagano, Hapuarachchi, & Wang, 2009). Besides, as mentioned by LIU and ZHANG (2006), initial water content has a significant effect on the accuracy of flood simulation. Hence, the initial soil water store So and the initial groundwater store Go are both taken as initial state parameters.

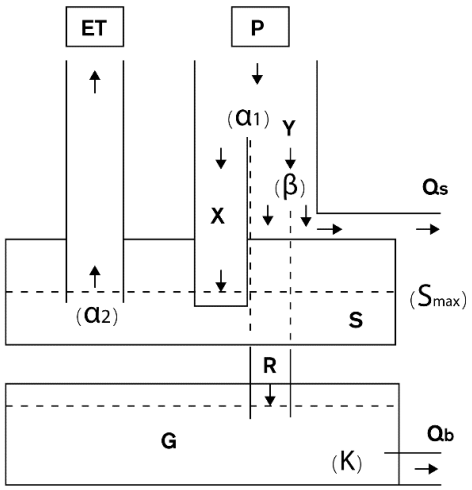

Figure 2-5: Water partitions in the Wapaba model. *Note. From Monthly versus daily water balance models in simulating monthly runoff, by Wang et al., 2011, p. 167, Figure 1. Copyright 2010 Elsevier.*

The collection of the model parameters can be represented as $\theta_w = \{\alpha_1, \alpha_2, \beta, K, S_{max}\}$.

The model takes into account the actual evapotranspiration, soil water storage, baseflow, and surface flow fluxes. Consistent with **section 2.2**, the study converts precipitation, evapotranspiration and river discharge over a month into monthly water fluxes. Therefore, all water fluxes, as well as water storage volumes within a month, are expressed in vertical extent of water. The unit is thus millimeter. Model calculation stages are as follows:

1. The consumption curves are adopted in the model to partition water into various components using the pre-requisite that water supply and demand are accessible. Wapaba model first partitions the total rainfall P(t) (mm month-1) into catchment water consumption X(t) (mm month-1) and catchment water yield Y(t) (mm month-1). This process examines the temporal and spatial heterogeneity of the catchment process (Pokhrel, Robertson, & Wang, 2013).

Table 2-2: Wapaba model parameters

Parameter [Unit]	Lower Bound	Upper Bound
α_1[-]	1	10
α_2[-]	1	10
β[-]	0	1
K[days]	1	3650
S_{max}[mm]	5	1000
S_0[mm]	0	S_{max}
G_0[mm]	0	-

Note. Adapted from Accounting for seasonal dependence in hydrological model errors and prediction uncertainty, by Li et al., 2013, p. 5916, Table 1. Copyright 2013, AGU.

The rainfall which replenishes the soil water store and returns to the atmosphere through evapotranspiration forms the catchment water consumption, while the water yield Y(t) is the remaining rainfall after the catchment water consumption in the catchment.

Catchment water consumption is given by

$$X\left(t\right) = X_0\left(t\right) F\left(\frac{P\left(t\right)}{x_0\left(t\right)}, \alpha_1\right) \tag{2-1}$$

in which parameter α_1 is the catchment consumption curve parameter, F(x) represents the consumption curves as follow:

$$\left(\frac{Consumption}{Demand}\right) = F\left(\frac{Supply}{Demand}, \alpha\right) = \ 1 \ + \frac{Supply}{Demand} - \ \left[1 + \left(\frac{Supply}{Demand}\right)^a\right]^{1/\alpha} \tag{2-2}$$

The catchment water consumption potential X0(t) is calculated as

$$X_0\left(t\right) = S_{max} - \ S\left(t-1\right) + \ ET_0\left(t\right) \tag{2-3}$$

in which S_{max} (mm) is the maximum soil water holding capacity in the catchment, taken as a parameter; $S\left(t-1\right)$ represents water remaining in the soil water store at the beginning of period t and $ET_0\left(t\right)$ (mm month-1) is the potential evapotranspiration.

The other partitioned component, catchment water yield, is given by

$$Y\left(t\right) = P\left(t\right) - X\left(t\right) \tag{2-4}$$

2. Total water available for evapotranspiration W(t) (mm month-1) comprises actual evapotranspiration ET(t) (mm month-1).

$$W\left(t\right) = S\left(t-1\right) + X\left(t\right) \tag{2-5}$$

The actual evapotranspiration is given by

$$ET\left(t\right) = ET_0\left(t\right) F\left(\frac{w\left(t\right)}{ET_0\left(t\right)}, \ \alpha_2\right) \tag{2-6}$$

in which parameter α_2 is the evapotranspiration curve coefficient.

Water storage in the soil water at the end of t is given by

$$S(t) = W(t) - ET(t) \tag{2-7}$$

3. The catchment water yield is partitioned into water that replenishes the groundwater store R(t) (mm month-1) and surface runoff Qs(t) (mm month-1).

$$R(t) = \beta\ Y(t) \tag{2-8}$$

$$Q_S(t) = Y(t) - R(t) \tag{2-9}$$

in which β is the proportion of the catchment water yield as groundwater.

4. The groundwater store is drained to produce base flow $Q_b(t)$ (mm month-1), which is given by

$$Q_b(t) = G(t-1)\left(1 - e^{-TK}\right) + R(t)\left(1 - \left(\frac{K}{T}\right)\left(1 - e^{-Tk}\right)\right) \tag{2-10}$$

in which T is the length of time step t (in the same time unit as the groundwater store time constant K, days in this study). Since there is not enough data-based evidence for the store time, K is calibrated as a model parameter. The base flow refers to the amount of infiltrated groundwater that returns to the surface (Muvundja et al., 2014).

Therefore, the remaining water storage in the groundwater $G(t)$ (mm) is

$$G(t) = G(t-1) + R(t)\ Qbt \tag{2-11}$$

Next, water storage in the soil water and the groundwater should be added to derive the total terrestrial water storage:

$$TWS(t) = S(t) + G(t) \tag{2-12}$$

5. The total monthly flow Q(t) is obtained by adding surface runoff and base flow

$$Q(t) = Q_S(t) + Q_b(t) \tag{2-13}$$

Chapter 3

Methodology

This section provides details on the three main steps of the methodology (see Figure 3-1). Different types of errors in the conceptual monthly water balance model are analyzed and reduced.

Corresponding to the three goals outlined above, the methodology, as shown in Figure 3.1, is divided into three parts. The first part investigates the effectiveness of quantifying and reducing errors in satellite data. Then, the model error impact and its solution are analyzed in the second part. In the final part, the improved strategy is tested.

In the phase of evaluation of the strategy, the original model and unprocessed satellite data are used for the simulation of the discharge first (Scenario 1 in Figure 3-2). In Scenario 2, the study calibrates the original model with the cleaned remote sensing data (data with known uncertainty) from step 1. We compare their performances on predicting monthly runoff to test the hypothesis that the error-corrected satellite remote sensing data can make up for the deficient ground observations over the basin (Hiep et al., 2018). By correct, it means to close the water balance through a single iterative approach for the estimation of a consistent set of data errors and hydrological variables. Then, Scenario 3 simulates the discharge using corrected inputs together with the model from step 2 to see if it can prove the benefit of the structurally enhanced model. By comparing the results of doing this with or without the correction for data errors and flawed model structure, their effectiveness and practicability in variable simulation and discharge prediction in catchments with limited ground observations can be confirmed. Therefore, the results of the study are expected to be a contribution to predictions in areas with insufficient discharge measurement.

3-1 Quantifying and reducing data errors using data fusion

In the first stage, the study focuses on errors in remote sensing data and in-situ observation of discharge. To study the uncertainty of all hydrological variables comprehensively, we work on the water balance closure, which is feasible due to the increasing availability of remote sensing products for components of the terrestrial water cycle (Sheffield et al., 2009). Recent

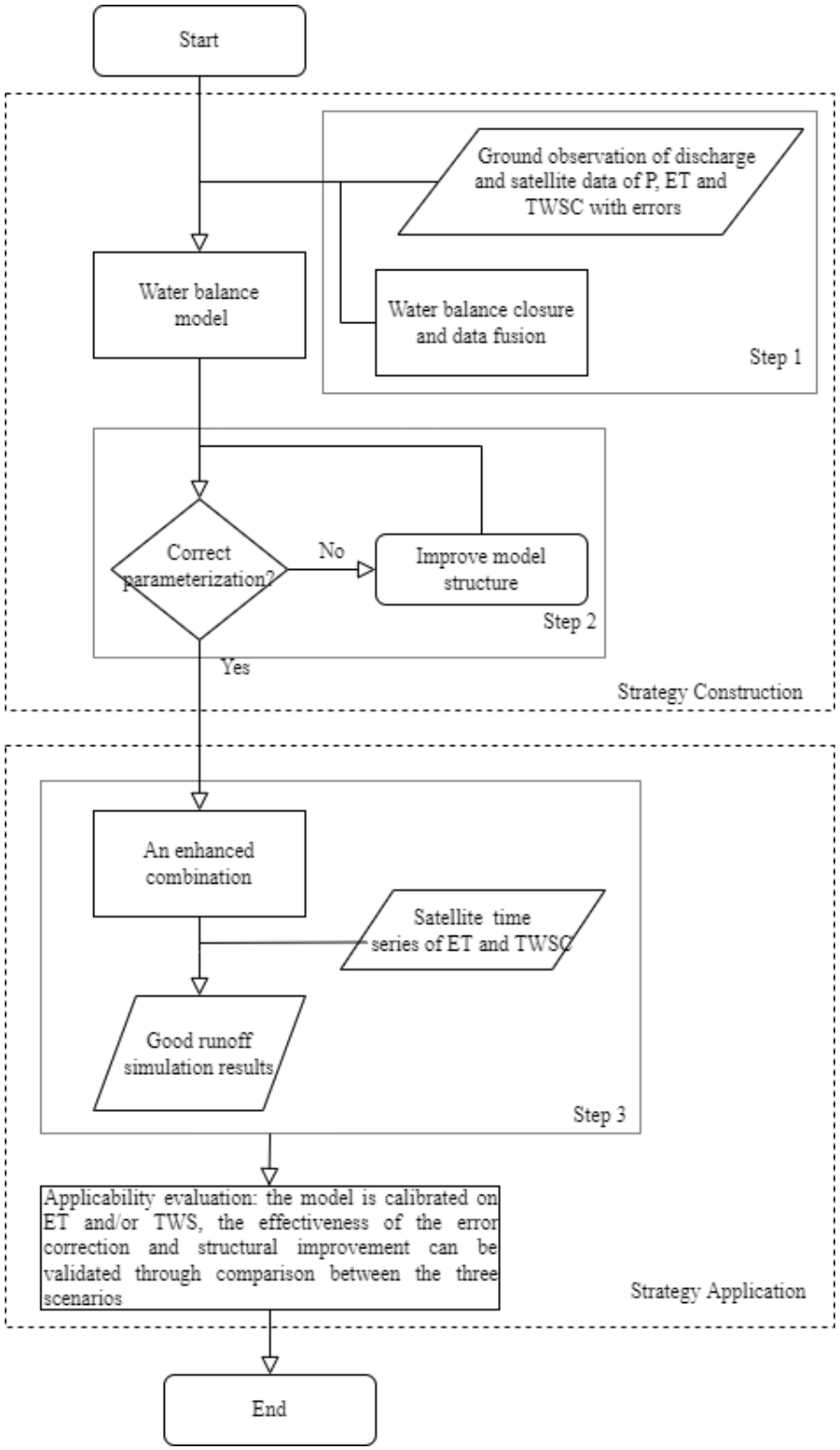

Figure 3-1: Logic flowchart of the study

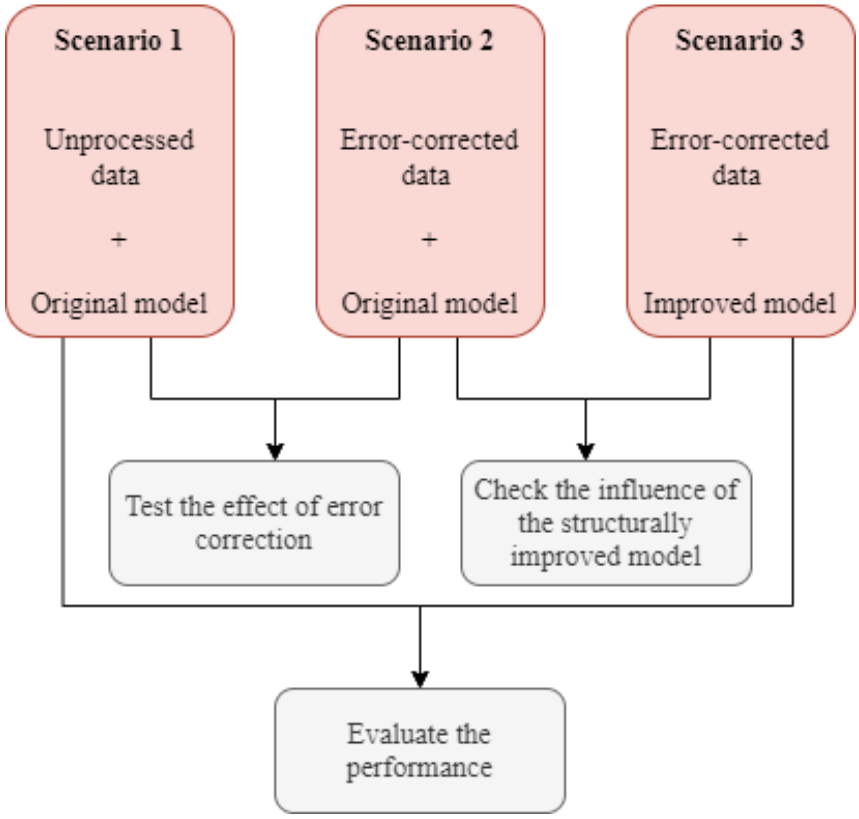

Figure 3-2: Comparing different scenarios to assess the effects of data and model errors

error estimation and data fusion methodology proposed by Schoups and Nasseri (2020) will be used for automatically cleaning water balance datasets. Monthly water balance variables for every month are taken as inputs, they were spatially averaged so as to derive basin-scale data values. Barely can true values that can be employed as a reference for bias and random data errors estimation be discovered, because no dataset or estimate is excused of errors. For this cause, the water balance fusion and error estimation method does not assume a reference dataset. Instead, it assumes every water balance variable as subject to unrevealed bias and errors. Subsequently, an internally consistent set of data errors and values of variables that can close water balance needs finding. This goal is achieved through a single iterative scheme (Schoups & Nasseri, 2020).

This scheme combines the error estimation and water balance fusion processes into an integrated methodology: it first uses a single iterative method which forms data error models for every water balance component with a probabilistic model that can be used for the amalgamation of water balance constraints. Next, the results from the former step are processed with Markov Chain Monte Carlo sampling and an iterative form of Kalman smoothing. In so doing, all accessible information can be fused together in order to produce optimized estimates with uncertainty for all hydrological components as well as error parameters. The output of the methodology is a distribution that gives the mean value and the standard deviation of every water balance variable (Schoups & Nasseri, 2020). Hence, it provides an estimated value and the uncertainty of each variable for each month.

After this, data used in the model (i.e., precipitation as input, river discharge, evapotranspiration, and water storage for calibration) are anticipated to be error-filtered and bias-corrected and they lead to a satisfactory water balance closure.

3-2 Quantifying and reducing model errors using model calibration and evaluation

This section argues the method used to examine errors brought by model structure. It first provides the method to demonstrate the effectiveness of data fusion in hydrological modelling. Next, after eliminating the interference of data error, the error still displayed in the simulation results is the model structure error. This error, then, is quantified and reduced. This section also elaborates on objective functions used for each step.

3-2-1 Calibration scheme

To conduct the parameter calibration and to display the outcomes, several additional parameters are incorporated (see Table 3-1). The first research question focuses on data errors, in which model input error is of vital significance (see Figure 3-3). To take into account errors in model inputs, the model treats precipitation in each month individually as a parameter. The bound of each P_t is $(\mu - 3SD,\ \ \mu + 3SD)$, in which μ and SD are the mean value and standard deviation of P given by data fusion. This range can include 99.73% of the possible actual P and is considered enough for this study.

Besides, it is assumed that the model error for each variable is independent and identically distributed according to a normal distribution with an estimated variance σ^2. The model error indicators for the simulation forced by the raw data from the two satellite products on discharge (Scenario 1) are denoted as σ_{prism} and σ_{chirps}. When using error-corrected data, model errors for discharge, ETa and TWSA are σ_Q, σ_E and σ_S.

In addition, when comparing modeled TWS with GRACE data or calibrating on water storage, the transform parameter M needs to be introduced. Since GRACE data are a series of deviations of observations from a reference period (anomalies), the modeled water storage cannot be compared with it directly. Instead, M is subtracted for each simulated value over the entire time series to convert it into anomalies. For the former case, M is set in such a way that the modeled TWS in the first month is equal to the GRACE mean value. For the latter case, parameter M is calibrated to make its objective function reach the optimal value. In this case, parameter M also makes the simulated value not much different from the observed value in the first month (due to a relatively low σ_S brought by the optimal objective function). These additional parameters are found through the same joint calibration approach as other parameters.

According to scenarios in Figure 3.2, the research set up the following steps.

Step a. To force the Wapaba model with data from the two satellite products, respectively. The reproductions of TWSA and ETa are also given.

Step b. To use the error-corrected precipitation time series and GLEAM potential evapotranspiration to force the Wapaba model. This step can be divided into two sub-steps.

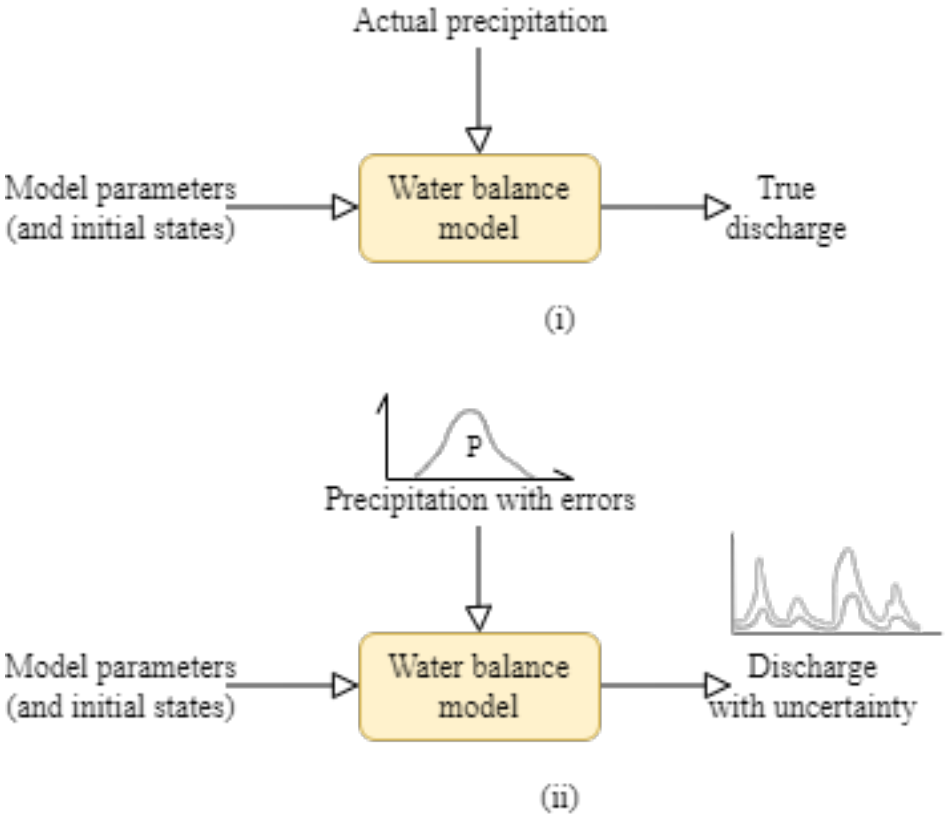

Figure 3-3: Analysis scenarios for the assessment of input uncertainties. *Note. Adapted from Investigating the impact of remotely sensed precipitation and hydrological model uncertainties on the ensemble streamflow forecasting, by Moradkhani et al. (2006), p. 3, Figure 1. Copyright 2006 by the American Geophysical Union. 0094-8276/06/2006GL026855.Analysis scenario: (i) Calibrated true, (ii) forcing data uncertainty.*

The first is to use the mean values derived from data fusion without considering precipitation uncertainty. The second is to take into account precipitation uncertainty by adding logLikelihood P in its objective function.

Then, to calibrate the parameters on solely discharge (by using logLikelihood Q as the objective function). The simulations of ETa and TWS are also required.

Step c. The study uses error-corrected data to force the chosen model and calibrate the parameters on all three fluxes to test whether the model has the ability to describe the physical process of each flux accurately.

Step d. To calibrate on actual evapotranspiration or terrestrial water storage anomalies. The obtained parameter set is denoted as θ_{ETa} or θ_{TWS}. Parameter sets θ_{ETa} or θ_{TWS} will be tested through the reproducing of other components. Next, this study calibrates model parameters on both actual evapotranspiration and terrestrial water storage anomalies. Then, it tests the parameter set using discharge simulation.

Step e and Step f. These two steps are the counterparts of Step c and Step d. The difference is that they will use improved models for simulation.

All objective functions used in the above steps are exhibited in Table 3.2. Through the

Table 3-1: Parameters for the whole calibration scheme and their bounds

Type	Parameter	Lower bound	Upper bound
Model parameter	Wapaba model parameters	See section 2.3	
Forcing data	P_t	$\max(\mu - 3SD,\ 0)$	$\mu + 3SD$
	σ_{prism}		
Model prediction error parameter	σ_{chirps}	0	$+\infty$
	σ_Q		
	σ_E		
	σ_S		
Transform parameter	M	0	1000

comparison of results from Step a and Step b, the influence of forcing data errors on streamflow prediction and the effectiveness of bias correction and error correction can be verified.

The second research question aims at adjustments in their structure that will be made to create an improved monthly water balance strategy. We investigate if there is the problem that the model produces unrealistic representations of hydrological processes over the catchment due to the limitation of parameters and equations. This can be examined first in Step b. If the model does produce unrealistic representations of hydrologic process across the watershed, a simulation of discharge does not guarantee the reliable reproduction of other hydrological components (ETa and water storage), which reveals the problem of the defective model structure (Bai et al., 2018; Muthuwatta et al., 2009; Rajib et al., 2018). This will also be studied, in Step c, by calibrating the model on all three output fluxes. The results can give a general impression of the model's ability to simulate all fluxes. The results of the simulation can yield insights about model deficiencies that are otherwise not available by using conventional methods and only in situ data (Sun et al., 2012).

One approach of the improvement is to replace the empirical model parameters, equations, or configurations of the model with physically robust ones (e.g., Qing-fang, WANGYintang, Ke-lin, and Zong-zhi, 2007) (Y. Q. Zhang, Chiew, Zhang, Leuning, & Cleugh, 2008; Jiang & Wang, 2019). Another way is to include hydrological processes ignored in the existing model (e.g., Anyan, Shenglian, Lihua, and Jing, 2008), since the systematic errors can be decreased as more hydrological processes are added to the model, which leads to an increase in its complexity (L. Zhang, Walker, & Dawes, 2002; Bai et al., 2018). After the modifications in model structure, in Step e and Step f, it is expected to produce more reliable discharge sim-

Table 3-2: Calibration scheme

	Flux(es) used for calibration	**Objective function**
Step a/Step b	Observed Q (without precipitation error or discharge measurement error)	logL (see Eq (3-4))
Step b	Q	Sub-step 1: logL (see (Eq (3-4))
		Sub-step 2: logLikelihood P + logLikelihood Q (see Eq (3.5) and (3.6))
Step c/Step e	ETa, TWSA and Q	logLikelihood P + logLikelihood E + logLikelihood S + logLikelihood Q
Step d	ETa	logLikelihood P + logLikelihood E
	TWSA	logLikelihood P + logLikelihood S
Step d/Step f	ETa and TWSA	logLikelihood P + logLikelihood E+ logLikelihood S

Note. Smybols Q, ETa and TWSA represent fluxes of discharge, actual evapotranspiration and terrestrial water storage anomalies. In step d, using only ETa or TWSA for calibration are not focal points and results are put in ***Appendix C****.*

ulation results without severe deteriorations in the accuracy of TWSA and ETa simulations compared with the original model and vice versa.

3-2-2 Objective function

Likelihood, a relative quantitative measure of model fit, is used as the objective function for parameter calibration. Higher likelihoods present higher probabilities of the model producing the observed time series. When carrying out different calibrations, different likelihood functions are employed.

1. Using unprocessed satellite data to force the model

As illustrated by Schoups (December, 2018), the main idea is to generate data to fit the measurement through a conceptual process by using a statistical model and to reason backward from the measurement to determine the parameter set that produces the generated data. More specifically, the procedures of building likelihood function for parameter calibration on discharge can be:

(1) Run the rainfall-runoff model with its parameters θ to obtain simulated runoff Q_{sim}:

$$Q_{sim} = MODEL\,(P, E_P, \theta) \tag{3-1}$$

in which P is the precipitation of the study area, E_P is the potential evapotranspiration.

(2) The generative model defines observed discharge values $Q_{obs,t}$ as a series of random draws from normal distribution depending on the modeled values $Q_{sim,\ t}$ and errors. When using raw data as model inputs, no data errors are considered. Hence, $Q_{obs,t}$ is drawing from a normal distribution with a mean value of $Q_{sim,t}$ and a standard deviation of σ indicating the hydrological model structure error:

$$Q_{obs,t} = Q_{sim,t} \ + \ \sigma z_t \tag{3-2}$$

where z_t is a normal distributed random variable and $z_t\ \mathcal{N}(0,\ 1)$.

(3) The distribution of observed discharge at time t $Q_{obs,t}$ is $\mathcal{N}\left(Q_{obs,t}|\, Q_{sim,t},\ \sigma^2\right)$. The probability L can be calculated through the product of every such distribution of every measurement:

$$L = \prod_t \mathcal{N}\left(Q_{obs,t}|\, Q_{sim,t},\ \sigma^2\right) \tag{3-3}$$

(4) Take the logarithm of both sides of the equation to obtain:

$$logL = \sum_t log\ \left(\mathcal{N}\left(Q_{obs,t}|\, Q_{sim,t},\ \ \sigma^2\right)\right) \tag{3-4}$$

in which σ is to be estimated from the data using calibration.

2. Using corrected precipitation to force the model

To further improve the model performance, the effect of uncertain forcing data should be reduced. For this purpose, a more effective series of precipitation is calibrated using an objective function incorporating log-likelihood (see Equation (3-5)) of precipitation.

$$logLikelihood\ P = \sum_t log\ \left(\mathcal{N}\left(P_{obs,t}|\, P_{sim,t},\ variance_{P,t}\right)\right) \tag{3-5}$$

where $P_{sim,t}$ for each month is calibrated as a parameter, $P_{obs,t}$ and $variance_{P,t}$ are the mean value and uncertainty of precipitation for the $t-th$ month produced by the data fusion method. 3. Using observations with errors for model calibration Similar to the first case, model prediction error of river discharge is denoted as σ_Q. Moreover, measurement errors need to be included in the likelihood function of discharge.

$$logLikelihood\ Q = \sum_t log\ \left(\mathcal{N}\left(Q_{obs,t}|\, Q_{sim,t},\ {\sigma_Q}^2 + variance_{Q,t}\right)\right) \tag{3-6}$$

where $Q_{sim,t}$ for each month is the simulation of discharge produced by the Wapaba model, $Q_{obs,t}$ and $variance_{Q,t}$ are the mean value and uncertainty of river discharge for the $t-th$ month produced by the data fusion method.

Likewise, this function can be modified for calibration on actual evapotranspiration and terrestrial water storage anomalies. The model simulation of actual evapotranspiration and terrestrial water storage anomaly are denoted as $E_{sim,t}$ and $S_{sim,t}$ for each month. Symbols σ_E and σ_S are their model structure errors. Their mean values and uncertainties for the $t-th$ month given by the data fusion method are denoted as $E_{obs,t}$, $S_{obs,t}$, $variance_{E,t}$ and $variance_{S,t}$.

As stated in the calibration scheme, from Step b to Step f combined objective functions, which are additions of log-likelihood functions of required terms, are used. When calibration on different datasets, in order to combine those single functions, weights of different terms are usually used. In this method, rather than weight, the variances in the likelihood terms are used. As mentioned before, the data variances are given by the data fusion method, and the model error variances are estimated through calibration.

The differential evolution (DE) algorithms (Storn & Price, 1997) is used to determine the optimal values for model parameters. DE is a metaheuristic search algorithm based on population that enhances a problem by iteratively developing a potential solution based on an evolutionary process (Georgioudakis & Plevris, 2020).

For the monthly water resources simulation, it is the low flow that researchers pay more attention to. Another index, the Box-Cox transformed root mean squared error (TRMSE) (equation (3-7)), can be put into service since it emphasizes model fitting during low-flow periods. As stated by P. M. d. L. Ferreira, Paz, and Bravo (2020), TRMSE can reduce the influence of heteroscedasticity in RMSE (root mean squared error) calculation. In general, a lower TRMSE is better than a higher one.

$$TRMSE = \sqrt{\frac{1}{n}\sum_{t=1}^{n}\left(\widehat{Q_{sim,\,t}} - \widehat{Q_{obs,\,t}}\right)^2} \tag{3-7}$$

$$\hat{Q} = \frac{(1+Q)^{\lambda}-1}{\lambda} \tag{3-8}$$

where n is the time step, $\widehat{Q_{sim,\,t}}$ refers to the transformed simulated discharge, $\widehat{Q_{obs,\,t}}$ is the transformed observed discharge. Following a previous study, the Box-Cox transformation coefficient λ is set at a value of 0.3, which gives a similar impact as the log transformation (Wagener, van Werkhoven, Reed, & Tang, 2009).

When considering errors in observation, the simulated discharge will be compared as the discharge mean value of each month on the basis that the uncertainty given by data fusion is small. Even so, TRMSEs disadvantage of disability in taking data uncertainty into account is still noticeable. Therefore, when simulating ETa and TWSA, who have remarkably larger uncertainty, this index is not a good reference. However, when no measurement uncertainty is considered, namely in Case a and Case b sub-step 1, TRMSE for ETa and TWSA can also be used. The calculation equation is similar to that of runoff in Eq (3-7) and (3-8).

Chapter 4

Results

This chapter illustrates and tests the outlined methodology with the study area. The data fusion is done before modeling and its effectiveness is illustrated in 4.1 and 4.2. In the following section 4.3, the results of structure modification are presented.

4-1 Data fusion

This section first presents the water balance error without correction. Then, results of data fusion are exhibited. Through comparison, part of the efficiency of the data fusion method can be illustrated before bringing in hydrological models.

4-1-1 Data fusion results

Before using datasets of hydrological variables, the water balance needs checking using Equation (4-1). Equation (4-2) is obtained by moving all terms to the left side. To allow for some computer setting and rounding errors, if the absolute value of the left side is smaller than 10^{-5}, it is believed that the water balance is closed.

$$S_t = S_{t-1} + P_t - E_t - Q_t \tag{4-1}$$

$$S_t - S_{t-1} - P_t + E_t + Q_t = 0 \tag{4-2}$$

in which S_{t-1} and S_t refer to total terrestrial water storage in the study area at the start and end of the $t-th$ month, P_t and E_t are basin-averaged precipitation and evapotranspiration in the $t-th$ month, and Q_t represents the river runoff at the basin outlet.

Figure 4-1 exhibits the results of water balance checking on original satellite data. First of all, in both graphs, there are missing points caused by missing values of one or more variables

(in this case, TWSA). This phenomenon reduces datasets' feasibility, although most of the other time series is long enough and of better quality. Secondly, errors in the two graphs are apparently beyond the acceptable threshold. In Graph (a), the maximal and the minimal errors are 47.40 and -110.20. In Graph (b), the maximal and the minimal errors are 95.83 and -67.89, far beyond the threshold. Therefore, original datasets do not close the water balance in the study area in both cases.

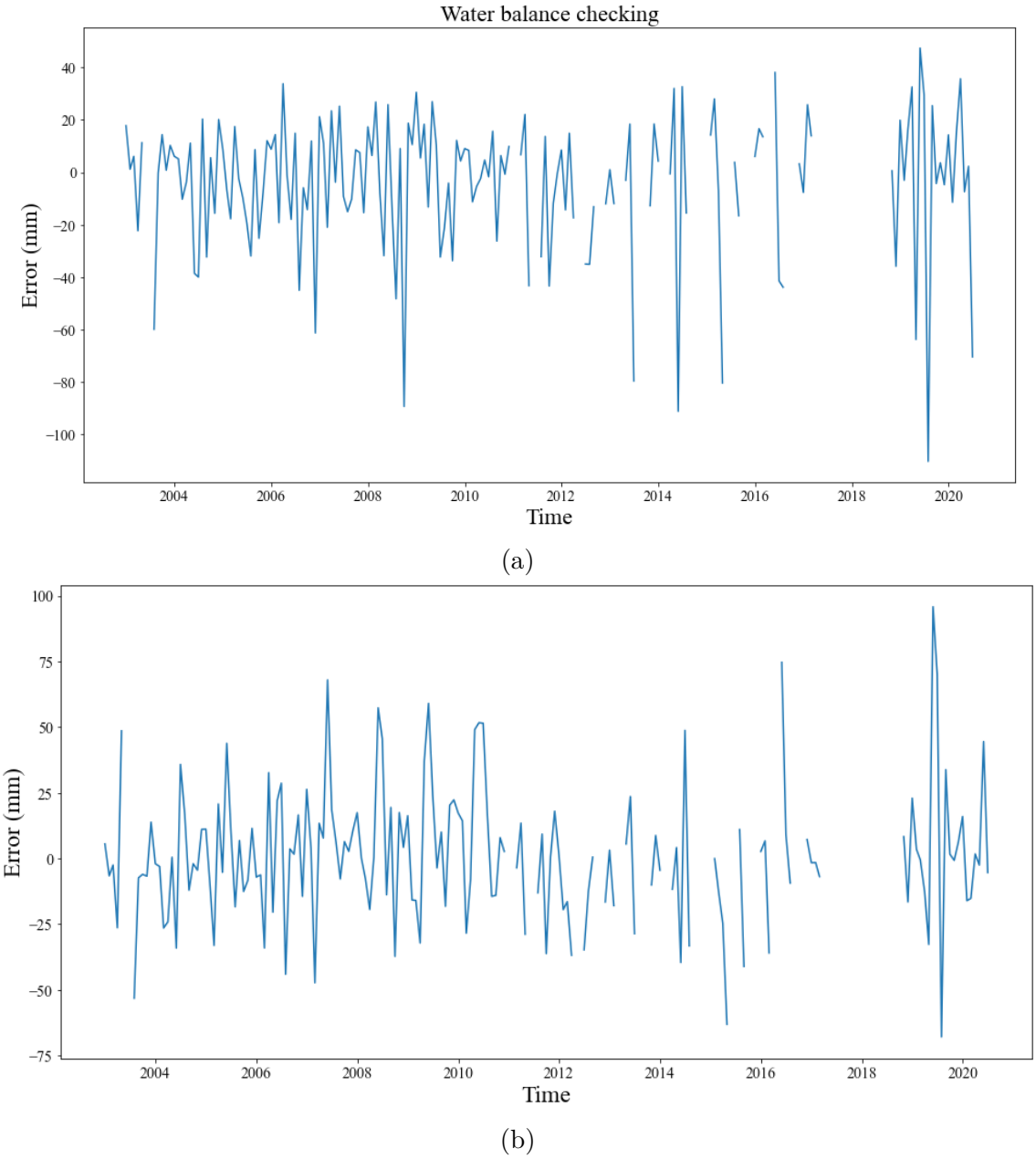

Figure 4-1: Water balance checking using original datasets. *Note. Graph (a) uses time series from PRISM and GLEAM for precipitation and ETa, while in Graph (b), Chirps and SSEBop v5 are used as precipitation and ETa. In both graphs, river discharge and TWSA use in-situ measurement and GRACE-JPL data.*

Water balance posteriors are shown in Figure 4-2. The four graphs from top to bottom represent ensemble P, ETa, TWSA and Q, respectively. Uncertainty bands of 90% are also presented in the figure to prevent the results from being overconfident. In the first graph, the corrected mean value is closer to the simulation using CHIRPS data (with TRSME = 0.7493) than PRISM data (with TRSME = 1.058), especially in the summer and autumn when the monthly rainfall is higher. In these periods, the PRISM dataset always overrates the P values, while in the low-value months, PRISM tends to underestimate P compared with CHIRPS. According to Schoups and Nasseri (2020), this suggests that a more prominent weight is given to the CHIRPS dataset.

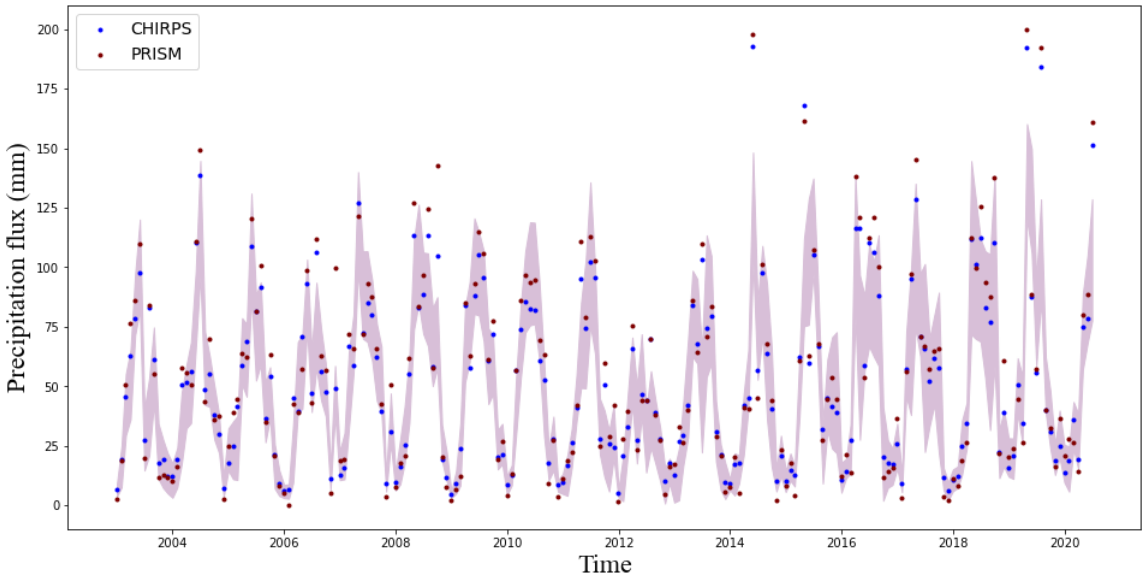

(a)

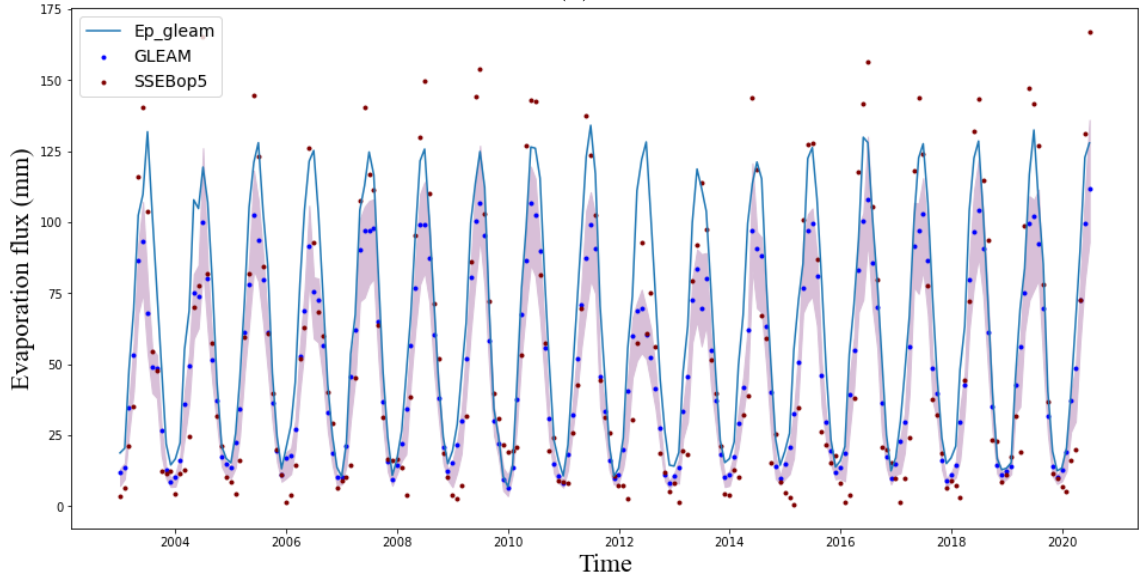

(b)

Figure 4-2: Monthly water balance estimates from January 2003 to July 2020 by data fusion.

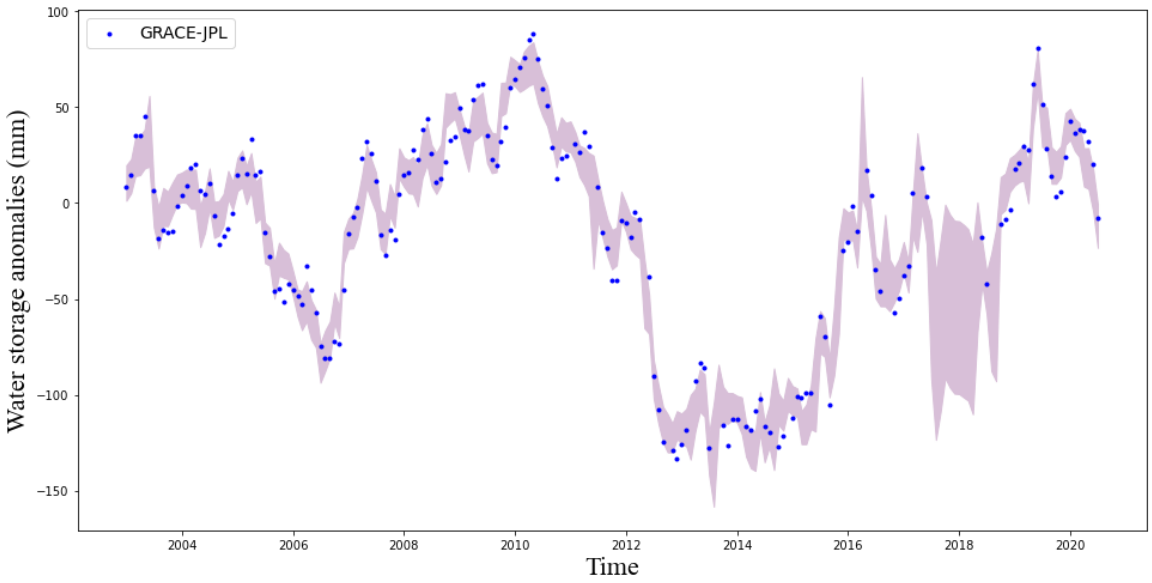

(c)

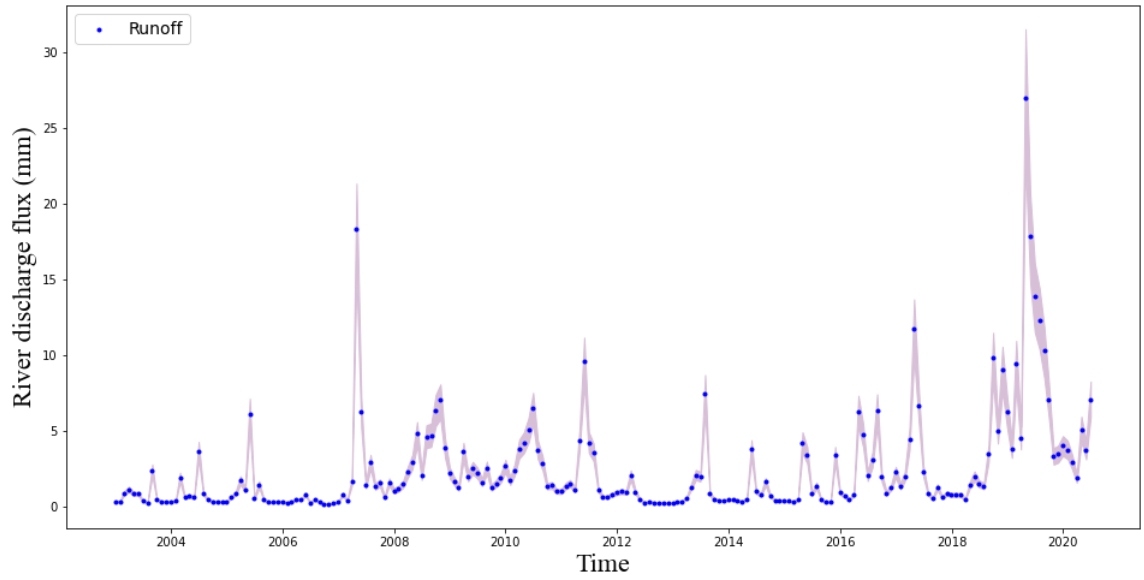

(d)

Figure 4-2: Monthly water balance estimates from January 2003 to July 2020 by data fusion. *Note. Graph (a) to (d) represents estimates for precipitation, evapotranspiration, terrestrial water storage anomalies and discharge. The subfigures show a 90% posterior uncertainty band. In Graph (b), the potential evapotranspiration from GLEAM is taken as the basin potential evapotranspiration.*

It can be seen from the second graph that there is a large difference between the GLEAM and the SSEBop datasets. The corrected result for ETa tends to much more nearly follow the value of GLEAM than that of SSEBop. The latter one is likely to fall out of the uncertainty band at peak value or valley value. Both P and ETa graphs demonstrate a more significant uncertainty at a higher value, indicating that the corrected values for these two variables are

more accurate at the lower level. This phenomenon results from discrepancies between two datasets often more prominent at peak values than at low values.

Inferred TWSA is presented in Graph (c). It basically follows the GRACE data, other than there is an abnormal period in 2017 and 2018, the uncertainty band is significantly wider than any other time. The rational explanation for this is that there are many missing records (see **Appendix A**) between July 2017 to May 2018, also in August and September 2018 (13 consecutive months in total, excluding June and July 2018). Although there are also a few sporadic data missed before, they do not lead to abnormity like that. To conclude, the occasional missing GRACE record does not remarkably differ its inferred posteriors from those with observation value. This is, as designed by Schoups and Nasseri (2020), due to the principle of data fusion that error parameters are obtained from months using data from the entire time series, and smoothing infers posteriors using data from all months. However, the significant disturbance in the posteriors elucidates that the data fusion method is less precise dealing with a long-range deficiency in observations.

Besides, the TWS anomalies in 2012 decrease significantly. The great diminish in the water store can be explained by the lower amount of precipitation, which results in a declined actual evapotranspiration (the potential ET remains stable). The low P also leads to less runoff in 2012 - likewise, the high P in 2019 accounts for the increase in TWS and river discharge.

The posterior uncertainty firmly follows its prior uncertainty, as revealed in the last graph of Figure 4-2. Like P and ET, data fusion generally gives higher uncertainty to peak flow and lower uncertainty to low flow. This characteristic can make it more accurate when simulating low flow, which is the primary focus of the monthly water balance model.

4-2 Efficiency analysis

This section provides results of, firstly, traditional model simulation (Scenario 1) in Case a. In the second place, it gives the performance from Scenario 2 in Case b. This case contains two sub-steps. Sub-step 1 only uses corrected data as model input and performance controls, without considering input or measurement uncertainty. Sub-step 2 combines the impact of forcing data error, measurement error and model error.

4-2-1 Case a: using raw data for calibration

When the likelihood reaches its maximum, the optimal parameter set is found (See Table 4-1). Using PRISM or CHIRPS to force model, both α_1 are around 3. PRIMS results in larger α_2, β and K than CHIRPS, but its S_{max} around 200 is much lower than S_{max} derived by CHIRPS exceeding 500. The initial states soil water storage by PRISM is approximately one-ninth as large as CHIRPS. The values of groundwater storage in both cases are close to zero.

Besides, Table 4-1 also lists both fitting results. The simulated discharge, together with the observation, is plotted in Figure 4.3 below. The two σ values are similar and larger than 1.6, and TRMSE values both exceeds 0.7 in the calibration period, consistent with the

Table 4-1: Calibrated parameters and precision indexes of simulations with Wapaba model forced by original inputs (Case a)

Input	**Parameter**						
	α_1 [-]	α_2 [-]	β [-]	K [**days**]	S_{max} [**mm**]	S_o [**mm**]	G_o [**mm**]
PRISM	3.546	2.753	0.7212	81.80	204.4	38.14	1.470
CHIRPS	2.855	1.621	0.5660	12.68	504.4	342.8	0.0004
Input	σ	**Calibration Likelihood**		**TRMSE**		**Validation TRMSE**	
PRISM	1.659	0.1458		0.8119		1.433	
CHIRPS	1.699	0.1424		0.7047		1.264	

Table 4-2: Parameters calibrated on discharge using Wapaba model and fitting precision indexes (Case b)

Sub-step	α_1 [-]	α_2 [-]	β [-]	K [**days**]	S_{max} [**mm**]
1: No P/Q uncertainty	3.762	2.379	0.5610	183.3	112.9
2: With P and Q uncertainty	3.658	2.358	0.4376	849.2	131.9
Sub-step	So [**mm**]	Go [**mm**]	M	σ_Q	$TRMSE_Q$
1: No P/Q uncertainty	22.95	3.423	(18.30)	1.654	0.5473
2: With P and Q uncertainty	35.12	13.47	(26.20)	0.4554	0.2864

phenomenon that the discharge in Graph (a) Figure 4-3 fitting is almost as bad as that in Graph (b) in general. The modeled discharge in Graph (a) fits the observation relatively worse at low flow. Besides, in the validation period, simulated discharge in Graph (b) in Figure 4.3 is better than that in Graph (a). Also, the TRMSE of discharge simulation forced by PRISM is larger than CHIRPS by about 0.17.

Figure 4-4 present the reproduction of ETa and TWS. In Graph (a), the two ETa simulations forced by PRISM and CHIRPS are broadly close to each other, especially at low values. At high values, PRISM-forcing ETa values are usually larger than CHIRPS-forcing ones, except for those in the dry years 2006 and 2012. TRMSE of ETa and TWSA can be computed in a similar way of that of discharge. The simulated ETa values are quite different from those of Ssebop5 (TRMSE for ETa simulation using PRISM and CHIRPS data are 1.696 and 1.771). Although the simulations, particularly the PRISM-forcing ones, are closer to GLEAM data (TRMSE for ETa simulation using PRISM and CHIRPS data are 0.4640 and 0.4526), no information of measurement uncertainty is provided. Moreover, Graph (b) shows that CHIRPS-forcing TWSA fluctuates more and better fits GRACE JPL data from 2005 to 2015 than the PRISM-forcing one. After 2016, both simulations are apparently larger than the observation. The value of TRMSE for water storage anomalies is larger than 4.

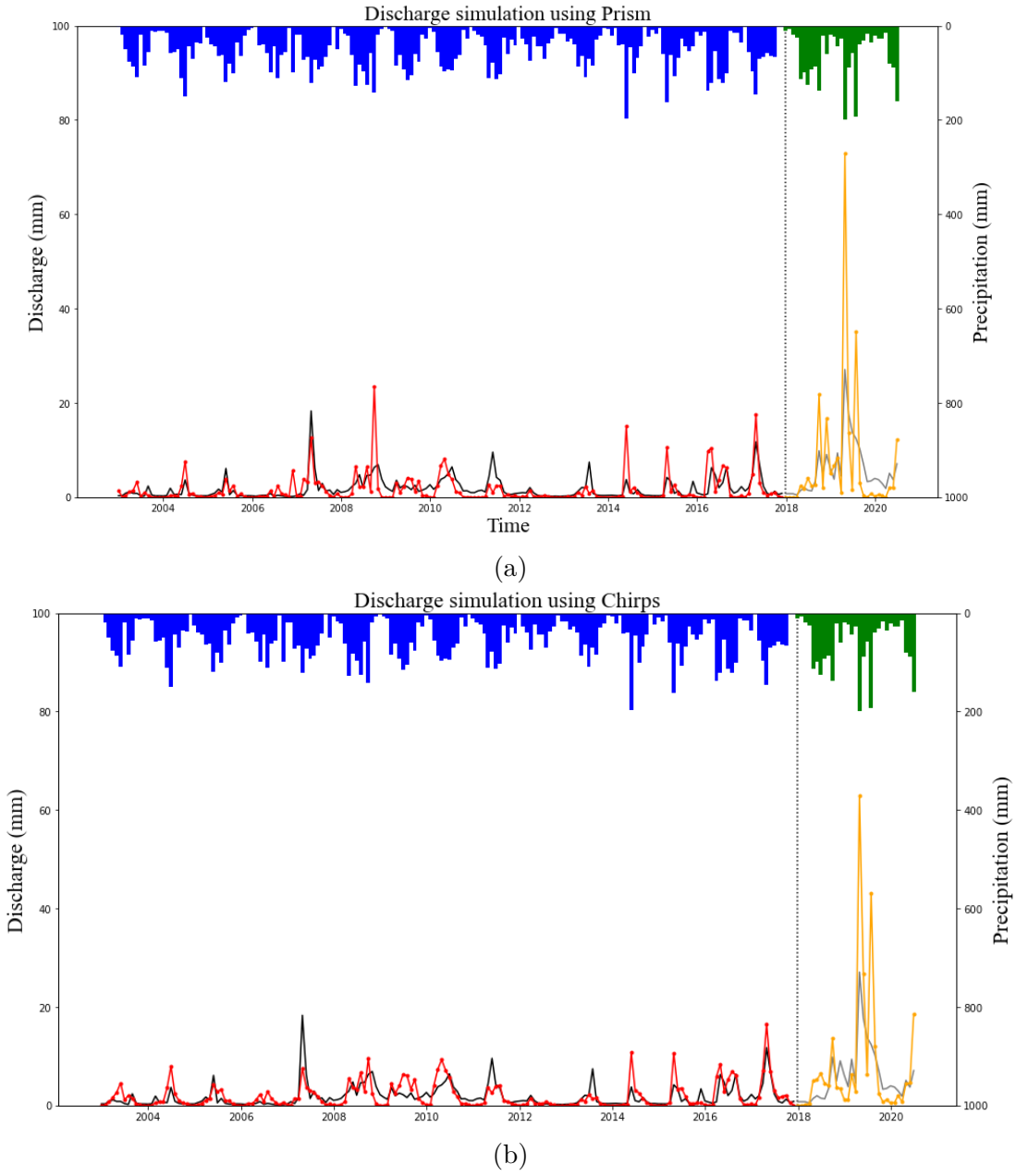

Figure 4-3: Discharge simulations with Wapaba model forced by raw satellite data (Case a)

4-2-2 Case b: Using clean data and calibration on Q

As the effects of inaccurate input are demonstrated, the next step is to examine the efficiency of the data fusion method. First of all, if considering no precipitation uncertainty, only one determined time series, in this sub-step the time series of mean values, is used as inputs. The optimal parameter sets are given in Table 4-2 and Figure 4-5 exhibits the simulated results. In this sub-step, the fitting precision index of discharge simulation σ_Q is 1.654, and TRMSE is 0.5473. The simulation of discharge fits the observation accurately in low flow but the simulation of recession limbs is not precise. For example, the simulated recession limbs in

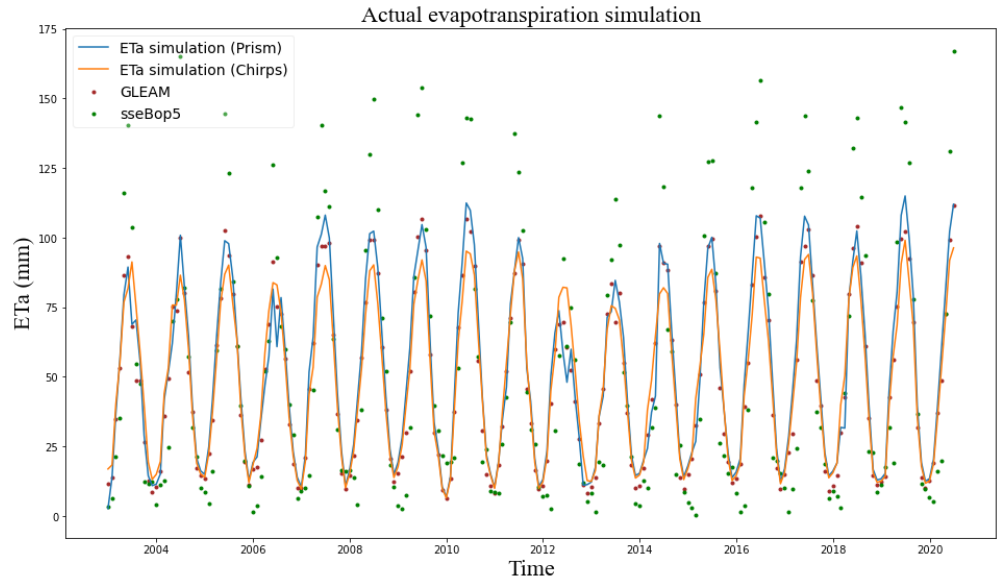

(a)

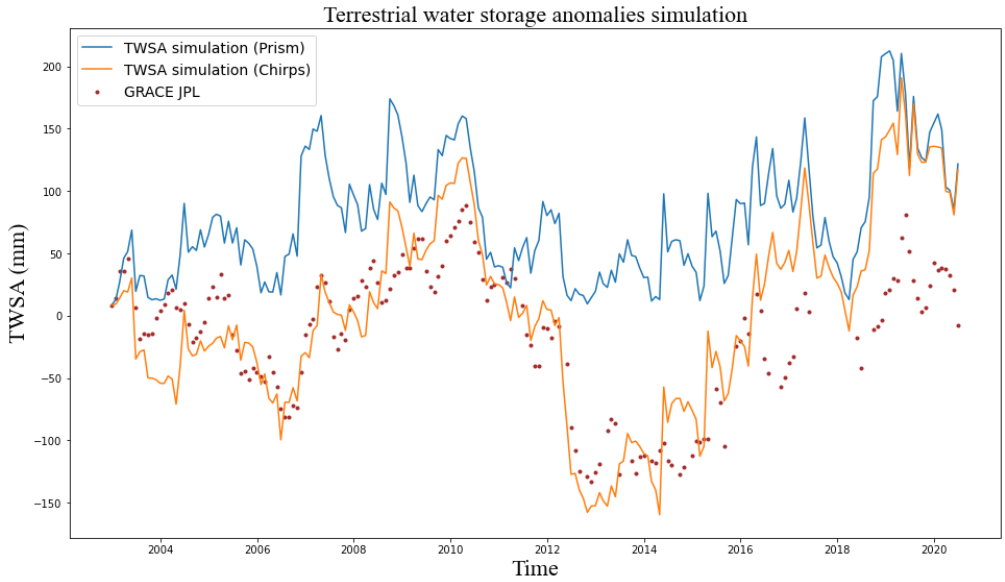

(b)

Figure 4-4: Actual evapotranspiration and water storage anomalies simulations with raw satellite data (Case a)

2004, 2005 and 2017 are higher than the observation, while that in 2011 is much lower. Even if we know that there are errors between the measured and the observed values, the magnitude of errors is still unavailable, due to unqualified uncertainty of the measurement. Graph (b) exhibits the observed and simulated ETa with TRMSE equal to 0.5109. The simulated TWSA is flat and quite different from the observation with TRMSE equal to 4.207.

While in the second sub-step, the uncertainty in precipitation is also incorporated. As stated above, precipitation values here are treated as parameters and given a much wider

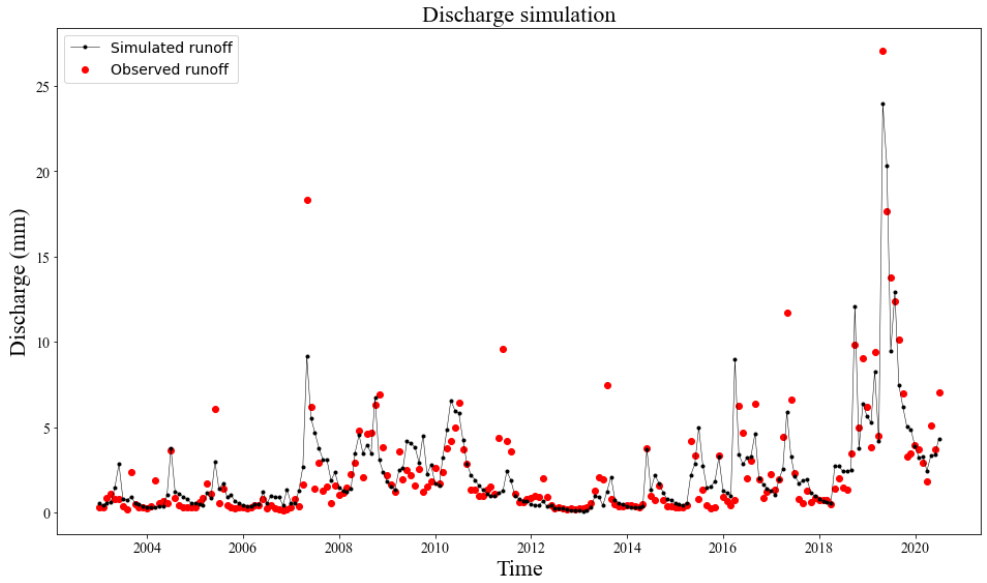

(a)

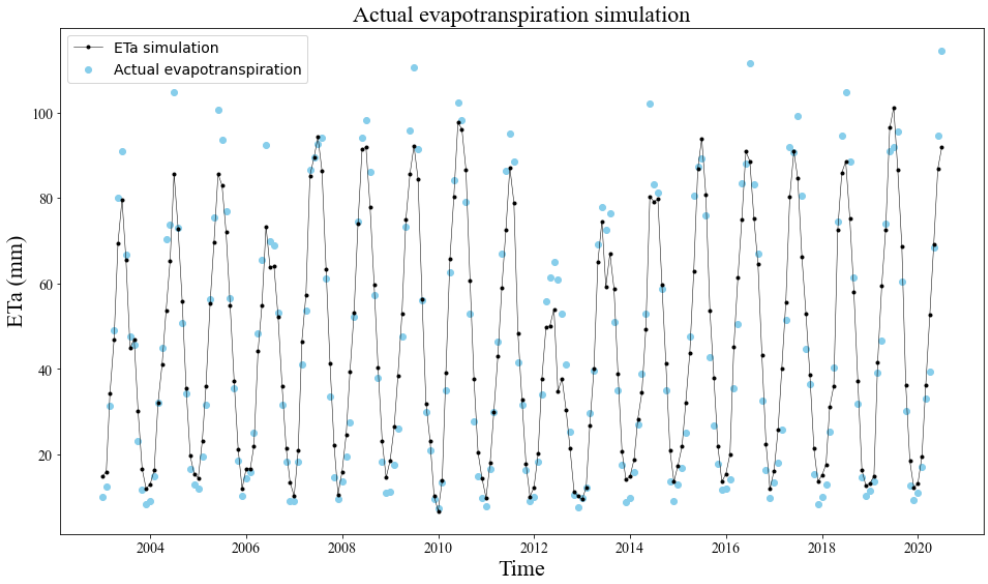

(b)

Figure 4-5: Simulation results without considering precipitation uncertainty (Case b sub-step 1)

range than the uncertainty band. However, due to the constraint of likelihood, the majority of the precipitation values used as inputs fall in the band (see Figure 4-6). The value of σ_Q (0.4554) and TRMSE (0.2864) are both remarkably lower than that in the previous sub-step. All simulated discharge can be explained by its measurement with 99.74% uncertainty, and even that with 90% uncertainty can account for the majority of the simulation (92.89%) (see Figure 4-7).

In Figure 4-8 Graph (a), 64.93% simulation of ETa can be accounted for by measurement with 90% uncertainty, and measurement with 99.74% uncertainty can explain 89.10%

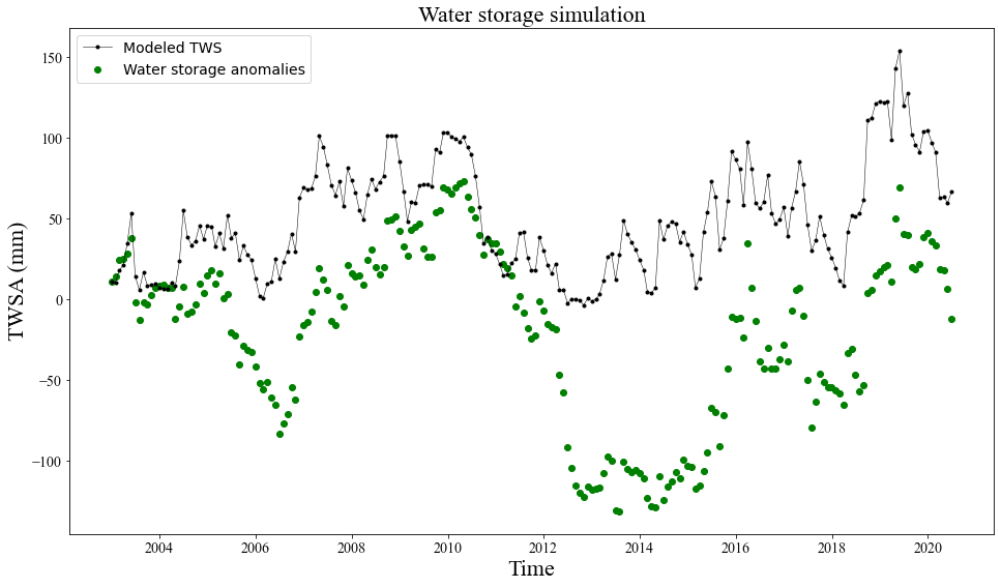

(c)

Figure 4-5: Simulation results without considering precipitation uncertainty (Case b sub-step 1)

simulated ETa values. Graph (b) presents a large difference between the simulated TWSA and the measurement, which cannot be explained fully by errors in model forcing data and observation. Thus, this reveals the defective model structure.

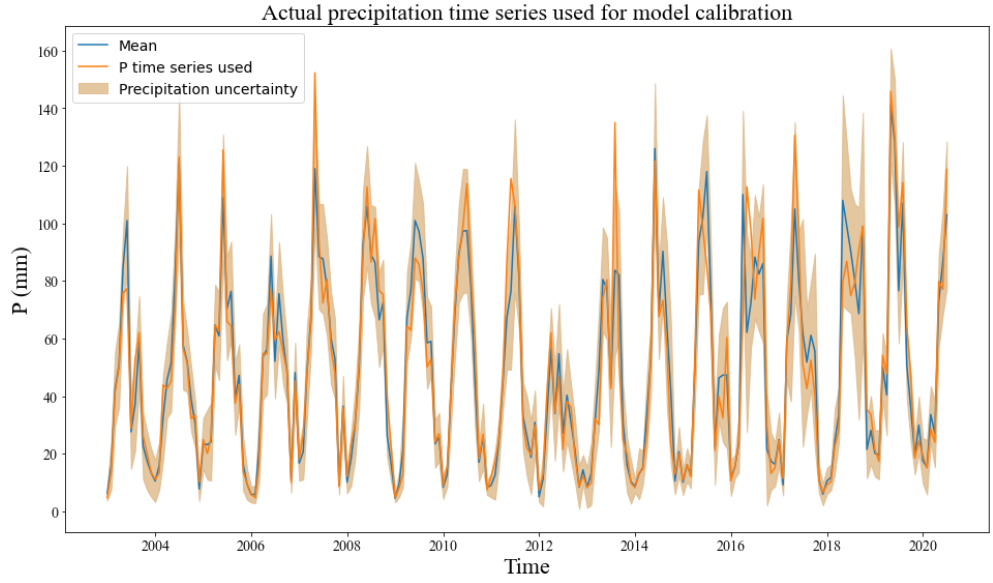

Figure 4-6: The calibrated precipitation (Case b sub-step 2)

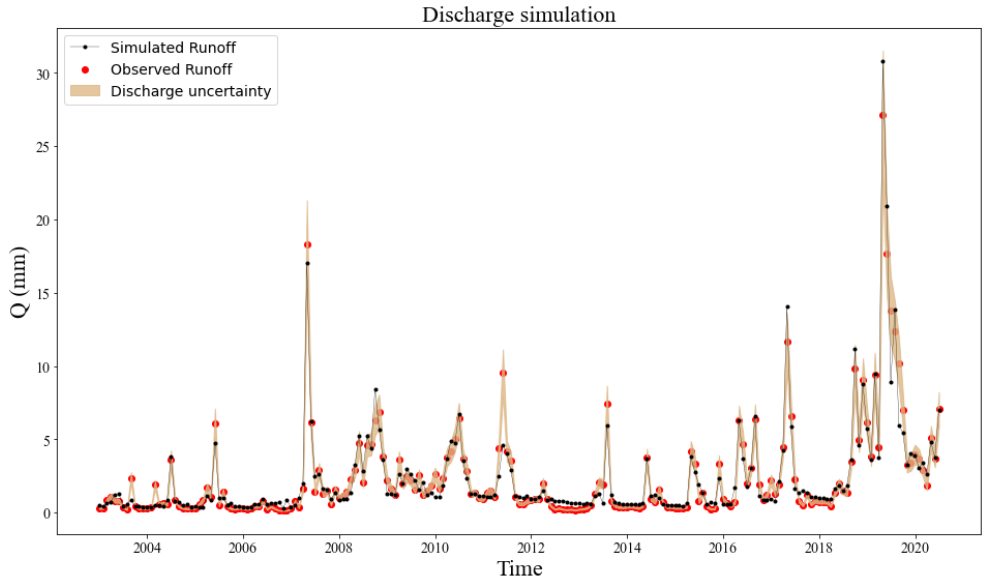

Figure 4-7: Discharge simulation process using parameters calibrated on discharge (uncertainty known, Case b sub-step 2)

4-3 Model structure analysis

This section presents outputs of Step c to Step f. The first two cases c and d use the original monthly Wapaba model, while the last two cases improve it and make use of the advanced model.

4-3-1 Case c: calibration on ETa, TWSA and discharge

This case calibrates model parameters on all three fluxes (using the objective function from Table 3-2). The simulated results using parameters calibrated are exhibited in Figure 4-9.

The optimal parameter set is in Table 4-3. With the better simulation of TWSA than exhibited in Figure 4-8, the accuracy of discharge simulation decreases. TRMSE increases to 0.8532, and the value of σ_Q rises to 2.174.

4-3-2 Case d: calibration on ETa and TWSA

Bai et al. (2018) argue that model calibration using GRACE-derived TWSA data alone cannot efficiently decides parameters associated with runoff generation and/or routing, because water storage is a state variable. Therefore, ETa is also incorporated for calibration in this case. The results are exhibited in Figure 4-10. All optimal parameters derived in Case c and Case d are presented in Table 4-3.

The performances of actual evapotranspiration simulation in Case c and Case d are similarly. Relatively, the simulated ETa in Case c fits the observation better, given a smaller fitting precision index ($\sigma_E = 4.013$) than that in Case d ($\sigma_E = 4.755$). Even though the result

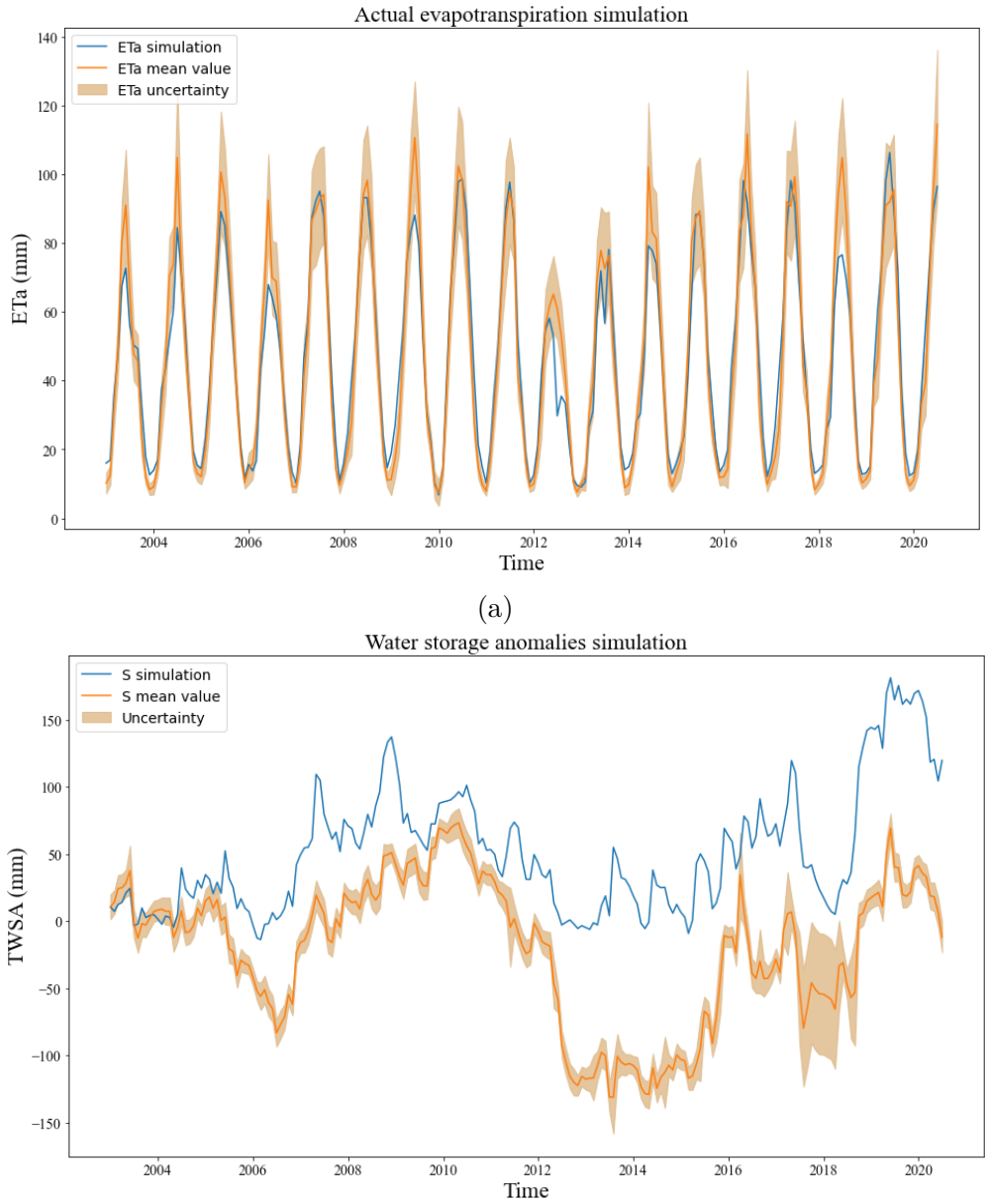

Figure 4-8: Simulation of ET (a) and TWS (b) using Wapaba parameters calibrated on discharge (Case b sub-step 2). *Note. In the simulation of TWSA, parameter M is set to be 26.1960.*

that the σ_S value in Case d is much lower than that in Case c seems to be an improvement, the simulation of runoff gets significantly worse. The index $TRMSE_Q$ increases from 0.8532 to 1.441. In graph (b) of Figure 4-10, the modeled discharge consists only of baseflow, which is inconsistent with the actual situation. It is found by analyzing the parameters of the case that the severe smooth and delay of flow results from the situation that sensitive parameters and K in Case d are much lower than those in Case c. Parameter β, indicating the proportion of the catchment yield as groundwater, is larger than 0.50 in Case c, but decreased to 0.1559 in Case d. Moreover, the groundwater store time K exceeds 2000 in the previous case, but is

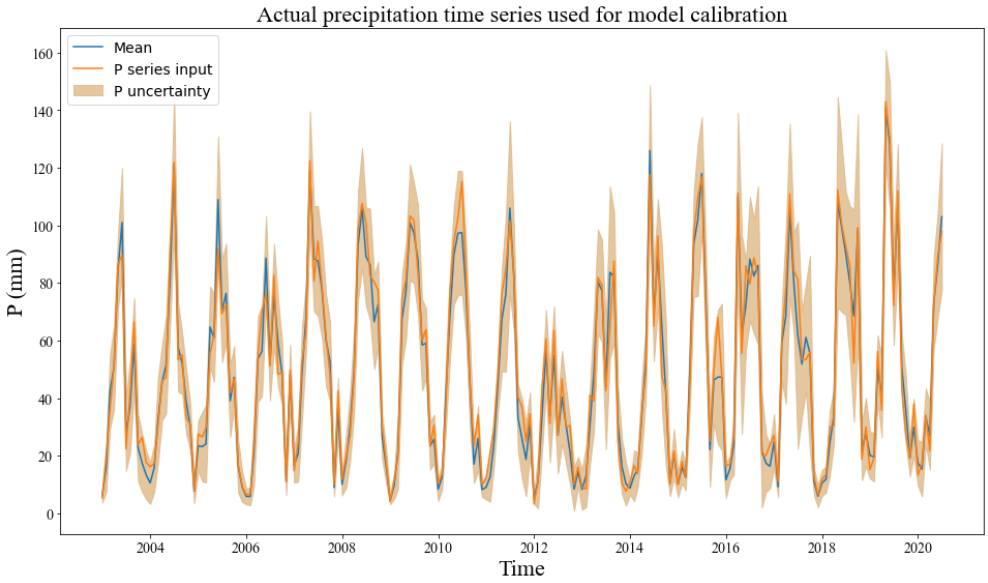

(a)

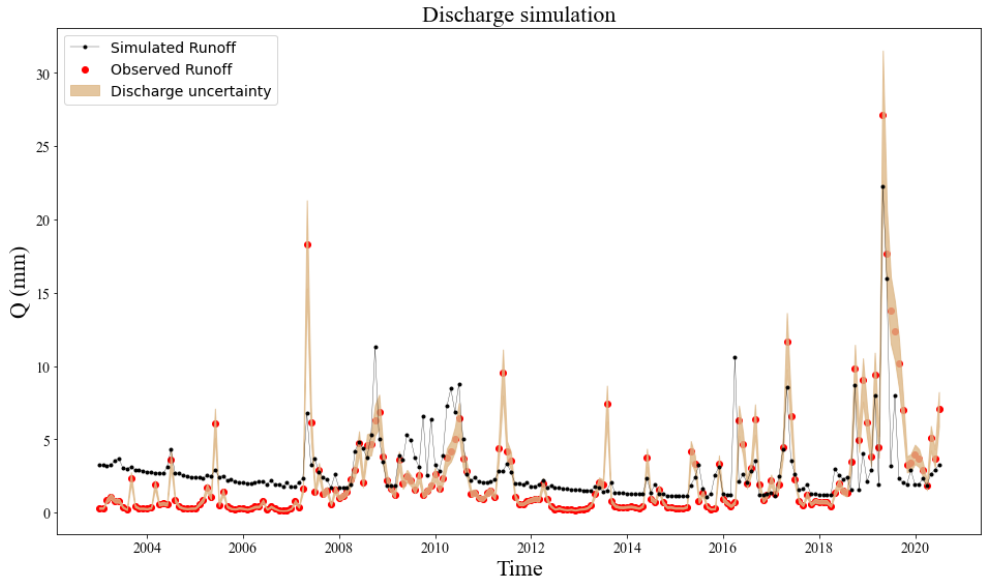

(b)

Figure 4-9: Simulation using all three fluxes for calibration (Wapaba model, Case c)

less than 1500 in Case d.

Therefore, more processes should be added in the model principle to constrain these parameters to more realistic values. A high β value shows high recharge to groundwater. Thus, it leads to the results that the proportion of river discharge as baseflow is high, but as surface runoff is low.

Besides, in both Case c and Case d, the amount of baseflow is too large. For example, in the beginning of 2003 in both cases, the actual amount of baseflow should be close to zero. However, both simulated values are around 4 millimeters, suggesting in the simulated results

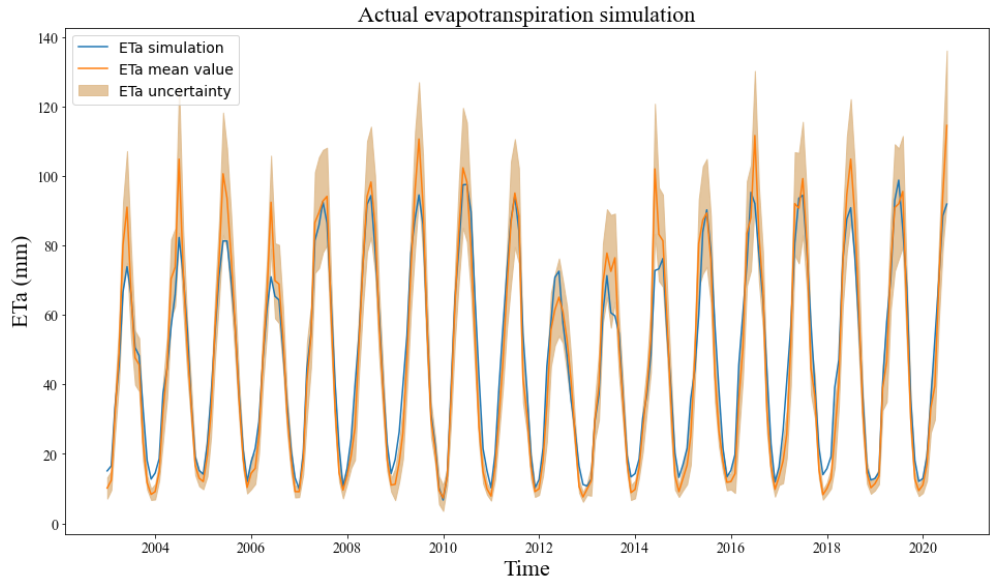

(c)

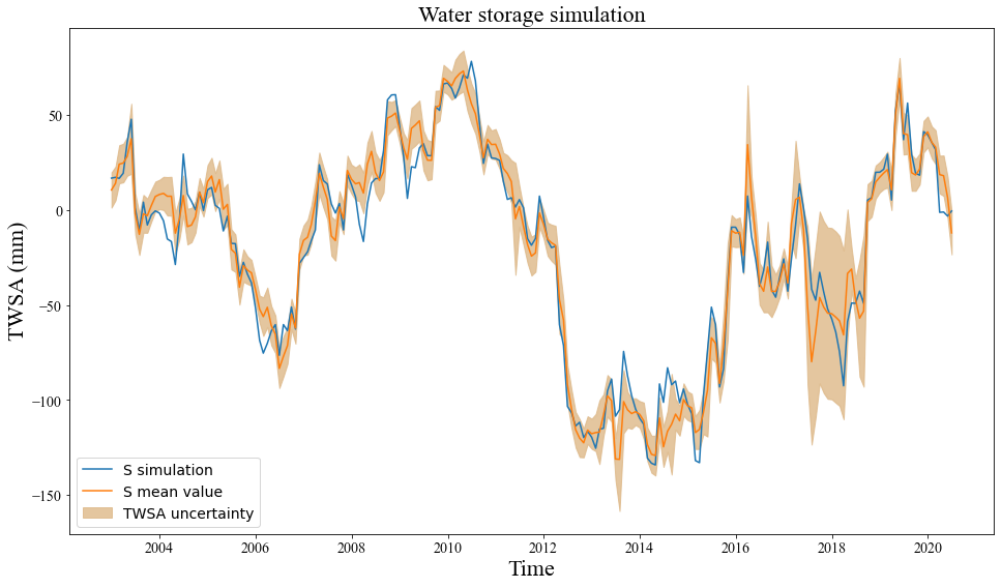

(d)

Figure 4-9: Simulation using all three fluxes for calibration (Wapaba model, Case c)

too much water are regarded as baseflow (of discharge) among all water balance fluxes. This inaccuracy can thus influence the amount of other fluxes.

4-3-3 Case e: model structure modification and calibration on ETa, TWSA and discharge

According to equation (2-9), to increase (the proportion of) surface runoff Qs, the recharge to groundwater store R for each time step needs to be reduced. The recharge R can be

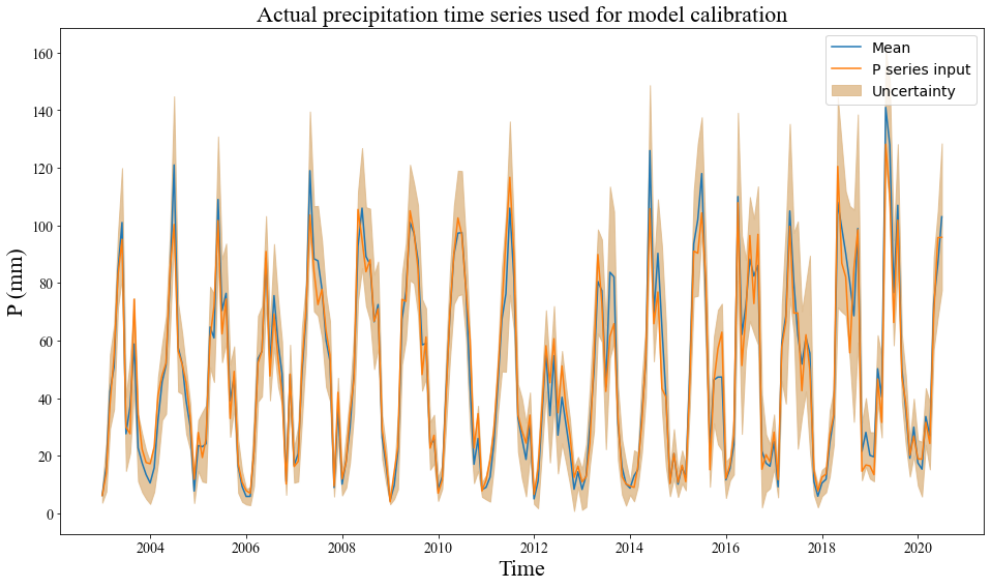

(a)

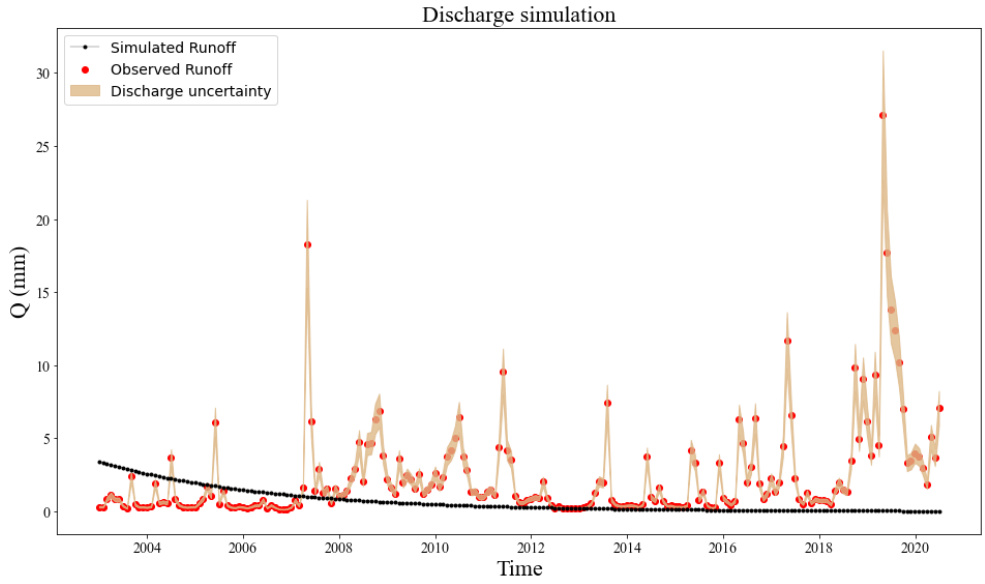

(b)

Figure 4-10: Simulation using ETa and TWSA for calibration (Wapaba model, Case d)

constrained.

This case assumes that the factors influencing groundwater recharge are similar to those influencing infiltration. That is, to ignore the influence brought by recharge from precipitation, i.e., precipitation duration, seasonal factors, topography and vegetation. The main factors affecting recharge are (a) the intensity of water supply, (b) the size of soil voids, (c) the amount of time given and (d) the amount of groundwater that can be held in store (related to water table, space in the ground and rate of groundwater discharge).

Consequently, according to the Wapaba models equation (2-8), the water supply (factor

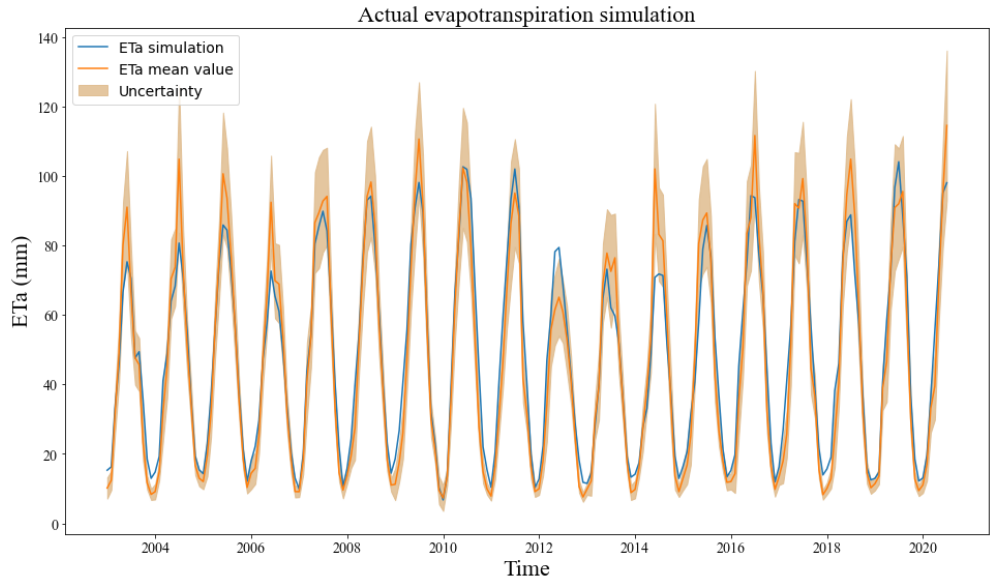

(c)

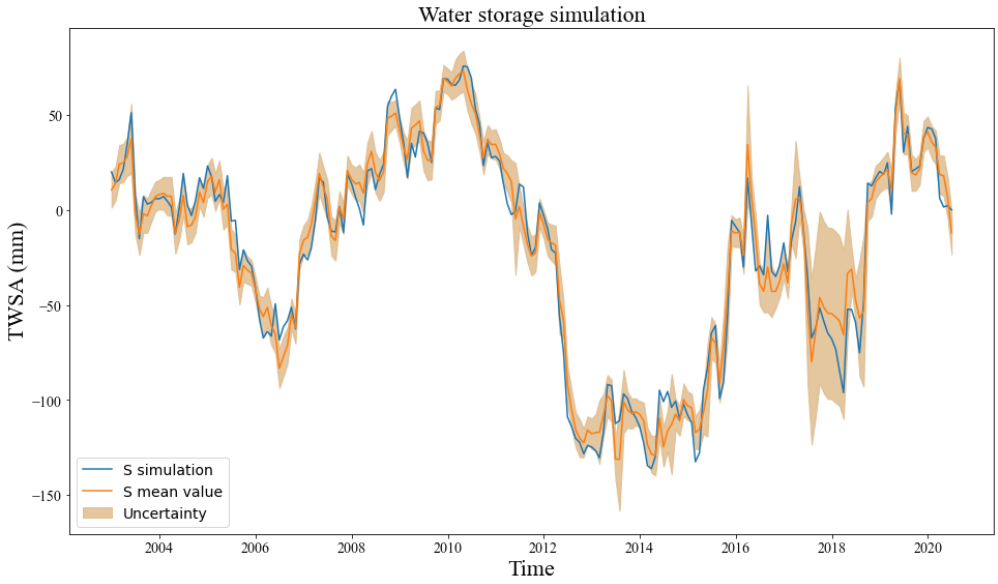

(d)

Figure 4-10: Simulation using ETa and TWSA for calibration (Wapaba model, Case d)

(a)) in month t is the product of β and catchment water yield $Y(t)$. A constant that works as the upper limit of infiltration rate f_{max} [mm/day] is introduced for factor (b). It reflects the permeability of rock and soil mass. For catchments without underlying surface information, f_{max} can be determined by trial and error. Factor (c) talks about the fact that recharge from catchment water yield is also related to time (usually the precipitation retention time on the ground) T. Since Y is catchment water yield, instead of precipitation, the $T(t)$ can be the number of days of the $t-th$ month. The factor (d) is neglected in this study since the groundwater store is considered to be infinitely large.

Table 4-3: Calibrated parameters and precision indexes for Cases c and Case e

Calibration on	α_1 **[-]**	α_2 **[-]**	β **[-]**	K **[days]**
ETa, TWSA and discharge (Case c)	4.055	1.988	0.5334	2173
ETa and TWSA (Case d)	3.830	2.007	0.1559	1332
Calibration on	S_{max} **[mm]**	S_o **[mm]**	G_o **[mm]**	M **[mm]**
ETa, TWSA and discharge (Case c)	177.2	41.85	232.2	244.3
ETa and TWSA (Case d)	2049	42.56	148.0	158.0
Calibration on	σ_Q	σ_E	σ_S	$TRMSE_Q$
ETa, TWSA and discharge (Case c)	2.174	4.013	8.019	0.8532
ETa and TWSA (Case d)	-	4.755	6.252	1.441

Table 4-4: Calibrated parameters and precision indexes in Case c and Case e

Case	α_1 **[-]**	α_2 **[mm]**	β **[mm]**	K **[days]**	S_{max} **[mm]**
c (Wapaba)	4.055	1.988	0.5334	2173	177.3
e (modified Wapaba)	4.028	1.875	0.3911	2816	195.9
Case	S_o **[mm]**	G_o **[mm]**	M **[mm]**	f_{max} **[mm/d]**	
c (Wapaba)	41.85	232.2	244.3	-	
e (modified Wapaba)	77.54	193.0	247.7	0.5	
Case	σ_Q	σ_E	σ_S	$TRMSE_Q$	
c (Wapaba)	2.174	4.013	8.019	0.8532	
e (modified Wapaba)	1.654	3.997	9.946	0.7069	

Hence, a modified equation for the calculation of $R(t)$ adapted from the work of Bennett, Wang, Schepen, Robertson, and Li (2015) can be:

$$R\left(t\right) = \min\left(\beta Y\left(t\right),\ f_{max}\ T\left(t\right)\right) \tag{4-3}$$

In this case, we calibrate parameters on all three output fluxes (see Figure 4-11) and compare the performances with those in Case c.

The value of the constant f_{max} is experimented with between 0 and 3 and determined by making the best model performances. For the study area, the most appropriate value for f_{max} is 0.5.

4-3-4 Case f: model structure modification and calibration on ETa and TWSA

Similar to what is done in Case d, the simulations of discharge, as well as other fluxes, use the parameter set calibrated on ETa and TWSA (see Table 4-5). The performances are exhibited in Figure 4-12. Graph (a) is the calibrated precipitation, while Graph (b) to Graph (d) represents the simulated results using the improved Wapaba model of discharge, actual

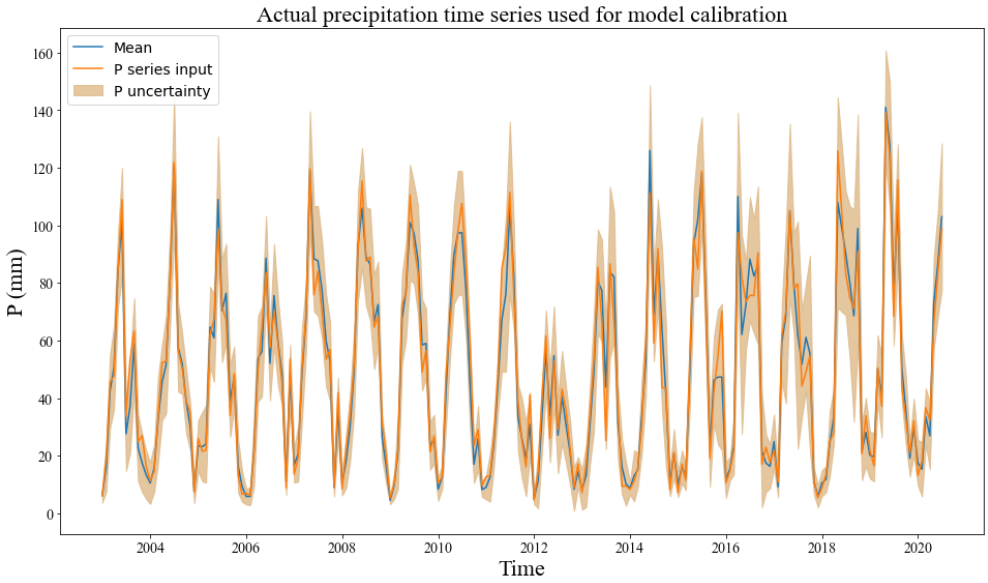

(a)

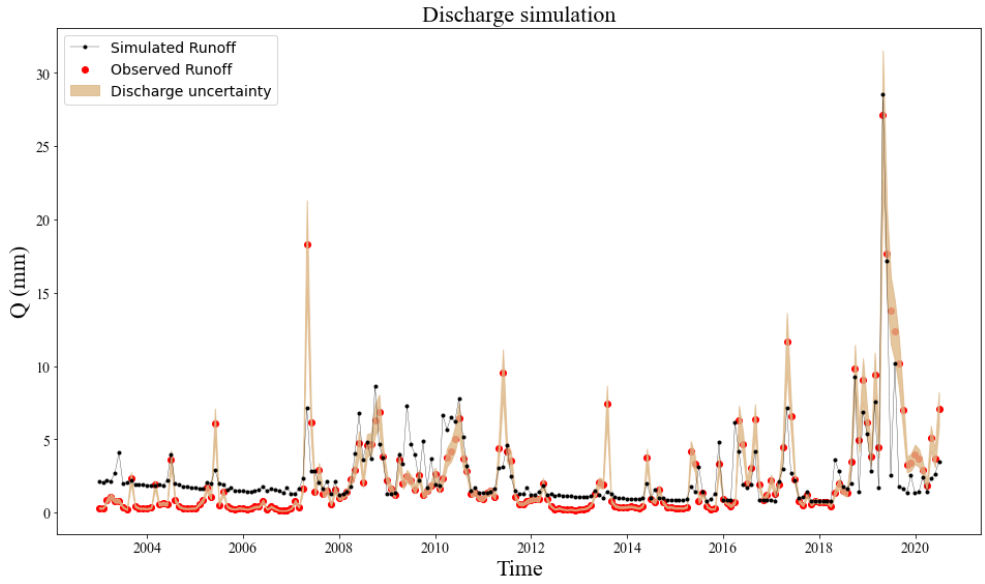

(b)

Figure 4-11: Simulations using parameters calibrated on ETa, TWSA and discharge (modified Wapaba model, Case e)

evapotranspiration and water storage anomalies. Similar to the previous case, the value of f_{max} is set as 0.5.

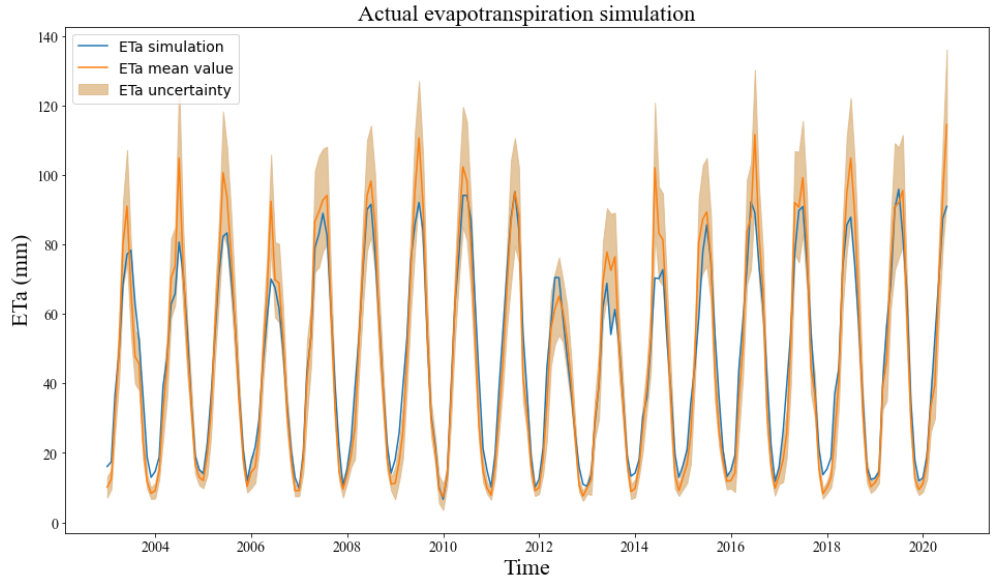

(c)

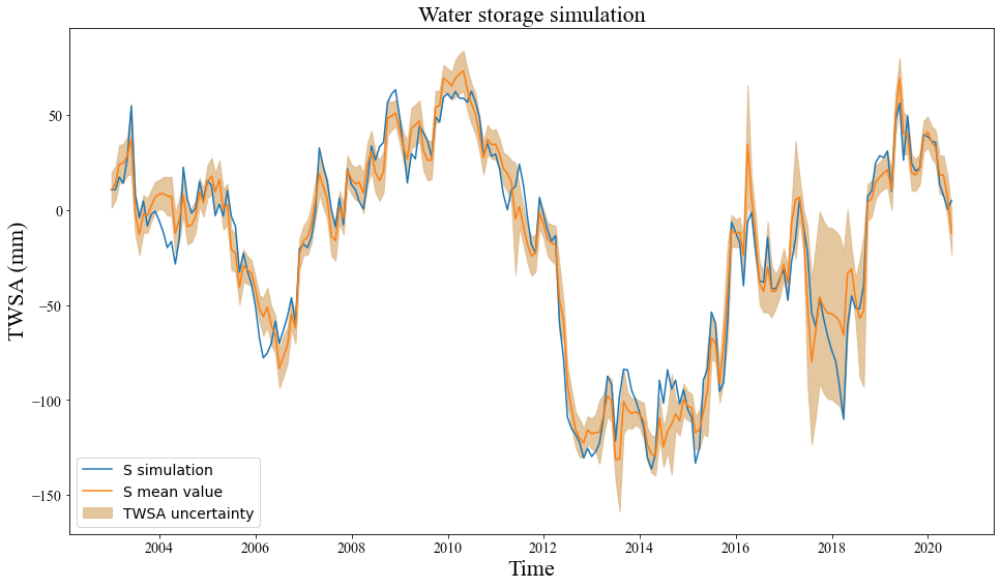

(d)

Figure 4-11: Simulations using parameters calibrated on ETa, TWSA and discharge (modified Wapaba model, Case e)

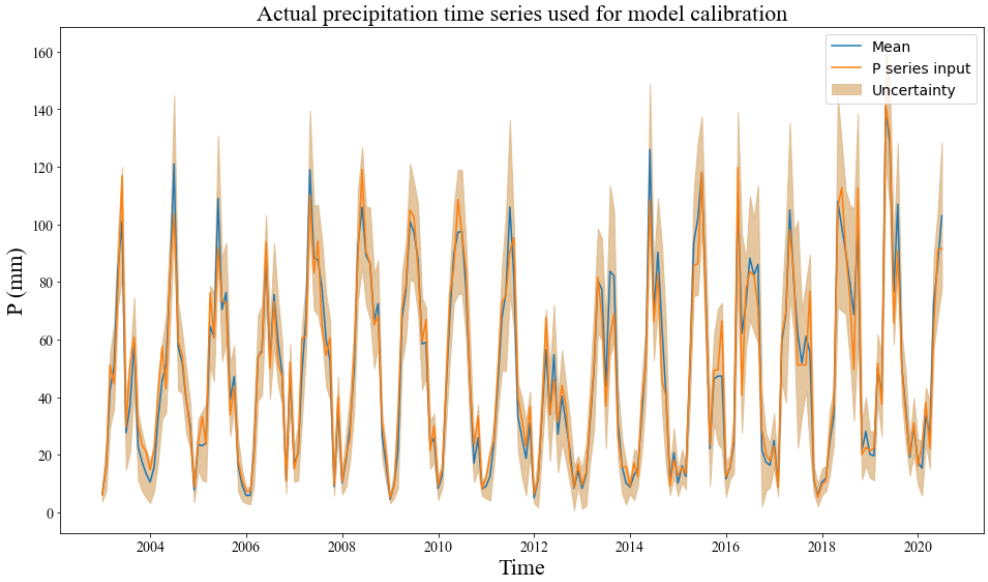

(a)

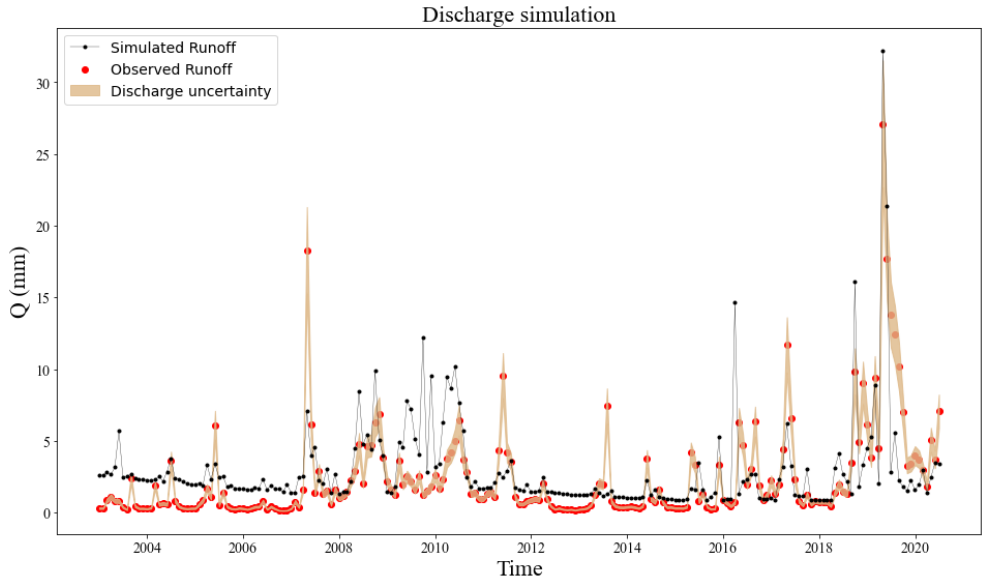

(b)

Figure 4-12: Simulations using parameters calibrated on ETa and TWSA (modified Wapaba model, Case f)

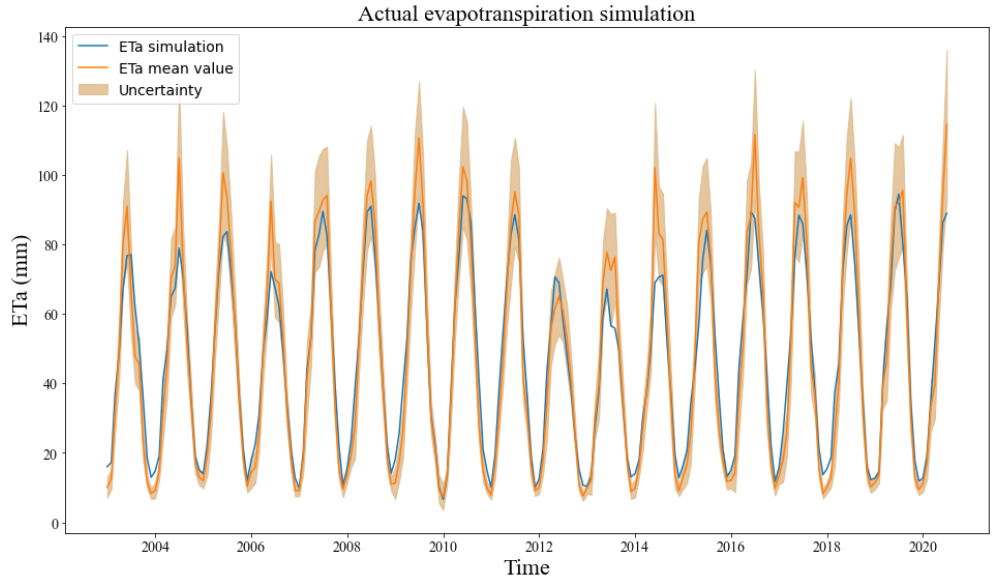

(c)

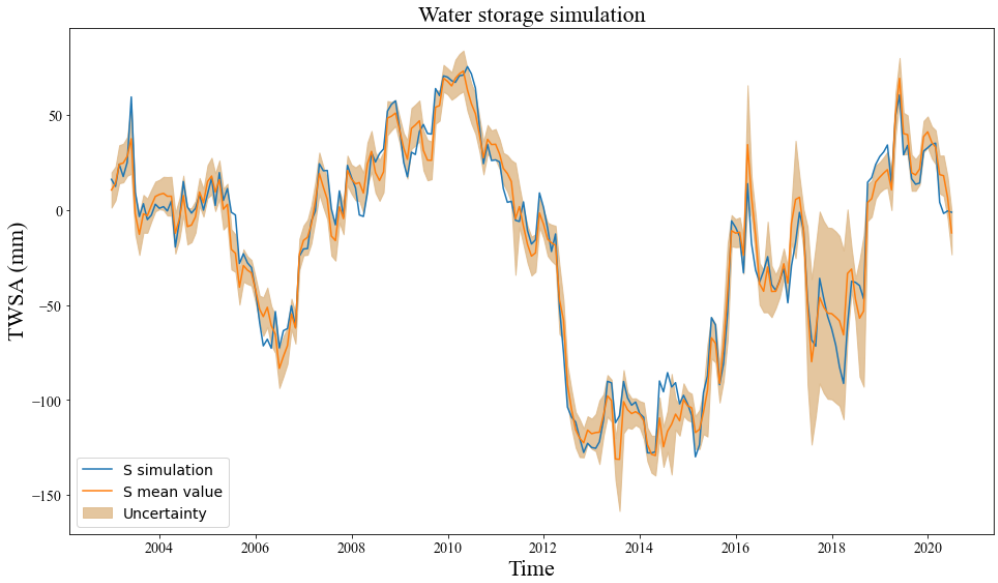

(d)

Figure 4-12: Simulations using parameters calibrated on ETa and TWSA (modified Wapaba model, Case f)

Table 4-5: Calibrated parameters and precision indexes in Case d and Case f

Case	α_1 **[-]**	α_2 **[mm]**	β **[mm]**	K **[days]**	S_{max} **[mm]**
d (Wapaba)	3.830	2.007	0.1559	1332	2049
f (modified Wapaba)	3.834	1.864	0.3842	2080	190.4
Case	S_o **[mm]**	G_o **[mm]**	M **[mm]**	f_{max} **[mm/d]**	
d (Wapaba)	42.56	148.0	157.9	-	
f (modified Wapaba)	77.27	178.0	226.5	0.5	
Case	σ_Q	σ_E	σ_S	$TRMSE_Q$	
d (Wapaba)	-	4.755	6.252	1.441	
f (modified Wapaba)	-	4.526	6.705	0.8790	

Chapter 5

Discussion

This chapter discusses those results derived from last chapter and answers research questions accordingly. The importance of data and model errors and their reduction are explained in detail. Finally, this chapter elaborates on the effects of the strategy.

5-1 The significance of water balance data errors and their reduction

Firstly, the original datasets fail in closing the water balance in the catchment, which does not correspond to the actual situation in the study catchment. The maximum water balance error is about four times the maximum runoff depth. Thus, the original datasets cannot be put into use directly. After introducing the data fusion method, the water balance is closed due to its internal principle. By doing so, the time series of all fluxes can be utilized for modeling. One set of those time series combinations is the mean value time series of all fluxes which is used in Case b sub-step 1. Judging from results in Table 4-1 and Table 4-2 sub-step 1, the values of parameter β and S_{max} drops; while values of K and G_o increase a lot. After data fusion, σ_Q decreases slightly and $TRMSE_Q$ drops greatly, indicating data fusion method successes in improving the performance of discharge simulation, particularly at low flows. More specifically, it increases the reliability of the input. It is concluded that the data fusion method can give the precipitation input more reasonable (with smaller errors) values by fusing them in the system.

Secondly, even though checking the inaccuracy of unprocessed data can reveal part of the inaccuracy of those datasets, the uncertainty is still not clear and cannot be quantified. With the help of the data fusion method, the normal distributions of each term each month are given, so uncertainty is shown in bands. For instruction, Table 4-2 shows both input and measurements with uncertainties of 90%. The mean value for each term is the most likely value for the actual data. Within the band, the closer a point is to the mean, the more likely it is to be the true value. In this way, data errors can be quantified with variances provided by data fusion and their negative influences on simulations can be reduced significantly.

Thirdly, apart from errors in forcing data, data fusion also provides normal distributions for output fluxes. The uncertainty band for discharge is very narrow because, instead of satellite products, the discharge data used in this study comes from in-situ observation, which is more reliable. Also, the magnitude of discharge in the study area is much smaller than ETa and TWSA. With larger values, ETa and TWSA have relatively larger standard deviation in their normal distribution as well as wider uncertainty bands. By using these, a lot of simulation errors of ETa and TWSA can be explained. Thus, data errors can be excluded from the synthesized errors and make it easier to analyze the model error.

Furthermore, the method can also make up for missing data. The missing data can be filled in by smoothing since error parameters are shared throughout the entire time series. For instance, from July 2017 to September 2018, many GRACE-JPL data are missing in this case. After processing, it can be seen from the third graph of Figure 4-2 that there is no missing data point in the new time series. As a result, the practicability of the method is improved. These two aspects together illustrate part of the advantages of the data fusion method.

5-2 The significance of errors in water balance models, and model error reduction

As stated in the last section, the total simulated errors apart from data errors are considered as model errors in this study. The goodness of fitting is also quantified with the estimated index σ. The Wapaba model used in this study has a very large model error. This is proved, firstly, by results from Case b and Case d. In these cases, when using one or more fluxes for calibration, the reproduction of other parameters is far from the (corrected) observations. Moreover, through the comparison of Case b and Case c, it is clear that by incorporating more fluxes for calibration, the reproduction capability of discharge is reduced. Compared to Figure 4-7, the simulated discharge in Figure 4-9 performs worse in both peak flow and baseflow, indicating by much higher σ of discharge.

Therefore, the model requires modification. Nevertheless, the hydrological process within a watershed is considered as a whole. Changes in one component must lead to changes in another one. Thus, it is challenging to improve the model in such a way that three outputs can be simulated perfectly at the same time. In this research, the improved model structure is made to the degree that, first of all, the principle of the model structure is more suitable for the realistic catchment conditions. In section 4.3.3 Case e, we constrain the infiltration of catchment water yield. This assumption is perfectly in line with the natural condition here that the Smoky Hill area is famous for the stratum with noticeable amount of silt (and siltstone) and a resultant low permeability. Secondly, the model error indicator σ for some fluxes is reduced without greatly increasing σ for other fluxes.

5-3 The effectiveness of quantifying and reducing data and model errors

This section has three parts. Each part elaborates on one change made in the study. Together, this section systematically analyzes how quantifying and reducing data and model errors can

eliminate the trade-off in fitting multiple datasets. This section illustrates the strategy's effectiveness in improving the use of the monthly Wapaba model in poorly gauged areas.

5-3-1 Effects of reducing water balance data errors

The study investigates data fusion efficiency by comparing not only water balance checking but also the comparison of results from Case a and Case b. Scenario 1 in Figure 3-2 uses the traditional model simulation in Case a. Scenario 2 includes data fusion in decreasing data uncertainty, with results presented in Case b. In Case b, Sub-step 1 only uses one set of the corrected data (the mean value time series of precipitation) as the model input and performance controls. Sub-step 2 combines the impact of forcing data error, measurement error and model error.

In line with the assumption, there are noticeable biases and errors in satellite data. It is evident that discharge performance in Figure 4-5 fits better than that in both graphs in Figure 4-3 to the observation. The two indexes σ and TRMSE in sub-step 1 are lower than their counterparts in Case a. Although it seems possible that if we choose another data to force the Wapaba model in the study area and use another data as the reference of ETa, we get a similar discharge simulation result as the sub-step 1. However, with the help of the data fusion method, no such prior knowledge is required, leading to higher feasibility and efficiency of data utilization. Also, the data fusion method brings more than input uncertainty. The provided discharge uncertainty of 90% accounts for 24.64% simulated points, while 37.91% of them can be explained by 99.74% uncertainty. Similarly, for ETa or TWSA simulation, in Case a, the goodness of fitting is the only standard for performances. While in sub-step 1 of Case b, the given errors of measurement can help in the interpretation of results. Although the performance of TWSA is bad (the simulations cannot reproduce the observed values), 67.30% of the ETa simulation results can be explained by the 90% data errors, and 99.74% uncertainty can account for 90.52% of results.

5-3-2 Effects of accounting for precipitation uncertainty

The second benefit can be concluded by comparing the two sub-steps in Case b. The difference of the two sub-steps is whether they calibrate the input precipitation as a series of parameters, that is whether they consider input uncertainty. By comparing the modeled runoff in Figure 4-5 and Figure 4-7, the effect of the change is further improving the accuracy of runoff simulation is significant. First, in Figure 4-7, the simulations fit the observations better. The index TRMSE is decreased from more than 0.5 to 0.2864, indicating the simulation at low flow is much closer to the observed values than previously. Another index σ also drops to 0.4554 (see Table 4-2) from 1.654, implying a smaller model error. Also, the observation with 90% uncertainty can shed light on 31.28% of values in the simulation. The observation with 99.74% uncertainty can explain 52.61% of values in the simulation. Thus, incorporating forcing data uncertainty is necessary.

The reason for this great change in σ is that in Case a σ includes errors in measurement, model input as well as model structure. After data fusion processing, the model input error is removed from the synthesis error.

5-3-3 Effects of model structure modification

Compared to results from Case c, after the modification the fitting of discharge in Case e (Figure 4-11) is improved. The model error σ_Q drops (see Table 4-4) from 2.174 to 1.654 (about 23.93%, although still larger than 1) and the index TRMSE decreases from 0.8532 to 0.7069 (about 17.15%). A similar reduction is also identified in the model error for ETa σ_E, from 4.013 to 3.997 (about 0.40%), but it is not that significant. The improvement of discharge and ETa simulations are at the expense of lowering the fitting accuracy from the σ_S equal to 8.019 to the σ_S equal to 9.946 (about 24.03%). Since in this study we focus mostly on discharge reproduction, and 24.03% is no larger than the sum of the percentage of decrease in discharge and ETa, the results are acceptable.

Case d and Case f offer results of the application of the original and the advanced model in ungauged area and the calibrated parameters as well as indexes are presented in Table 4-5. By comparing results in Case d and Case f, it can be seen that after modification, the simulation of discharge is improved significantly, indicated by a much lower TRMSE from 1.441 to 0.8790 (approximately 39.02%). This is done on the basis of an also improved actual evapotranspiration simulation (σ_E from 4.755 to 4.526, around 4.82%) and no severe deterioration on the simulation of TWSA (σ_S increases from 6.252 to 6.704, by 7.24%).

The comparison of results in Case f to those in Case c and Case e shows that, even without using discharge time series for simulation, Case f still succeeds in producing simulated discharge whose TRMSE (0.8790) is not much larger than that in Case e (0.7069). Despite the fact that the improved model (Case f) cannot achieve the same efficiency as using only the discharge (Figure 4-7) for its simulation results, the simulation results obtained by the improved model are close to the simulation results of considering all fluxes (Case c (TRMSE = 0.8532)). Although the simulation of TWSA becomes slightly worse, the simulation effects of both ETa and runoff are improved (smaller σ_E and σ_S). This shows the potential of the method in areas with deficient discharge observation.

Apart from numerical results, seen from Figure 4-12 Graph (b), the discharge result in Case e is more theoretically reasonable than that in Case d. In Case d, the only component in discharge is baseflow, so there is no response to precipitation input nor any peak corresponding to the measurement. However, by comparing the two sets of parameters, it can be seen that the improved model has a reduced value for the sensitive parameter β and an increased value for the sensitive parameter K. Hence, the proportion of surface flow in the runoff from the basin outlet has increased. Also, the simulated flow in Figure 4-12 is less smoothed. After modification the new model enables the simulation to capture much more peaks, for example the ones in 2007 and in 2019, although it is still not perfect.

Therefore, it can be concluded that the strategy is able to reproduce the flow regime, without using in-situ data, and results in a similar result as that achieved by using all three hydrological components for calibration. Through the modified Wapaba model, it is more feasible to simulate river discharge without in-situ measurement to get a largely satisfactory result.

One problem presented in Case c to Case f is that when calibrating on ETa and TWSA, the initial condition cannot be constrained effectively. In poorly gauged areas, the initial soil water storage and the initial groundwater can be assigned to inappropriate values. In these

cases, the too-large values of initial states lead to overestimation of discharge at the beginning of the study period.

Chapter 6

Conclusions and prospects

6-1 Research conclusions

The in-situ discharge time series has been used as the only measurement for hydrological model calibration in traditional methods for decades. An improved monthly water balance strategy that allows the absence of in-situ measurement and the usage of satellite data is a valuable tool for streamflow simulations and predictions in poorly gauged river basins. This study first demonstrates the effectiveness of the data fusion method in correcting data bias and errors as well as describing data uncertainty. Then, it tests the improvement in model performances brought by model structure modification and thus, confirms its ability to use fluxes other than river runoff for calibration.

This study takes the Smoky hill river basin as the study area. It incorporates the data fusion method so as to correct bias and errors in satellite data. When no uncertainty is used in modeling, the mean value time series of precipitation given by data fusion succeeds in improving discharge simulation, especially at low flow (TRMSE decreases from greater than 0.70 to 0.55). The error for each month in forcing data or measurements of discharge, actual evapotranspiration (ETa) and terrestrial water storage anomalies (TWSA) is described with a normal distribution. These distributions of precipitation values work as their ranges. The best input time series can be decided as a set of parameters when the loglikelihood of P reaches its maximum. Discharge simulation is further improved (TRMSE = 0.29). Estimates of the three fluxes with uncertainty can explain more than 31.28% simulated points in discharge and more than 64.93% simulated points in ETa.

The study also enables the model to use satellite data for modeling and produce satisfactory results indicating its potential in being applied in ungauged areas. The imperfect model structure is improved by adding a constraint to the recharge to groundwater. The idea comes from the comparison of sensitive parameters as well as the proportion of different water sources in total runoff. The modification effects are that the discharge ($TRMSE_Q$ drops from 1.44 to 0.88) and ETa (σ_E decreases from 4.76 to 4.53) simulation results are improved without severely deteriorating the performance of TWSA simulation (σ_S slightly

increase from 6.2517 to 6.7045). The study uses the original Wapaba model to simulate the three fluxes using parameters calibrated on all fluxes. The improved model is employed to simulate the discharge using parameters derived from calibration on ETa and TWSA. The effect of the improvement is that the latter experiment ($TRMSE_Q = 0.88$) achieves similar results as the former one ($TRMSE_Q = 0.85$) does.

6-2 Prospects for further study

The long-term goal is to fully benefit from the data fusion method and the relative strategy. The improved model in this paper inherits Wapaba models advantage of being straightforward, parsimonious and fast. The value of the added infiltration constant f_{max} can be easily determined through trial and error for different catchments. Being simple and highly comprehensible, technicians can quickly learn how to use it, so it is possible to apply and popularize this methodology widely. Besides, due to the exploitable structure, incorporating some extra modules and applying this methodology in catchments under other climate types is within the bounds of possibility. For instance, if adding a snowmelt water module and including more parameters like ground surface temperature (also accessible through satellite products), the methodology may be applicable in basins dominated by snow and snowmelt water.

The large drainage area of the study catchment may be one reason for the imperfect performances of lumped models. In this study, the methodology can only be applied in basins with large drainage areas since GRACE data requires basin area to be larger than 10000 km^2 . The inhomogeneity of precipitation distribution, underlying surface characteristics and river network characteristics in such a large catchment still affect the simulation accuracy significantly. Although the diversity of the catchment process in temporal and spatial scales can be expressed with the consumption curve to some extent. It is still difficult for a lumped conceptual model to represent hydrological processes in such a large basin. For instruction, precipitation with spatially distributed characteristics is regarded as a lumped input, which is clearly inconsistent with the actual situation that the rainfall-runoff system takes dispersed inputs and gives lumped runoff output. Fortunately, this disadvantage can be mitigated by downscaling GRACE data.

Additionally, the problem of inaccurate estimation of initial storage can be solved with the help of prior knowledge of the study area. Discharge is not sensitive to initial soil water storage and initial groundwater. Therefore, their values can be appropriated from adjacent similar watersheds with data. Another method is to assign initial state values to basins accordingly to climate types of study areas. For example, if the study pried starts in the dry season, the initial storage of an arid basin can be assigned as 0.

Lastly, the method does not take into account hydrological processes under changing conditions. Human activities/climate changing/influences of vegetation (growth period). To deal with problems like this, more efforts should be taken in future works for model structure improvement. One feasible method is to investigate parameters that change with climate or land cover change. Also, for areas affected greatly by human activities (i.e., reservoirs, cisterns, water diversions, rooftop water storage works and underground water cellar works), some virtual free water reservoirs (either for surface water or groundwater) can be added in the model to delineate the abrupt variations in fluxes.

Appendix A

Dataset information

This appendix exhibits first the annual peak flow for SMOKY HILL R AT ENTERPRISE (06877600) ("USGS 06877600 SMOKY HILL R AT ENTERPRISE, KS. USGS Water Resources", n.d.). Next, the record index of GRACE/GRACE-FO during the study period is provided.

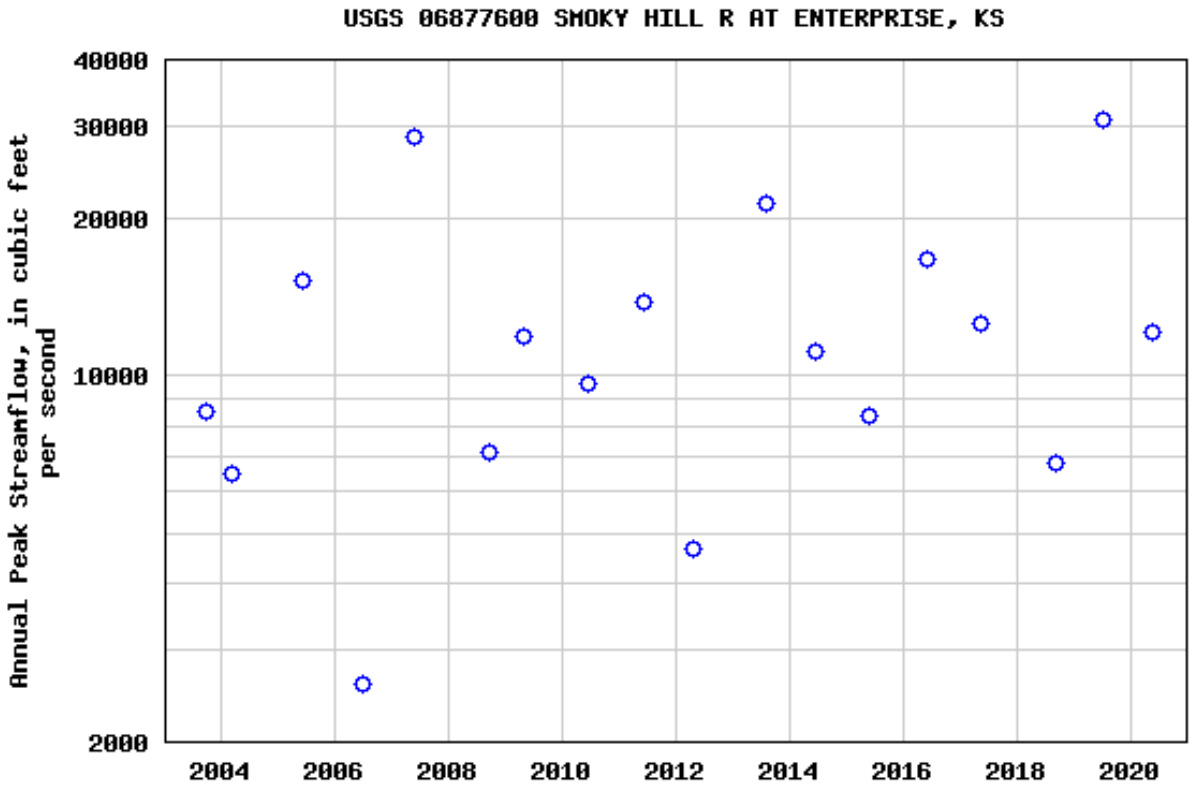

Figure A-1: Annual peak flow for 06877600 SMOKY HILL R AT ENTERPRISE, KS (Jan 1st 2003 to July 30th 2020)

Table A-1: Record index (RI) of GRACE/GRACE-FO during Jan 2003-July 2020

Year	Month	RI	Year	Month	RI	Year	Month	RI
2003	JAN	8	2008	DEC	78	2014	NOV	140
2003	FEB	9	2009	JAN	79	2014	DEC	NA
2003	MAR	10	2009	FEB	80	2015	JAN	141
2003	APR	11	2009	MAR	81	2015	FEB	142
2003	MAY	12	2009	APR	82	2015	MAR	143
2003	JUN	NA	2009	MAY	83	2015	APR	144
2003	JUL	13	2009	JUN	84	2015	MAY	145
2003	AUG	14	2009	JUL	85	2015	JUN	NA
2003	SEP	15	2009	AUG	86	2015	JUL	146
2003	OCT	16	2009	SEP	87	2015	AUG	147
2003	NOV	17	2009	OCT	88	2015	SEP	148
2003	DEC	18	2009	NOV	89	2015	OCT	NA
2004	JAN	19	2009	DEC	90	2015	NOV	NA
2004	FEB	20	2010	JAN	91	2015	DEC	149
2004	MAR	21	2010	FEB	92	2016	JAN	150
2004	APR	22	2010	MAR	93	2016	FEB	151
2004	MAY	23	2010	APR	94	2016	MAR	152
2004	JUN	24	2010	MAY	95	2016	APR	NA
2004	JUL	25	2010	JUN	96	2016	MAY	153
2004	AUG	26	2010	JUL	97	2016	JUN	154
2004	SEP	27	2010	AUG	98	2016	JUL	155
2004	OCT	28	2010	SEP	99	2016	AUG	156
2004	NOV	29	2010	OCT	100	2016	SEP	NA
2004	DEC	30	2010	NOV	101	2016	OCT	NA
2005	JAN	31	2010	DEC	102	2016	NOV	157
2005	FEB	32	2011	JAN	NA	2016	DEC	158
2005	MAR	33	2011	FEB	103	2017	JAN	159
2005	APR	34	2011	MAR	104	2017	FEB	NA
2005	MAY	35	2011	APR	105	2017	MAR	160
2005	JUN	36	2011	MAY	106	2017	APR	161
2005	JUL	37	2011	JUN	NA	2017	MAY	162
2005	AUG	38	2011	JUL	107	2017	JUN	163
2005	SEP	39	2011	AUG	108	2017	JUL	NA
2005	OCT	40	2011	SEP	109	2017	AUG	NA
2005	NOV	41	2011	OCT	110	2017	SEP	NA
2005	DEC	42	2011	NOV	111	2017	OCT	NA
2006	JAN	43	2011	DEC	112	2017	NOV	NA
2006	FEB	44	2012	JAN	113	2017	DEC	NA
2006	MAR	45	2012	FEB	114	2017	JAN	NA
2006	APR	46	2012	MAR	115	2017	FEB	NA
2006	MAY	47	2012	APR	116	2017	MAR	NA
2006	JUN	48	2012	MAY	NA	2017	APR	NA

Continued on next page

Table A-1 – *Continued from previous page*

Year	Month	RI	Year	Month	RI	Year	Month	RI
2006	JUL	49	2012	JUN	117	2017	MAY	NA
2006	AUG	50	2012	JUL	118	2018	JUN	164
2006	SEP	51	2012	AUG	119	2018	JUL	165
2006	OCT	52	2012	SEP	120	2018	AUG	NA
2006	NOV	53	2012	OCT	NA	2018	SEP	NA
2006	DEC	54	2012	NOV	121	2018	OCT	166
2007	JAN	55	2012	DEC	122	2018	NOV	167
2007	FEB	56	2013	JAN	123	2018	DEC	168
2007	MAR	57	2013	FEB	124	2019	JAN	169
2007	APR	58	2013	MAR	NA	2019	FEB	170
2007	MAY	59	2013	APR	125	2019	MAR	171
2007	JUN	60	2013	MAY	126	2019	APR	172
2007	JUL	61	2013	JUN	127	2019	MAY	173
2007	AUG	62	2013	JUL	128	2019	JUN	174
2007	SEP	63	2013	AUG	NA	2019	JUL	175
2007	OCT	64	2013	SEP	NA	2019	AUG	176
2007	NOV	65	2013	OCT	129	2019	SEP	177
2007	DEC	66	2013	NOV	130	2019	OCT	178
2008	JAN	67	2013	DEC	131	2019	NOV	179
2008	FEB	68	2014	JAN	132	2019	DEC	180
2008	MAR	69	2014	FEB	NA	2020	JAN	181
2008	APR	70	2014	MAR	133	2020	FEB	182
2008	MAY	71	2014	APR	134	2020	MAR	183
2008	JUN	72	2014	MAY	135	2020	APR	184
2008	JUL	73	2014	JUN	136	2020	MAY	185
2008	AUG	74	2014	JUL	NA	2020	JUN	186
2008	SEP	75	2014	AUG	137	2020	JUL	187
2008	OCT	76	2014	SEP	138			
2008	NOV	77	2014	OCT	139			

Appendix B

Water balance check

To check the water balance within the Wapaba model, the water balance equation is used. The figures below are the results of the water balance equation. When the result is equal to zero ($<10^{-5}$), the water balance in the model is considered to be met.

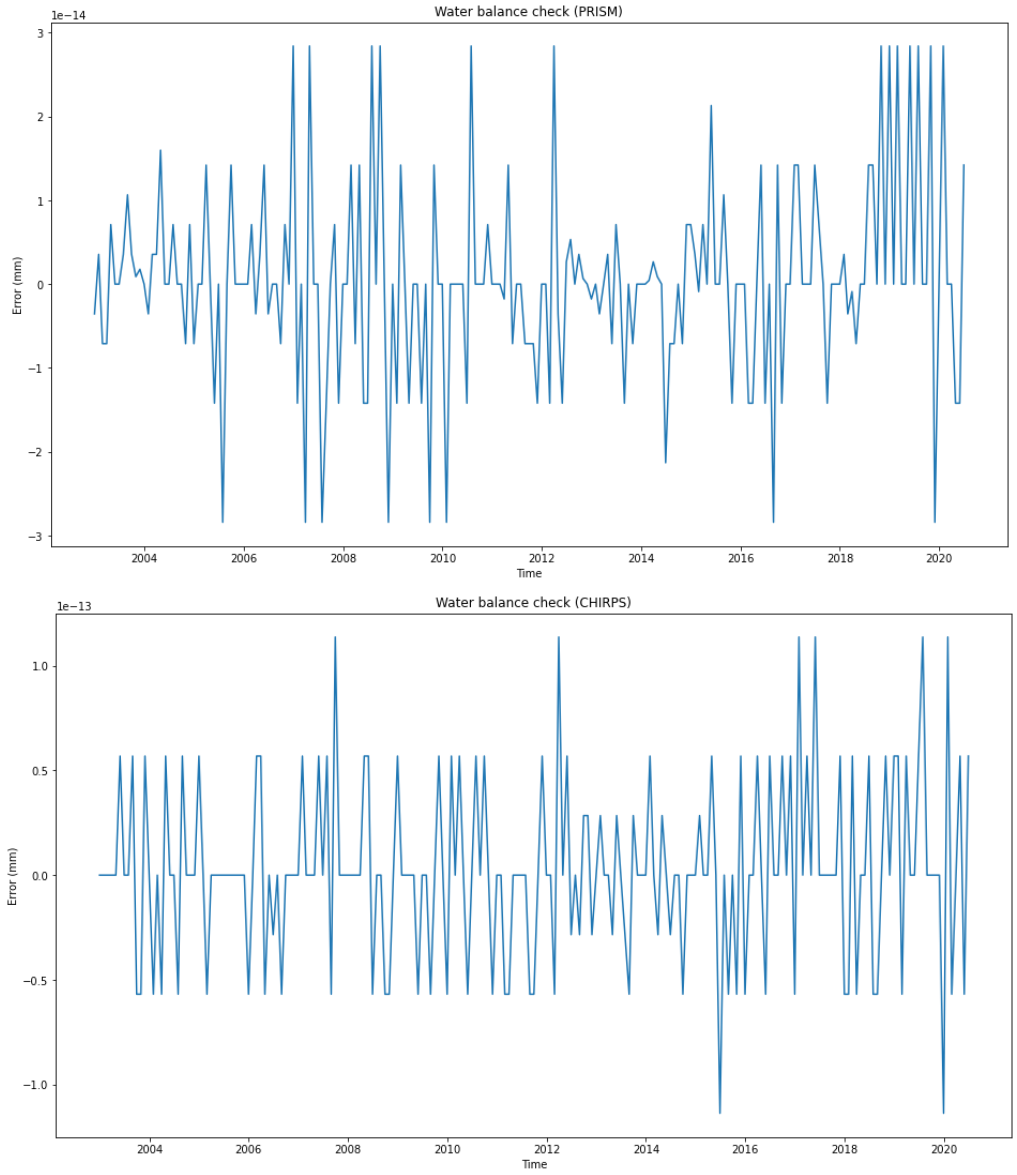

Figure B-1: Water balance check for simulation in Case a

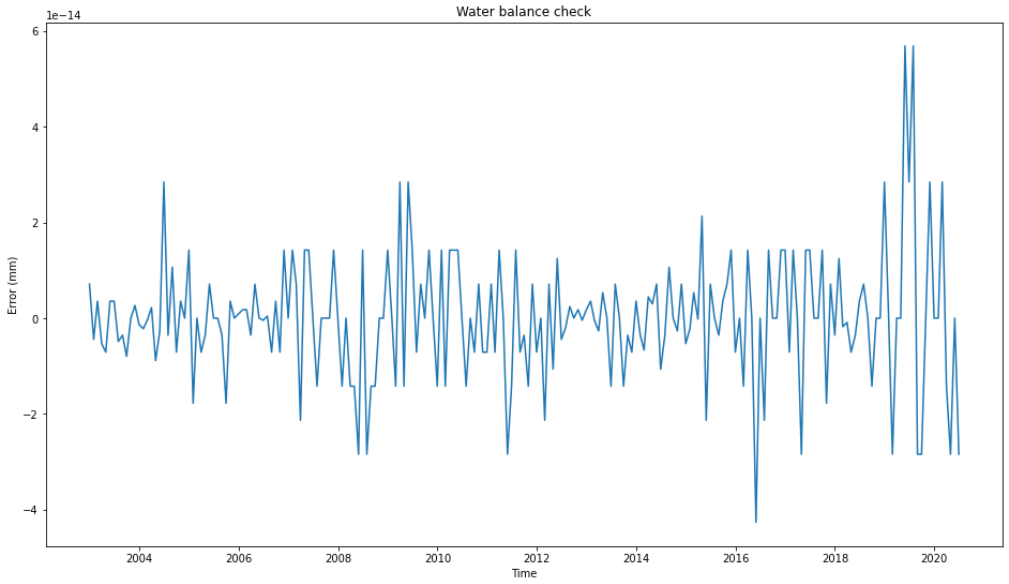

Figure B-2: Water balance check for simulation in Case b

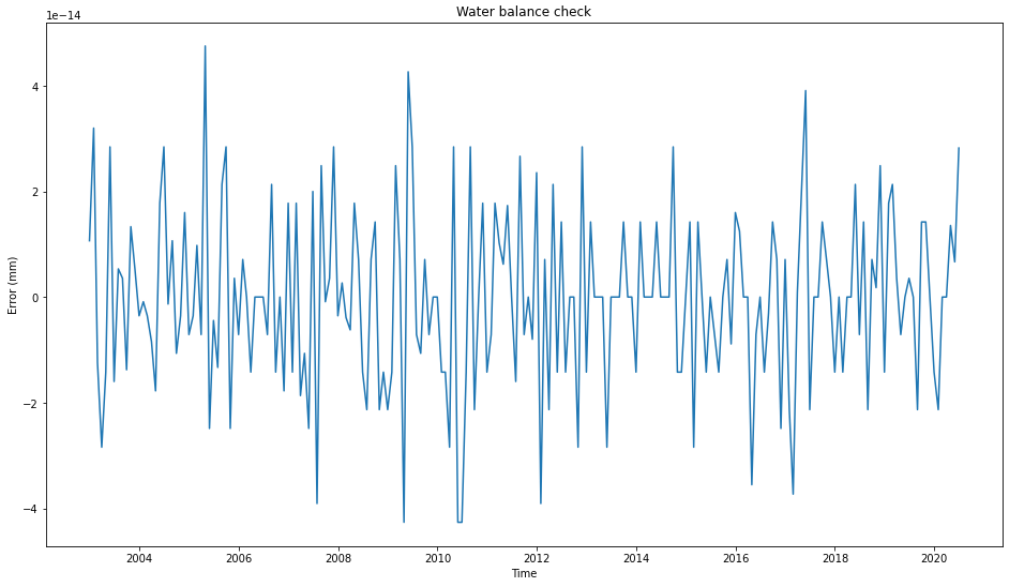

Figure B-3: Water balance check for simulation (Case c: parameters calibrated on ETa and TWSA)

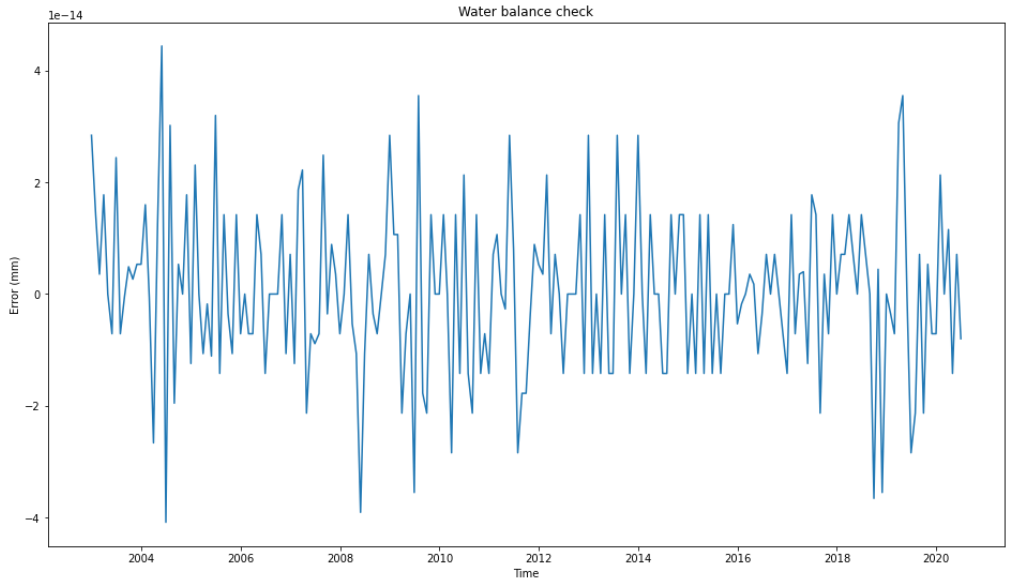

Figure B-4: Water balance check for simulation (Case d: parameters calibrated on ETa and TWSA)

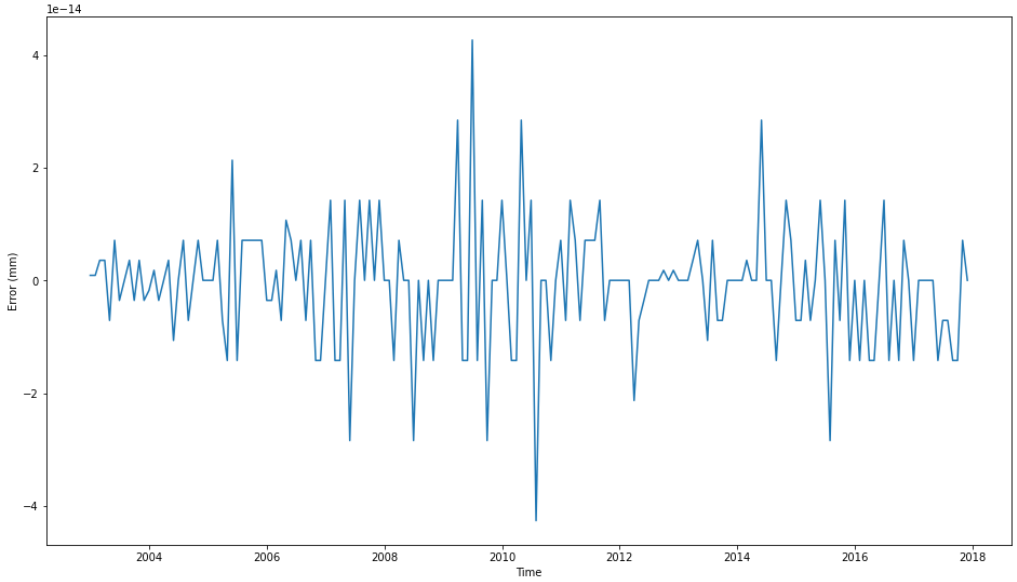

Figure B-5: Water balance check for simulation (Case f: parameters calibrated on ETa and TWSA using the improved model)

Appendix C

Other simulation results

Case d uses fluxes other than discharge for parameter calibration. Apart from results provided in Chapter 4, simulated results using parameter calibrated with only ETa and only TWSA are exhibited as follows.

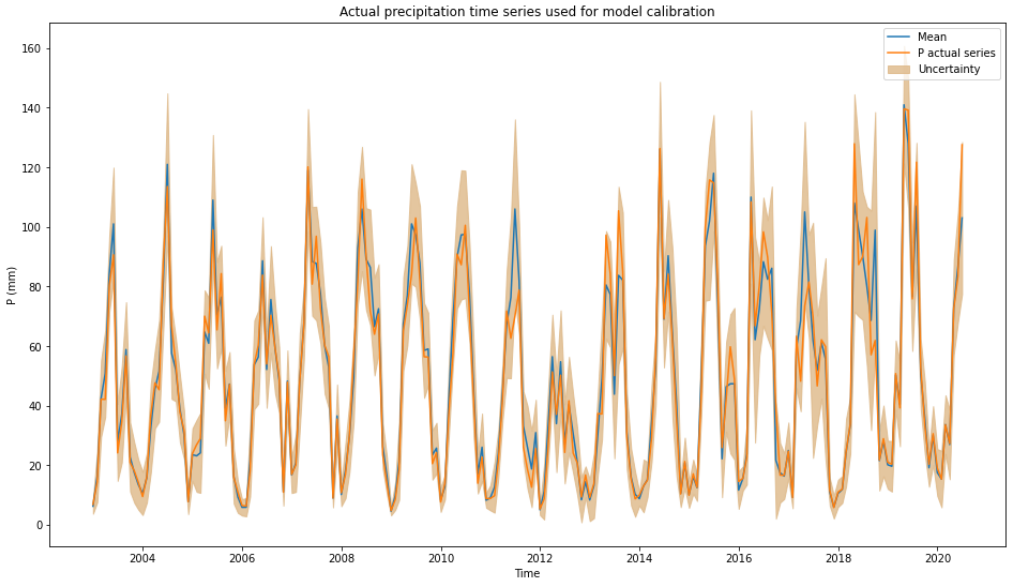

Figure C-1: The optimal precipitation input when using parameters calibrated with ETa

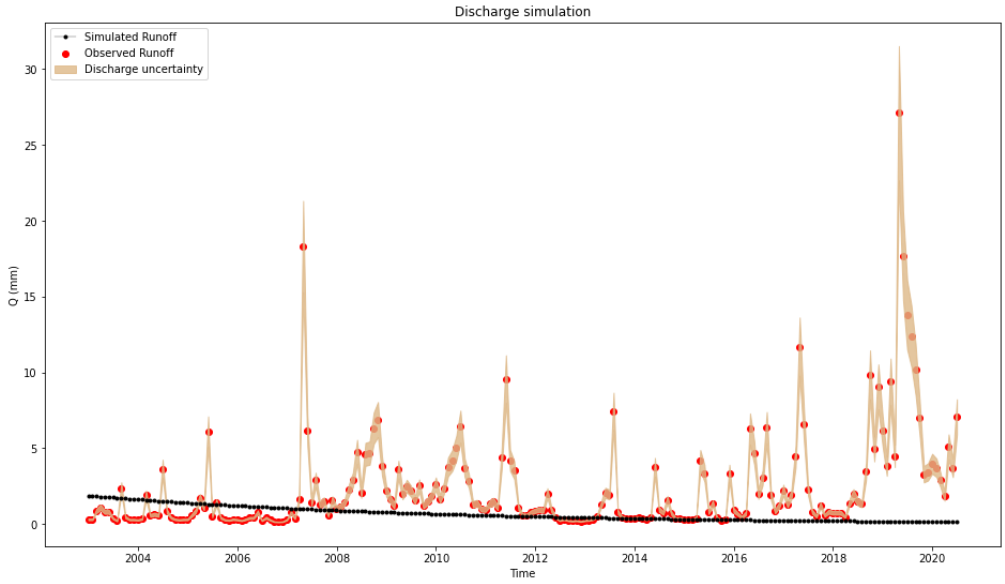

Figure C-2: Discharge simulation results using parameters calibrated with ETa

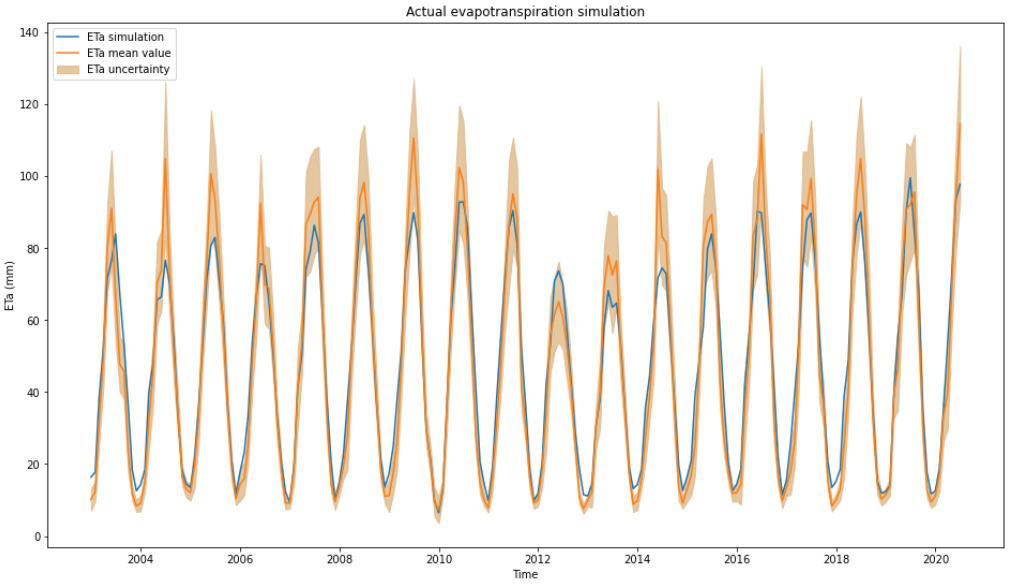

Figure C-3: ETa simulation results using parameters calibrated with ETa

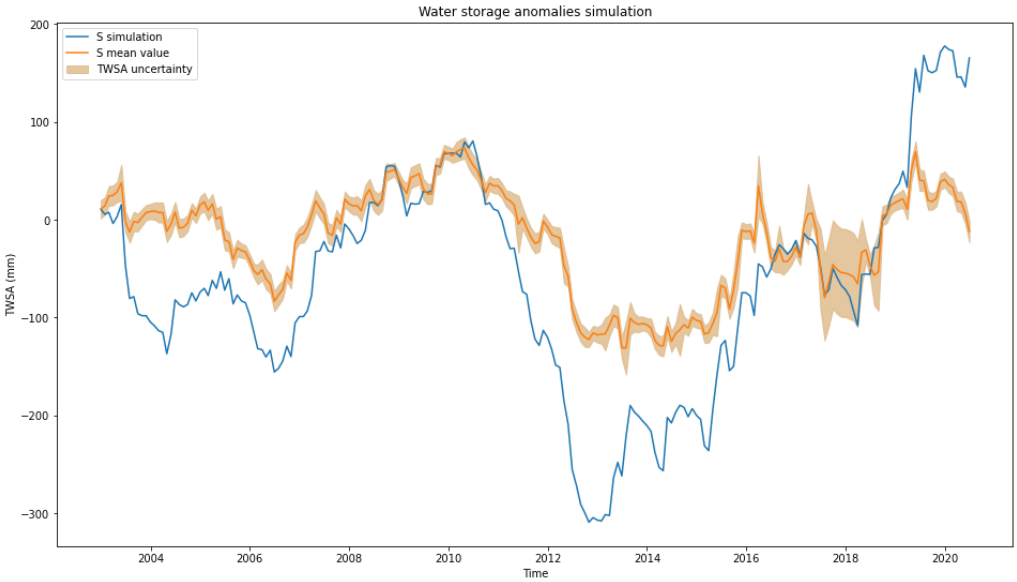

Figure C-4: TWSA simulation results using parameters calibrated with ETa

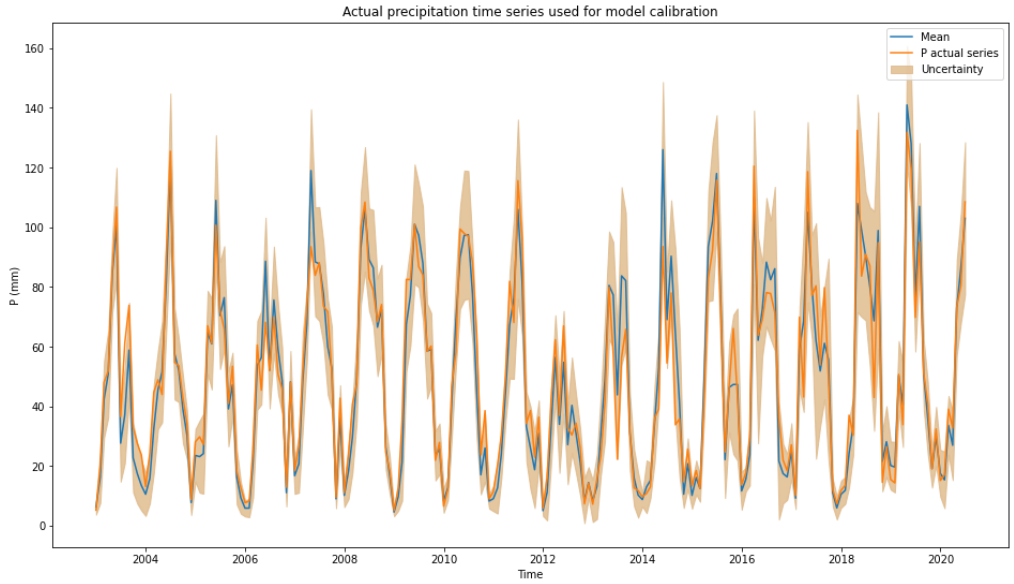

Figure C-5: The optimal precipitation input when using TWSA for calibration

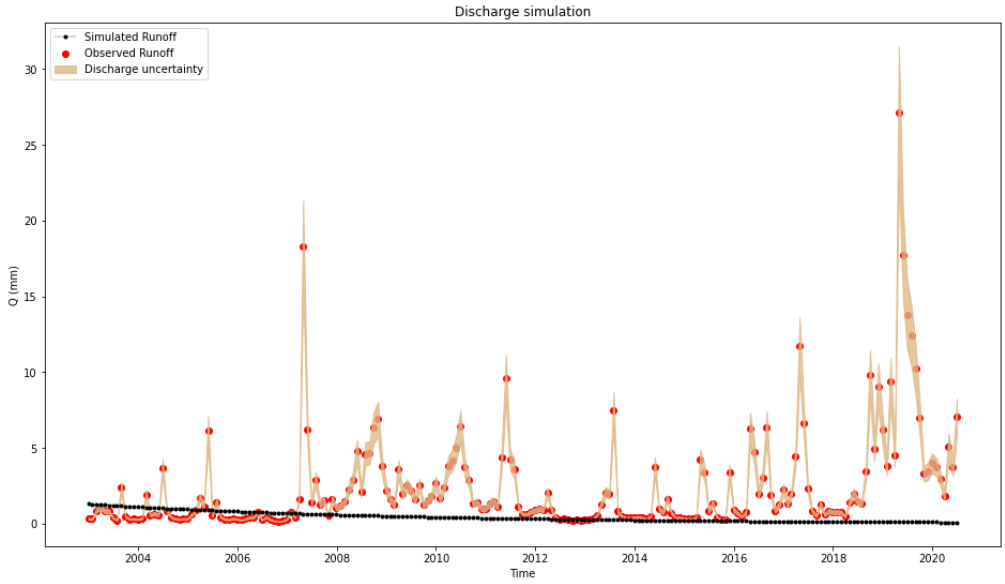

Figure C-6: Discharge simulation using TWSA for calibration

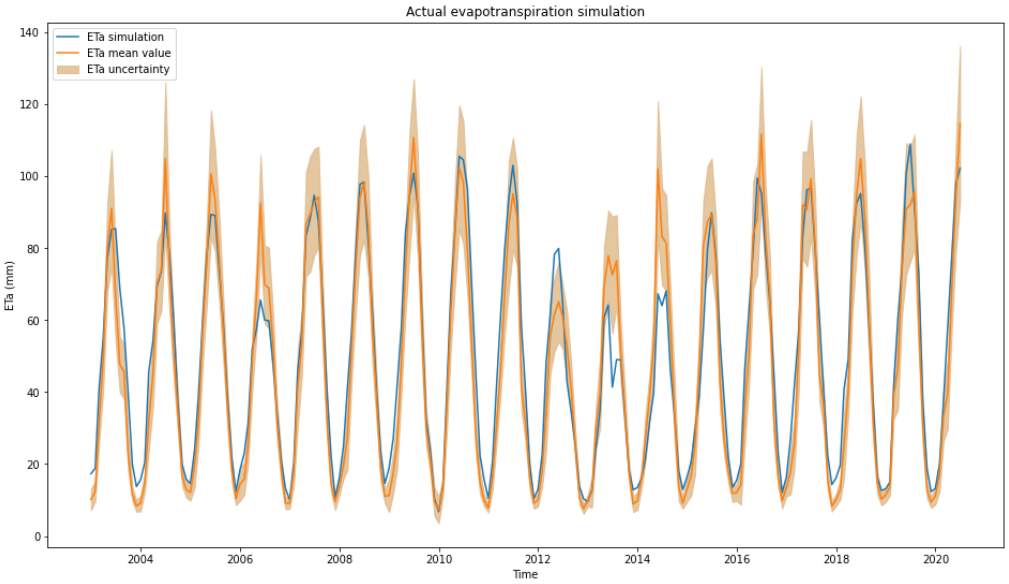

Figure C-7: ETa simulation using TWSA for calibration

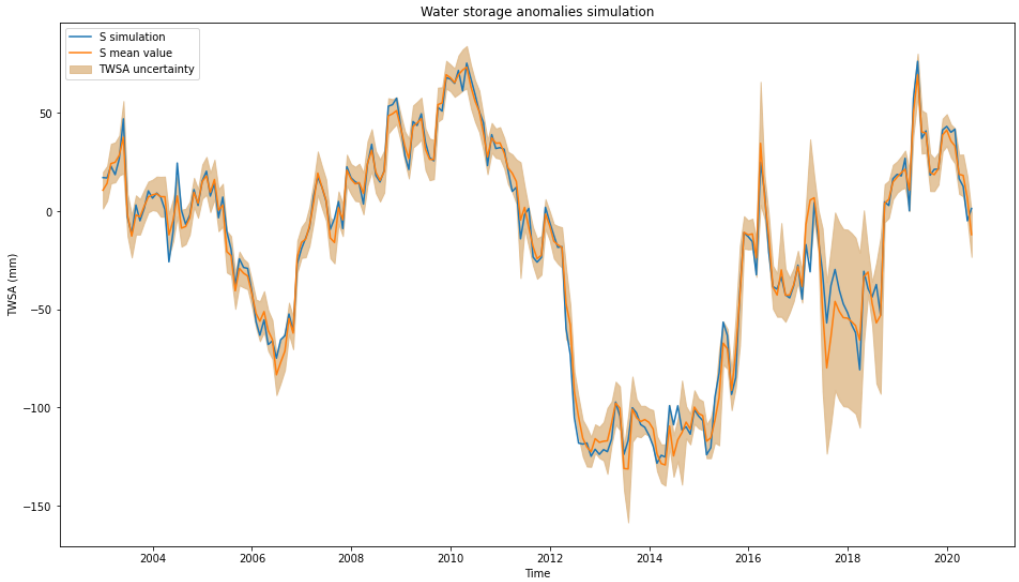

Figure C-8: TWSA simulation using TWSA for calibration

References

Abera, W., Formetta, G., Borga, M., & Rigon, R. (2017). Estimating the water budget components and their variability in a pre-alpine basin with jgrass-newage [Journal Article]. *Advances in Water Resources*, *104*, 37-54. Retrieved from https://www.scopus.com/inward/record.uri?eid=2-s2.0-85015793470&doi=10.1016%2fj.advwatres.2017.03.010&partnerID=40&md5=45aede70b11575296de3eb1020c63afa doi: 10.1016/j.advwatres.2017.03.010

Anyan, H., Shenglian, G., Lihua, X., & Jing, G. (2008). Three-parameter monthly water balance model and its application [Journal Article]. , *26(004), 8-10.*. doi: 10.3969/j.issn.1000-7709.2008.04.003

Azarderakhsh, M., Rossow, W. B., Papa, F., Norouzi, H., & Khanbilvardi, R. (2011). Diagnosing water variations within the amazon basin using satellite data [Journal Article]. *Journal of Geophysical Research Atmospheres*, *116*(24). Retrieved from https://www.scopus.com/inward/record.uri?eid=2-s2.0-84855303324&doi=10.1029%2f2011JD015997&partnerID=40&md5=87709646032ddb5d216960c86c230e09 doi: 10.1029/2011JD015997

Bai, P., Liu, X., & Liu, C. (2018). Improving hydrological simulations by incorporating grace data for model calibration [Journal Article]. *Journal of Hydrology*, *557*, 291-304. doi: 10.1016/j.jhydrol.2017.12.025

Bardossy, A. (2007). Calibration of hydrological model parameters for ungauged catchments [Journal Article]. *Hydrology and Earth System Sciences*, *11,2(2007-01-17), 11(2), 703-710*. doi: 10.5194/hess-11-703-2007

Bennett, J., & Wang, Q. (2017). Seasonal streamflow forecasting in ungauged catchments: a review [Journal Article]. *CSIRO, Australia*.

Bennett, J., Wang, Q., Schepen, A., Robertson, D., & Li, M. (2015). Improving the fogss system: generating streamflow forecasts beyond 3 months [Journal Article]. *CSIRO Water for a Healthy Country Flagship, Australia*.

Blasone, R.-S., Vrugt, J. A., Madsen, H., Rosbjerg, D., Robinson, B. A., & Zyvoloski, G. A. (2008). Generalized likelihood uncertainty estimation (glue) using adaptive markov chain monte carlo sampling [Journal Article]. *Advances in Water Resources*, *31*(4), 630-648. doi: 10.1016/j.advwatres.2007.12.003

Bock, A. R., Hay, L. E., McCabe, G. J., Markstrom, S. L., & Atkinson, R. D. (2016). Parameter regionalization of a monthly water balance model for the conterminous united states [Journal Article]. *Hydrology and Earth System Sciences*, *20*(7), 2861-2876. doi: 10.5194/hess-20-2861-2016

Cao, W., Bowden, W. B., Davie, T., & Fenemor, A. (2006). Multi-variable and multi-site calibration and validation of swat in a large mountainous catchment with high spatial variability [Journal Article]. *Hydrological Processes*, *20*(5), 1057-1073. doi: 10.1002/hyp.5933

Chaplin, S., Cook, T., Dinerstein, E., Simms, P., & Carney, K. (n.d.). Central and southern mixed grasslands | ecoregions | wwf. (n.d.) [Journal Article]. *World Wildlife Fund. Retrieved September 25, 2021, from https://www.worldwildlife.org/ecoregions/na0803*.

Climate [Journal Article]. (2013). *The Central Peoples Government of the Peoples Republic of China*, http://www.gov.cn/test/2005-07/27/content$_1$7402.*htm*.

da Silva, M. G., de Aguiar Netto, A. d. O., de Jesus Neves, R. J., do Vasco, A. N., Almeida, C., & Faccioli, G. G. (2015). Sensitivity analysis and calibration of hydrological modeling of the watershed northeast brazil [Journal Article]. *Journal of Environmental Protection*, *06*(08), 837-850. doi: 10.4236/jep.2015.68076

Falck, A. S., Maggioni, V., Tomasella, J., Vila, D. A., & Diniz, F. L. R. (2015). Propagation of satellite precipitation uncertainties through a distributed hydrologic model: A case study in the tocantinsaraguaia basin in brazil [Journal Article]. *Journal of Hydrology*, *527*, 943-957. doi: 10.1016/j.jhydrol.2015.05.042

Falcone, J. (2011). Gages-ii: Geospatial attributes of gages for evaluating streamflow [Journal Article]. *U.S. Geological Survey*.

Famiglietti, J. S., & Rodell, M. (2013). Water in the balance [Journal Article]. *Science*, *340*(6138), 1300-1301. Retrieved from https://www.scopus.com/inward/record.uri?eid=2-s2.0-84878940540&doi=10.1126%2fscience.1236460&partnerID=40&md5=1ebd9205fa5c2d4819e3dfa29c93a561 doi: 10.1126/science.1236460

Ferreira, P. M. d. L., Paz, A. R. d., & Bravo, J. M. (2020). Objective functions used as performance metrics for hydrological models: state-of-the-art and critical analysis [Journal Article]. *Rbrh*, *25*. doi: 10.1590/2318-0331.252020190155

Ferreira, V., Gong, Z., He, X., Zhang, Y., & AndamAkorful, S. (2013). Estimating total discharge in the yangtze river basin using satellite-based observations [Journal Article]. *Remote Sensing*, *5*(7), 3415-3430. doi: 10.3390/rs5073415

Forman, B. A., Reichle, R. H., & Rodell, M. (2012). Assimilation of terrestrial water storage from grace in a snow-dominated basin [Journal Article]. *Water Resources Research*, *48*(1). Retrieved from https://www.scopus.com/inward/record.uri?eid=2-s2.0-84856013055&doi=10.1029%2f2011WR011239&partnerID=40&md5=e1cfd224acc0ca494c414ff811ee3cf8 doi: 10.1029/2011WR011239

Funk, C., Peterson, P., Landsfeld, M., Pedreros, D., Verdin, J., Shukla, S., ... Michaelsen, J. (2015). The climate hazards infrared precipitation with stations - a new environmental record for monitoring extremes [Journal Article]. *Scientific Data*, *2*. Retrieved from https://www.scopus.com/inward/record.uri?eid=2-s2.0-84961120091&doi=10.1038%2fsdata.2015.66&partnerID=40&md5=d94ac51fea6314b27c45c55128a23b05 doi: 10.1038/sdata.2015.66

Georgioudakis, M., & Plevris, V. (2020). A comparative study of differential evolution variants in constrained structural optimization [Journal Article]. *Front. Built Environ.*. doi: https://doi.org/10.3389/fbuil.2020.00102

Green, G. (1992). The digital geologic map of colorado in arc/info format: U.s. geological survey open-file report [Journal Article]. , 92-0507, 9 p.; http://pubs.usgs.gov/of/1992/ofr-92-0507/.

Hadachek, A. G. (2019). Flooding continues and spreads to more states as snow melts and rain falls [Journal Article]. *The Fence Post | Flooding Continues and Spreads to More States as Snow Melts and Rain Falls*, https://www.thefencepost.com/news/flooding-continues-and-spreads-to-more-states-as-snow-melts-and-rain-falls/.

Hallema, D., & Moussa, R. (2009). A multi-criteria parameterisation strategy for the hydrological modelling of storm events in an agricultural catchment [Journal Article].

Hiep, N. H., Luong, N. D., Viet Nga, T. T., Hieu, B. T., Thuy Ha, U. T., Du Duong, B., ... Lee, H. (2018). Hydrological model using ground- and satellite-based data for river flow simulation towards supporting water resource management in the red river basin, vietnam [Journal Article]. *Journal of Environmental Management*, *217*, 346-355. Retrieved from https://www.scopus.com/inward/record.uri?eid=2-s2.0-85055844350&doi=10.1016%2fj.jenvman.2018.03.100&partnerID=40&md5=8d43dd5df1b7690b997eb13e489b7d6e doi: 10.1016/j.jenvman.2018.03.100

Immerzeel, W. W., & Droogers, P. (2008). Calibration of a distributed hydrological model based on satellite evapotranspiration [Journal Article]. *Journal of Hydrology*, *349*(3-4), 411-424. Retrieved from https://www.scopus.com/inward/record.uri?eid=2-s2.0-38349075022&doi=10.1016%2fj.jhydrol.2007.11.017&partnerID=40&md5=aa2ecb24be3c9f674c6c354237324055 doi: 10.1016/j.jhydrol.2007.11.017

Jeremiah, E., Sisson, S., Marshall, L., Mehrotra, R., & Sharma, A. (2011). Bayesian calibration and uncertainty analysis of hydrological models: A comparison of adaptive metropolis and sequential monte carlo samplers [Journal Article]. *Water Resources Research*, *47*(7). doi: 10.1029/2010wr010217

Jiang, D., & Wang, K. (2019). The role of satellite-based remote sensing in improving simulated streamflow: A review [Journal Article]. *Water (Switzerland)*, *11*(8). Retrieved from https://www.scopus.com/inward/record.uri?eid=2-s2.0-85070288045&doi=10.3390%2fw11081615&partnerID=40&md5=142a934e0855ad07ffa603cd34632227 doi: 10.3390/w11081615

John, A., Fowler, K., Nathan, R., Horne, A., & Stewardson, M. (2021). Disaggregated monthly hydrological models can outperform daily models in providing daily flow statistics and extrapolate well to a drying climate [Journal Article]. *Journal of Hydrology*, *598*. doi: 10.1016/j.jhydrol.2021.126471

Landerer, F. W., Flechtner, F. M., Save, H., Webb, F. H., Bandikova, T., Bertiger, W. I., & al, e. (2020). Extending the global mass change data record: Grace followon instrument and science data performance [Journal Article]. *Geophysical Research Letters*, , *47*, *e2020GL088306*. doi: https://doi.org/10.1029/2020GL088306

Li, M., Wang, Q. J., & Bennett, J. (2013). Accounting for seasonal dependence in hydrological model errors and prediction uncertainty [Journal Article]. *Water Resources Research*, *49*(9), 5913-5929. doi: 10.1002/wrcr.20445

LIU, J.-t., & ZHANG, J.-b. (2006). Effect of antecedent soil water content on the uncertainty of hydrological simulation [Journal Article]. *Journal of Glaciology and Geocryology*, *028(004)*, 519-525. doi: 10.3969/j.issn.1000-0240.2006.04.009

Lo, M. H., Famiglietti, J. S., Yeh, P. J. F., & Syed, T. H. (2010). Improving pa-

rameter estimation and water table depth simulation in a land surface model using grace water storage and estimated base flow data [Journal Article]. *Water Resources Research*, *46*(5). Retrieved from https://www.scopus.com/inward/record.uri?eid=2-s2.0-85018194023&doi=10.1029%2f2009WR007855&partnerID=40&md5=4d0f43853151a2b65456bc278381f7b2 doi: 10.1029/2009WR007855

Long, D., Longuevergne, L., & Scanlon, B. R. (2014). Uncertainty in evapotranspiration from land surface modeling, remote sensing, and grace satellites [Journal Article]. *Water Resources Research*, *50*(2), 1131-1151. Retrieved from https://www.scopus.com/inward/record.uri?eid=2-s2.0-84893675286&doi=10.1002%2f2013WR014581&partnerID=40&md5=8bae0e0d644c46c30271f11967b1b8ed doi: 10.1002/2013WR014581

Lu, Z., Zou, S., Xiao, H., Zheng, C., Yin, Z., & Wang, W. (2015). Comprehensive hydrologic calibration of swat and water balance analysis in mountainous watersheds in northwest china [Journal Article]. *Physics and Chemistry of the Earth*, *79-82*, 76-85. Retrieved from https://www.scopus.com/inward/record.uri?eid=2-s2.0-84931009802&doi=10.1016%2fj.pce.2014.11.003&partnerID=40&md5=c301d8450e4a502a6f7d7925c6cc356e doi: 10.1016/j.pce.2014.11.003

López, P. L., Sutanudjaja, E. H., Schellekens, J., Sterk, G., & Bierkens, M. F. P. (2017). Calibration of a large-scale hydrological model using satellite-based soil moisture and evapotranspiration products [Journal Article]. *Hydrology and Earth System Sciences*, *21*(6), 3125-3144. Retrieved from https://www.scopus.com/inward/record.uri?eid=2-s2.0-85021648829&doi=10.5194%2fhess-21-3125-2017&partnerID=40&md5=2f46b05a14a31c499016d84173d1f4e8 doi: 10.5194/hess-21-3125-2017

Ma, J., & Chen, G. S. (2014). Analysis and application of parameter uncertainty of xin 'anjiang river model based on glue. [glue] [Journal Article]. *(2)*, 46-49.

Miralles, D., Holmes, T., de Jeu, R., Gash, J., Meesters, A., & Dolman, A. (2011). Global land-surface evaporation estimated from satellite-based observations [Journal Article]. *Hydrology and Earth System Sciences*(The current v3.5 datasets have been produced by Dr. Akash Koppa and Dr. Dominik Rains.), 15, 453469. doi: 10.5194/hess-15-453-2011

Moradkhani, H., Hsu, K., Hong, Y., & Sorooshian, S. (2006). Investigating the impact of remotely sensed precipitation and hydrologic model uncertainties on the ensemble streamflow forecasting [Journal Article]. *Geophysical Research Letters*, *33*(12). doi: 10.1029/2006gl026855

Moreira, A. A., Ruhoff, A. L., Roberti, D. R., Souza, V. D. A., da Rocha, H. R., & de Paiva, R. C. D. (2019). Assessment of terrestrial water balance using remote sensing data in south america [Journal Article]. *Journal of Hydrology*, *575*, 131-147. Retrieved from https://www.scopus.com/inward/record.uri?eid=2-s2.0-85066110539&doi=10.1016%2fj.jhydrol.2019.05.021&partnerID=40&md5=a665b74b56734c40ebb1a5cb234af6af doi: 10.1016/j.jhydrol.2019.05.021

Muthuwatta, L. P., Booij, M. J., Rientjes, T. H. M., Bos, M. G., Gieske, A. S. M., & Ahmad, M. U. D. (2009). Calibration of a semi-distributed hydrological model using discharge and remote sensing data [Conference Proceedings]. In (Vol. 333, p. 52-58). Retrieved from https://www.scopus.com/inward/record.uri?eid=2-s2.0-78751672103&partnerID=40&md5=0ad63c1ad61ba193ffe8f81ba18329ab

Muvundja, F. A., Wüest, A., Isumbisho, M., Kaningini, M. B., Pasche, N., Rinta, P., & Schmid, M. (2014). Modelling lake kivu water level variations over the last seven

decades [Journal Article]. *Limnologica*, *47*, 21-33. doi: 10.1016/j.limno.2014.02.003

Noaas 19812010 climate normals. (n.d.) [Journal Article]. (n.d.). *National Centers for Environmental Information (NCEI) Formerly Known as National Climatic Data Center (NCDC)*. Retrieved from https://www.ncdc.noaa.gov/oa/climate/normals/usnormals.html

Pagano, T. C., Hapuarachchi, P., & Wang, Q. J. (2009). Development and testing of a multi-model rainfall-runoff streamflow forecasting application [Journal Article]. *CSIRO: Water for a Healthy Country National Research Flag*. Retrieved from https://www.researchgate.net/publication/255738174_Development_and_testing_of_a_multi-model_rainfall-runoff_streamflow_forecasting_application

Pokhrel, P., Robertson, D. E., & Wang, Q. J. (2013). A bayesian joint probability post-processor for reducing errors and quantifying uncertainty in monthly streamflow predictions [Journal Article]. *Hydrology and Earth System Sciences*, *17(2)*, 795-804. doi: 10.5194/hessd-9-11199-2012

Prism climate group [Journal Article]. (2021). *Oregon State University. http://prism.oregonstate.edu, created 2 June 2021.*.

Qing-fang, H., WANGYin-tang, Ke-lin, L., & Zong-zhi, W. (2007). Monthly runoff simulation based on improved two-parameter monthly water volume balance model [Journal Article]. *Journal of Hohai University(Natural Sciences)*, *35 6 2007 11* . doi: CNKI:SUN:HHDX.0.2007-06-007

Rajib, A., Evenson, G. R., Golden, H. E., & Lane, C. R. (2018). Hydrologic model predictability improves with spatially explicit calibration using remotely sensed evapotranspiration and biophysical parameters [Journal Article]. *Journal of Hydrology*, *567*, 668-683. doi: 10.1016/j.jhydrol.2018.10.024

Razavi, S., & Gupta, H. V. (2015). What do we mean by sensitivity analysis? the need for comprehensive characterization of global sensitivity in earth and environmental systems models [Journal Article]. *Water Resources Research*, *51*(5), 3070-3092. doi: 10.1002/2014wr016527

Rientjes, T. H. M., Muthuwatta, L. P., Bos, M. G., Booij, M. J., & Bhatti, H. A. (2013). Multi-variable calibration of a semi-distributed hydrological model using streamflow data and satellite-based evapotranspiration [Journal Article]. *Journal of Hydrology*, *505*, 276-290. Retrieved from https://www.scopus.com/inward/record.uri?eid=2-s2.0-84886399520&doi=10.1016%2fj.jhydrol.2013.10.006&partnerID=40&md5=0abccec74d52294263f62c4323cc3a66 doi: 10.1016/j.jhydrol.2013.10.006

Ross, J. A. (1992). A digital representation of the geological map of kansas: Kansas geological survey, map m-23 scale 500,000, http://gisdasc.kgs.ku.edu/ [Journal Article].

Sahoo, A. K., Pan, M., Troy, T. J., Vinukollu, R. K., Sheffield, J., & Wood, E. F. (2011). Reconciling the global terrestrial water budget using satellite remote sensing [Journal Article]. *Remote Sensing of Environment*, *115*(8), 1850-1865. Retrieved from https://www.scopus.com/inward/record.uri?eid=2-s2.0-79957587195&doi=10.1016%2fj.rse.2011.03.009&partnerID=40&md5=adeea347914358eb4e8d6f6b3a348323 doi: 10.1016/j.rse.2011.03.009

Schoups, G. (December, 2018). Likelihood-based calibration of hydrological models.

Schoups, G., & Nasseri, M. (2020). Gracefully closing the water balance: a data-driven probabilistic approach applied to river basins in iran [Journal Article]. *Earth and Space Science Open Archive*. doi: 10.1002/essoar.10504775.1

Senay, G. B., & Kagone, S. (2019). Daily ssebop evapotranspiration: U. s. geological survey data release [Journal Article]. doi: https://doi.org/10.5066/P9L2YMV

Sheffield, J., Ferguson, C. R., Troy, T. J., Wood, E. F., & McCabe, M. F. (2009). Closing the terrestrial water budget from satellite remote sensing [Journal Article]. *Geophysical Research Letters*, *36*(7). Retrieved from https://www.scopus.com/inward/record.uri?eid=2-s2.0-67549115197&doi=10.1029%2f2009GL037338&partnerID=40&md5=7ab8c4afc22033cdefa2c73379885e8dhttps://agupubs.onlinelibrary.wiley.com/doi/pdfdirect/10.1029/2009GL037338?download=true doi: 10.1029/2009GL037338

Smoky-saline river basin total maximum daily load [Journal Article]. (n.d.). *Kansas Department of Health Environment*, *Waterbody: Smoky Hill River, Salina to Junction City Water Quality Impairment: Total Phosphorous. (n.d.)*, Retrieved September 21, 2021, from https://www.kdheks.gov/.

Storn, R., & Price, K. (1997). Differential evolution a simple and efficient heuristic for global optimization over continuous spaces [Journal Article]. *Journal of Global Optimization 11*, 341359. doi: https://doi.org/10.1023/A:1008202821328

Sun, A. Y., Green, R., Swenson, S., & Rodell, M. (2012). Toward calibration of regional groundwater models using grace data [Journal Article]. *Journal of Hydrology*, *422-423*, 1-9. Retrieved from https://www.scopus.com/inward/record.uri?eid=2-s2.0-84856406533&doi=10.1016%2fj.jhydrol.2011.10.025&partnerID=40&md5=fad3455f85ac331f69c900273752872f doi: 10.1016/j.jhydrol.2011.10.025

Tangdamrongsub, N., Steele-Dunne, S. C., Gunter, B. C., Ditmar, P. G., Sutanudjaja, E. H., Sun, Y., ... Wang, Z. (2017). Improving estimates of water resources in a semi-arid region by assimilating grace data into the pcr-globwb hydrological model [Journal Article]. *Hydrology and Earth System Sciences*, *21*(4), 2053-2074. Retrieved from https://www.scopus.com/inward/record.uri?eid=2-s2.0-85018493477&doi=10.5194%2fhess-21-2053-2017&partnerID=40&md5=badd39350c6ec6e96bd329538e705aac doi: 10.5194/hess-21-2053-2017

Tian, S., Tregoning, P., Renzullo, L. J., van Dijk, A. I. J. M., Walker, J. P., Pauwels, V. R. N., & Allgeyer, S. (2017). Improved water balance component estimates through joint assimilation of grace water storage and smos soil moisture retrievals [Journal Article]. *Water Resources Research*, *53*(3), 1820-1840. Retrieved from https://www.scopus.com/inward/record.uri?eid=2-s2.0-85014272734&doi=10.1002%2f2016WR019641&partnerID=40&md5=aee37fcdb3c4f1e845f3563b6cb8d8ed doi: 10.1002/2016WR019641

Us census bureau. [Journal Article]. (2021, October 8). *Cartographic Boundary Files - Shapefile. Census.Gov. Retrieved December 12, 2021, from https://www.census.gov/geographies/mapping-files/time-series/geo/carto-boundary-file.html*.

Usdas national agricultural statistics service kansas field office (part of the northern plains regional field office) [Journal Article]. (2021, September 15). *United States Department of Agriculture National Agricultural Statistics Service*. Retrieved from https://www.nass.usda.gov/Statistics_by_State/Kansas/Publications/County_Estimates/index.php

U.s. geological survey [Journal Article]. (2018). *3D Elevation Program 1-Meter Resolution*

Digital Elevation Model (published 20180618), accessed November 13, 2021. Retrieved from https://apps.nationalmap.gov/services/

Usgs 06877600 smoky hill r at enterprise, ks. usgs water resources [Journal Article]. (n.d.). *U.S. Department of the Interior, U.S. Geological Survey. (n.d.)*, Retrieved September 21, 2021, from https://waterdata.usgs.gov/nwis/inventory/?site$_no$ = 06877600.

van Griensven, A., Meixner, T., Grunwald, S., Bishop, T., Diluzio, M., & Srinivasan, R. (2006). A global sensitivity analysis tool for the parameters of multi-variable catchment models [Journal Article]. *Journal of Hydrology*, *324*(1-4), 10-23. doi: 10.1016/j.jhydrol.2005.09.008

Wagener, T., van Werkhoven, K., Reed, P., & Tang, Y. (2009). Multiobjective sensitivity analysis to understand the information content in streamflow observations for distributed watershed modeling [Journal Article]. *Water Resources Research*, *45*(2). doi: 10.1029/2008wr007347

Wang, Q. J., Pagano, T. C., Zhou, S. L., Hapuarachchi, H. A. P., Zhang, L., & Robertson, D. E. (2011). Monthly versus daily water balance models in simulating monthly runoff [Journal Article]. *Journal of Hydrology*, *404*(3-4), 166-175. doi: 10.1016/j.jhydrol.2011.04.027

Watkins, M. M., Wiese, D. N., Yuan, D.-N., Boening, C., & Landerer, F. W. (2015). Improved methods for observing earths time variable mass distribution with grace using spherical cap mascons [Journal Article]. *J. Geophys. Res. Solid Earth*, 120. doi: 10.1002/2014JB011547

Wei, Z. (2017). Study on the influence of uncertainty of input data on the simulation results of hydrological model-taking the swat model as an example [Journal Article]. *(Doctoral dissertation)*. doi: CNKI:CDMD:2.1017.126053

Wiese, D. N., Landerer, F. W., & Watkins, M. M. (2016). Quantifying and reducing leakage errors in the jpl rl05m grace mascon solution [Journal Article]. *Water Resour. Res.*, *52*, 74907502. doi: 10.1002/2016WR019344

Wiese, D. N., Yuan, D.-N., Boening, C., Landerer, F. W., & Watkins, M. M. (2018). Jpl grace mascon ocean, ice, and hydrology equivalent water height release 06 coastal resolution improvement (cri) [Journal Article]. *Filtered Version 1.0. Ver. 1.0. PO.DAAC, CA, USA. Dataset accessed [2021-06-15] at http://dx.doi.org/10.5067/TEMSC-3MJC6*.

Xu, C. Y., & Singh, V. P. (1998). A review on monthly water balance models for water resources investigations [Journal Article]. *Water Resources Management*, *12*(1), 31-50.

Xu, Y. M., Lin, K. R., & Li, P. J. (2015). Parameter uncertainty analysis of hymod model based on bayesian method. [hymod]. [Journal Article]. , *036(004)*, 1-4. doi: 10.3969/j.issn.1001-9235.2015.04.001

Yang, A. H. (2007). Hydrological modelling of the chaohe basin in china: statistical model formulation and bayesian inference [Journal Article]. *Journal of Hydrology*. doi: 10.1016/j.jhydrol.2007.04.006

Yassin, F., Razavi, S., Wheater, H., Sapriza-Azuri, G., Davison, B., & Pietroniro, A. (2017). Enhanced identification of a hydrologic model using streamflow and satellite water storage data: A multicriteria sensitivity analysis and optimization approach [Journal Article]. *Hydrological Processes*, *31*(19), 3320-3333. Retrieved from https://www.scopus.com/inward/record.uri?eid=2-s2.0-85028320786&doi=10.1002%2fhyp.11267&partnerID=40&md5=c32cae387315f51010176de498f2aa7c doi: 10.1002/hyp.11267

Yu, S. (2015). Time instability of hydrological model parameters under changing environ-

ment[] [Journal Article]. *Doctoral Dissertation, Tsinghua University*.

Zaitchik, B. F., Rodell, M., & Olivera, F. (2010). Evaluation of the global land data assimilation system using global river discharge data and a source-to-sink routing scheme [Journal Article]. *Water Resources Research*, *46*(6). Retrieved from https://www.scopus.com/inward/record.uri?eid=2-s2.0-77954399216&doi=10.1029%2f2009WR007811&partnerID=40&md5=4ffc5ae94256b9918cbaa1c7a62817af doi: 10.1029/2009WR007811

Zhang, L., Potter, N., Hickel, K., Zhang, Y., & Shao, Q. (2008). Water balance modeling over variable time scales based on the budyko framework model development and testing [Journal Article]. *Journal of Hydrology*, *360*(1-4), 117-131. doi: 10.1016/j.jhydrol.2008.07.021

Zhang, L., Walker, G., & Dawes, W. (2002). Water balance modelling: concepts and applications. in: Mcvicar, t.r., li rui, walker, j., fitzpatrick, r.w. and liu changming (eds) [Journal Article]. *Regional Water and Soil Assessment for Managing Sustainable Agriculture in China and Australia, ACIAR, Monograph No. 84*, 3147.

Zhang, Y., Pan, M., Sheffield, J., Siemann, A. L., Fisher, C. K., Liang, M., ... Wood, E. F. (2018). A climate data record (cdr) for the global terrestrial water budget: 1984-2010 [Journal Article]. *Hydrology and Earth System Sciences*, *22*(1), 241-263. Retrieved from https://www.scopus.com/inward/record.uri?eid=2-s2.0-85040601242&doi=10.5194%2fhess-22-241-2018&partnerID=40&md5=a77fa5da2e555e08ab831d2eebee2923 doi: 10.5194/hess-22-241-2018

Zhang, Y. Q., Chiew, F. H. S., Zhang, L., Leuning, R., & Cleugh, H. A. (2008). Estimating catchment evaporation and runoff using modis leaf area index and the penman-monteith equation [Journal Article]. *Water Resources Research*, *44*(10). Retrieved from https://www.scopus.com/inward/record.uri?eid=2-s2.0-57149084701&doi=10.1029%2f2007WR006563&partnerID=40&md5=4dd76c1ad6b3fd7c5186eefa4a3e0760 doi: 10.1029/2007WR006563